

City Research Online

City St George's, University of London

Citation: Brown, I. C. (1973). Two-dimensional biharmonic analysis and some applications. (Unpublished Doctoral thesis, The City University)

This is the accepted version of the paper.

This version of the publication may differ from the final published version. To cite this item please consult the publisher's version.

Permanent repository link: https://openaccess.city.ac.uk/id/eprint/38381/

Copyright and Reuse: Copyright and Moral Rights remain with the author(s) and/or copyright holders. Copies of full items can be used for personal research or study, educational, or not-for-profit purposes without prior permission or charge, unless otherwise indicated, provided that the authors, title and full bibliographic details are credited, a hyperlink and/or URL is given for the original metadata page and the content is not changed in any way. For full details of reuse please refer to City Research Online policy.

City Research Online: http://openaccess.city.ac.uk/ publications@citystgeorges.ac.uk

Two-dimensional Biharmonic Analysis and some Applications

by Ian Colin Brown, M.A.

A thesis submitted for the Degree of
Doctor of Philosophy

Department of Mathematics,
The City University, London.

June 1973

THE CITY UNIVERSITY LIBRARY,
ST. JOHN STREET, LONDON, E.C.1.

C O N T E N T S

		Page
List of tables		3
List of figures		4
Acknowledgements		5
Abstract		6
Glossary		7
Introduction..		10
PART I :	THE GARABEDIAN PROBLEM	
Chapter 1	Introduction	14
" 2	Harmonic function analysis	18
" 3	Numerical potential theory: Dirichlet problem ...	28
" 4	Numerical potential theory: Neumann problem ...	49
" 5	Biharmonic boundary value problems ..	56
" 6	Study of the Garabedian problem ...	67
PART II :	ELLIPTIC CAVITY PROBLEMS	
Chapter 7	Introduction	104
" 8	Exact solutions in confocal elliptic coordinates. ...	112
" 9	Exterior numerical solutions	125
PART III :	ELASTO-PLASTIC STRESS ANALYSIS	
Chapter 10	Introduction	142
" 11	Exact solution for a circular cavity.	148
" 12	Elasto-plastic iteration procedure...	160
" 13	Elliptic cavity subject to uniform internal pressure	171
Appendix 1	The Γ-contour : analytical considerations ...	184
" 2	The Γ-contour : numerical considerations ...	186
" 3	A trial harmonic problem	189
" 4	Representation of an arbitrary biharmonic function ...	192
" 5	Confocal elliptic coordinates	193
REFERENCES		195

LIST OF TABLES

Table	Page	Table	Page
1	36	33	52
2	36	34	53
3	37	35	53
4	37	36	53
5	38	37	54
6	38	38	54
7	39	39	54
8	39	40	55
9	40	41	63
10	40	42	64
11	41	43	64
12	41	44	64
13	42	45	65
14	42	46	65
15	43	47	65
16	43	48	66
17	43	49	66
18	43	50	66
19	43	51	73
20	44	52	74
21	44	53	74
22	45	54	75
23	45	55	75
24	45	56	76
25	46	57	76
26	46	58	77
27	46	59	78
28	47	60	122
29	47	61	168
30	48	62	169
31	52	63	169
32	52	64	187

LIST OF FIGURES

Figure	Page	Figure	Page
1	35	30	130
2	35	31	131
3	70	32	132
4	79	33	133
5	80	34	134
6	81	35	135
7	82	36	136
8	83	37	137
9	84	38	138
10	85	39	139
11	86	40	140
12	87	41	143
13	88	42	143
14	89	43	151
15	90	44	159
16	91	45	165
17	92	46	170
18	93	47	174
19	94	48	175
20	95	49	177
21	96	50	178
22	97	51	179
23	98	52	180
24	99	53	181
25	100	54	182
26	101	55	188
27	102	56	190
28	108	57	191
29	118		

ACKNOWLEDGEMENTS

The author has much pleasure in thanking his supervisor, Professor M.A. Jaswon, for his counsel and guidance.

He also acknowledges the help of the City of London Polytechnic (formerly Sir John Cass College), at which he has held the post of Senior Lecturer in Mathematics throughout the course of this research. Some research relaxation from teaching has been allowed; expenses of attending colloquia have been met; the Librarians have been helpful in obtaining journals; and the facilities of the City of London Polytechnic Computer Unit have been available.

ABSTRACT

This thesis lies within the subject area of the mathematical theory of elasticity and plasticity. Integral equation methods are applied to three problems lying broadly within the field of applied biharmonic analysis. The first concerns the deflection of a thin clamped elliptic plate subject to a concentrated transverse load. The second is that of determining the elastic stress field in the neighbourhood of a cavity of elliptic cross-section within an infinite medium. Finally, the previous problem is extended to the analysis of the plastic zone that develops near the tips of the cavity. This problem has relevance to the analysis of crack growth, and an approximation for the equilibrium elasto-plastic boundary is obtained.

This work is analytical and computational. Numerical solutions are obtained on a digital computer. Extensive use is made of numerical analysis and some developments in the field of techniques have been achieved.

GLOSSARY

List of Symbols.

a	Semi-major axis of ellipse.
b	Semi-minor axis of ellipse.
B	Domain.
c	(with reference to ellipses) $\sqrt{a^2-b^2}$.
c	(with reference to circular cavity problems) Radius of elasto-plastic boundary.
C	Elasto-plastic boundary.
C_i	Approximations to elasto-plastic boundary; $i = 1,2,3,...$
$\bar{C}_i$	Modified approximations to elasto-plastic boundary.
∂B	Boundary of domain B.
D	Flexural rigidity.
e	The base of natural logarithms, 2.71828183...
e	(as subscript) denotes "exterior".
(e)	(as subscript) denotes "in the elastic zone".
(e)	(as superscript) denotes "elastic component".
E	Young's modulus.
F_x, F_y	Traction components per unit length.
G	Biharmonic Green's function.
h_m	Half of an interval length.
h	Thickness of plate.
h, H	Critical axial ratios.
i	(as subscript) denotes "interior".
J	Yield stress.
K	Bulk modulus.
$\ln$	Natural logarithm.
L	Yield stress.
m	Scaling parameter.
n	Number of nodal points.
$\underline{n}$	Unit normal to boundary.
(p)	(as subscript) denotes "in the plastic zone".
(p)	(as superscript) denotes "plastic component".
P	Pressure.
P_0	Initial yield pressure.
$\underline{p}$	Vector variable specifying a point on ∂B.
$\underline{P}$	Vector variable specifying a point in B.
$\underline{q}$	Vector variable specifying a point on ∂B.
r	Plane polar coordinate.
s	"Capacity" of ellipse ($= \int_{\partial B} \sigma(\underline{q})\, dq$).
s	(In chapter 11) Increasing radius of plastic zone.

$\underline{s}$	Unit tangent to boundary.
$\underline{S}$	Source point.
S	Numerical approximation for s, the capacity of ellipse.
S	(In chapter 8) Shear.
T	Tension.
u	Cartesian displacement component.
v	Cartesian displacement component.
V	Strain energy per unit length.
$V(\underline{P})$	Harmonic function.
w	Cartesian displacement component; transverse deflection of plate.
W	Strain energy density.
$W(\underline{P})$	Double layer potential.
x	Cartesian coordinate.
y	Cartesian coordinate.
z	Cartesian coordinate.
α, β, γ	Constants which take values depending on the context.
Γ	An exceptional contour.
$\delta(\underline{P}-\underline{S})$	The Dirac delta function.
δ_{pq}	The Kronecker delta ($\delta_{pq} = 1$ if $p = q$; $\delta_{pq} = 0$ if $p \neq q$)
Δ	$\varepsilon_{xx} + \varepsilon_{yy} + \varepsilon_{zz}$, the divergence of the displacement vector.
$\in$	"is in", "is a member of".
ε_{pq}	Strain components; $p, q = x, y, z$; r, θ, z etc.
η	Confocal elliptic coordinate.
θ	Plane polar coordinate.
θ	(In chapters 12 and 13) Characteristic Coordinate.
$\textcircled{H}$	$\hat{x}x + \hat{y}y$
Θ	$\hat{x}x + \hat{y}y + \hat{z}z$, the dilatation.
$\lambda(\underline{q})$	Solution of integral equation.
$\Lambda(\underline{q})$	Solution of integral equation.
$\mu(\underline{q})$	Solution of integral equation.
μ	Lamé constant.
υ	Poisson's ratio.
ξ	Confocal elliptic coordinate.
π	3.14159265...
$\rho(\underline{q})$	Solution of integral equation.
$\sigma(\underline{q})$	Solution of integral equation; source density.
ϕ	Plane polar coordinate.
$\phi(\underline{q})$	Solution of integral equation.
$\phi(\underline{P})$	Two-dimensional harmonic function.
χ	Two-dimensional biharmonic function.
$\Psi(\underline{P})$	Two-dimensional harmonic function.
ω	Characteristic coordinate.

Notation

The symbol $\widehat{\ }$ connecting two letters denotes the stress component characterized by the directions associated with those letters. Thus $\widehat{xy}$ ($= \widehat{yx}$) is the component in the x-direction of stress on an element with normal in the y-direction.

A prime ($'$) above a function denotes the inward normal derivative, i.e. the expression $\phi' \equiv \frac{\partial \phi}{\partial n}$ where n is a normal to the boundary ∂B drawn into B.

In chapters 10 and 11, however, a prime on a stress or strain component denotes the deviatoric component. Thus

$$\widehat{pq}' = \widehat{pq} - \frac{\Theta}{3}\delta_{pq},$$

$$\varepsilon_{pq}' = \varepsilon_{pq} - \frac{\Delta}{3}\delta_{pq},$$

where

$$\Theta = \widehat{xx} + \widehat{yy} + \widehat{zz},$$

$$\Delta = \varepsilon_{xx} + \varepsilon_{yy} + \varepsilon_{zz} = \frac{\partial u}{\partial x} + \frac{\partial v}{\partial y} + \frac{\partial w}{\partial z}.$$

The two-dimensional Laplacian operator is denoted by ∇^2.

The two-dimensional biharmonic operator is denoted by ∇^4. In Cartesian coordinates,

$$\nabla^4 = \frac{\partial^4}{\partial x^4} + 2\frac{\partial^4}{\partial x^2 \partial y^2} + \frac{\partial^4}{\partial y^4}$$

Exhibition of Results

Numerical results are rounded off to the number of decimal places indicated. For example, the expression 3.464 denotes a real number x satisfying the inequality $3.4635 \leqslant x < 3.4645$. In some places, however, the context will make it clear that a decimal representation is exact.

INTRODUCTION

Biharmonic analysis traces its origins to Sir George Airy who, for the greater part of the last century, was Astronomer Royal of England. At the Royal Observatory, Greenwich, he developed an interest in elasticity in order to improve astronomical results by accounting for the deflection experienced by a telescope under its own weight. In 1862 he introduced the stress function, now usually called the Airy stress function, which satisfies the biharmonic equation of classical elasticity.

The earliest significant mathematical advance in biharmonic analysis was made by Hadamard (1908). He showed that a function χ which is continuous, and has continuous derivatives up to the fourth order throughout a finite domain B, and which satisfies the biharmonic equation in B, exists and is uniquely defined in B if χ and its normal derivative have prescribed values on the boundary of B.

There are two areas of elasticity in which the biharmonic equation plays a fundamental role. The first includes the theory of beams and thin elastic plates in which the deflection satisfies a biharmonic equation. The second comprises plane strain and generalized plane stress conditions. Here the second order partial derivatives of the Airy stress function determine the stress components.

An outstanding problem of classical elasticity concerns the deflection of a clamped plate under concentrated transverse loading. Translated into mathematical terms, the problem is that of determining a biharmonic Green's function G throughout the domain B of the plate, subject to appropriate conditions on the boundary ∂B. The earliest substantial advance was made by Hadamard (1908) when he conjectured that G has the same sign throughout B, i.e. the deflection has everywhere the same direction as the applied load. This conjecture was proved false by Garabedian in 1951. He demonstrated that, for a concentrated load located on the major axis of a clamped elliptic plate of axial ratio 5/3, the deflection along this axis changes sign if the load is located sufficiently near an extremity. Although Garabedian's result is extremely interesting and important, it involves rather complicated complex variable analysis of limited

applicability and leaves several questions unanswered. Firstly, it does not specify if there is a critical axial ratio below which the conjecture holds and above which it fails. Secondly, for Garabedian's particular axial ratio, no information is available about the deflection behaviour for different locations of the point force along the major axis. Thirdly, no expression is available for the deflection profile along the major axis. These questions seem sufficiently interesting to warrant further investigation. They are answered in part I of this thesis, and the conclusions reached are a significant contribution to the originality of the present work.

Returning to the other application of biharmonic analysis to elasticity, i.e. two-dimensional stress analysis, we may ascribe considerable worth to the contribution of Muskhelishvili (1963). His well known complex variable approach requires the domain under consideration to be mapped into the unit circle or half-plane. Closed expressions for the mapping function exist for relatively few domains. Approximate expressions for the mapping function may sometimes be constructed, and numerous other approaches are available which are effective for specialized types of problem. However, these are not sufficiently general to cope with the variety of domains and boundary conditions that arise in modern engineering science. Numerical solutions are achieved in part II of this thesis by a method which is applicable to a wide class of boundary-value problems. Where comparison is possible, good agreement is found between our numerical results and available exact solutions. An interesting analytical solution has been achieved for a problem in terms of confocal elliptic coordinates. Although the results are also obtainable by the method of Muskhelishvili, the present formulation appears to be original.

Elasto-plastic stress analysis constitutes another field in which few exact solutions are available. In the case of contained plastic flow, exact solutions are only available for special problems such as those exhibiting circular or spherical symmetry. General methods are available for computing stresses in a domain known to behave plastically, but the extent of this domain is unknown in advance. In part III of this thesis we develop a numerical method which we term the "elasto-plastic iteration procedure".

Here, successive solutions of elastic problems are followed by slip-line solutions for plastic stresses. The procedure is tested against problems having known solutions, and a useful solution is given to the problem of an infinite cavity of elliptic cross-section within an infinite medium subject to uniform internal pressure.

The basic tool of the numerical work of this thesis is the integral equation formulation of potential theory initiated by Jaswon in 1963, and developed, for example, by Jaswon, Maiti and Symm (1967). Although the theory is now well established, much work remains to be done on the numerical analysis and on the further exploitation of the method. Contributions in both these directions are made by the present thesis. Scope exists for extending research in this field, particularly in refining numerical results near boundaries. Since we generate biharmonic functions in terms of two harmonic functions, the early chapters of part I are devoted to discussing the relevant theoretical and numerical background issues. In particular we are concerned with the representation of harmonic functions by simple layer potentials.

It can be fairly claimed that this thesis makes a significant advance in developing numerical techniques as well as solving specific problems. It therefore inspires the hope that the present work will stimulate the further development of integral equation methods for applications in engineering science.

P A R T I

THE GARABEDIAN PROBLEM

CHAPTER 1

INTRODUCTION

Description and History of the Problem

The aim of Part I of this thesis is to solve one of the outstanding problems of classical elasticity concerning the deflection of a thin clamped plate under concentrated transverse loading. Translated into mathematical terms, this so-called "Garabedian problem" is that of determining a biharmonic Green's function G throughout the domain B of the plate, subject to appropriate conditions on its boundary ∂B. A notable contribution in this field was made by Hadamard (1908) when he conjectured that G has the same sign throughout B, i.e. the deflection has everywhere the same direction as the applied load. No doubt Hadamard was guided by comparison with the harmonic Green's function which is known to have the same sign everywhere in B, i.e. for a membrane the deflection has everywhere the same sign as the applied load. Hadamard's biharmonic conjecture is known to be true for a circular domain.

Happel (1921) obtained the deflection of a clamped elliptic plate loaded at the centre and Ghosh (1929) placed the load at a focus. Sengupta (1948) generalised by allowing the load to be anywhere on the major axis and later (1949)anywhere on the ellipse. These solutions, however, all suffer from disadvantages, chiefly that the deflection is left in the form of an infinite series with extremely complicated coefficients. Not surprisingly no attempt was made to compute the deflection anywhere or even discuss its sign.

Szegö (1939) showed that Hadamard's conjecture is false for certain non-convex domains, but regarded it as intuitively plausible for convex domains. Spain (1940) proved Hadamard's conjecture true with the additional restriction that the bending moment must take the appropriate sign on the boundary. But he believed that, without this restriction, Hadamard's conjecture was true for a convex domain.

No significant advance was made until Garabedian (1951) demonstrated that the conjecture fails even for a convex domain. More precisely he proved that, for a concentrated load located on the major axis of a clamped elliptic plate, the deflection along this axis changes sign in the following circumstances :-

(i) the axial ratio a/b equals $5/3$.

(ii) the load is located sufficiently near an extremity.

Although Garabedian's result is extremely interesting and important it involves rather complicated complex variable analysis of limited applicability and leaves several questions unanswered. Firstly, it does not specify if a critical axial ratio exists in the neighbourhood of $5/3$, below which the conjecture holds and above which it fails. Secondly, in the case of Garabedian's particular axial ratio, no information is available about the deflection behaviour for different locations of the point force along the major axis, e.g. would the conjecture also fail if the source point S coincides with the centre of the ellipse. Thirdly, no expression is available for the deflection profile along the major axis. These questions seem sufficiently interesting to warrant further investigation. They are answered in this thesis on the basis of a numerical technique described in the later chapters of Part I and the results are as follows :-

(i) there exists a critical a/b in the neighbourhood of $\sqrt{2}/1$ below which Hadamard's conjecture holds and above which it fails.

(ii) for a/b less than $\sqrt{2}/1$ the conjecture remains true for any S along the major axis, whereas for a/b greater than $\sqrt{2}/1$ the conjecture remains false for S sufficiently near an extremity of the major axis.

(iii) for a/b greater than or equal to $3/1$ the conjecture is false for any S on the major axis.

(iv) deflection profiles have been drawn for various choices of S in each of the ellipses $2/2$, $2/\sqrt{3}$, $2/\sqrt{2}$, $2/\frac{2}{3}$, $2/\frac{2}{5}$.

Unlike all previous solutions to this problem, the numerical approach we have used will allow us, with little extra effort, to compute profiles for any other position of the load point and any other axial ratio of the ellipse (or indeed for any other domain). The case 2/2, i.e. that of a circle, admits an exact analytical solution (Love, 1952) which yields profiles indistinguishable from those obtained by our numerical technique.

Integral Equation Formulations.

Apart from the circular case just mentioned, comparatively few biharmonic boundary-value problems admit exact analytical solutions. Several numerical methods of attack have been devised, including particularly the finite difference approach and, more recently, the boundary integral equation approach. In the former, B is covered by a grid of pivotal points at each of which the differential equation is replaced by a finite difference approximation. This leads to a system of linear algebraic equations over B which may be solved on a computer. In the latter approach, the biharmonic function is expressed in terms of two harmonic functions whereupon the integral representations of potential theory are utilised. This leads to a pair of coupled integral equations to determine the boundary source distributions. We discretise the integral equations into a linear algebraic system readily amenable to computer techniques. This enables the harmonic functions to be generated from the boundary source distributions, and hence the biharmonic function is constructed.

The integral equation formulations of potential theory are discussed in chapter 2 and the associated numerical procedures in chapters 3 & 4. The representation of biharmonic functions in terms of harmonic functions is discussed in chapter 5. The complete biharmonic solution can be handled by a single computer programme which may be checked by suitable trial functions, and numerical conditioning can be examined with hardly any extra human effort. Numerical data and computed deflection profiles

are displayed in chapter 6. This method is certainly more flexible and more accurate than the finite difference method, and has the obvious advantage that nodal points are restricted to ∂B so that the number of simultaneous linear equations to be solved is much smaller than for a grid of nodes covering B.

The integral equation method was introduced by M.A.Jaswon (1963) and developed in papers by Jaswon and Ponter (1963) and by Symm (1963). An application to clamped plates under uniform transverse loads is given by Jaswon and Maiti (1968) but no reference is made to concentrated loads. A useful contribution was made by E.Jaswon (1969) who confirmed Garabedian's result by this method. The present thesis extends Garabedian's work and fills in some of the important gaps mentioned. Deflection profiles are computed with greater numerical accuracy than before and original cases are considered. Scope clearly exists for extending the work to rectangular and other domains of engineering interest, and for the load located along the minor axis of the ellipse.

CHAPTER 2

HARMONIC FUNCTION ANALYSIS

Introduction

Boundary value problems in potential theory are usually classified according to the form of boundary condition into three main categories. The first, known as the Dirichlet problem, is that of finding a function ϕ harmonic within some domain B and having continuous prescribed values over the whole boundary ∂B of the domain. If continuous values of its derivative ϕ' normal to the boundary are prescribed, the problem is called the Neumann problem or the second boundary-value problem of potential theory. A necessary condition for the existence of a solution to the interior Neumann problem is

$$\int_{\partial B} \phi'(\underline{p})\, d_p = 0$$

where $\underline{p} \in \partial B$ and d_p is the arc differential at $\underline{p}$. Clearly the solution of this problem has an arbitrary constant since a constant contributes nothing to $\phi'(\underline{p})$. Finally, if a linear relation between ϕ and ϕ' is assigned at each point of ∂B, we have the third boundary value problem of potential theory. This problem clearly embraces the first and second problems and includes as a particular special case the mixed boundary value problem - that of finding a harmonic function in B given ϕ over part of ∂B and ϕ' over the complementary part. If B extends to infinity (exterior problem), then the behaviour there of the harmonic function must also be specified for a unique solution to exist.

Methods of solution for the above boundary-value problems fall into three main groups. The first involves finding exact analytic solutions such as the method of separation of variables, the use of Green's functions, and (in two-dimensions) the conformal mapping approach (Muskhelishvili,1963). These all suffer from the limitations of being only applicable to a very restricted class of boundaries and boundary conditions. The second

group comprises approximate analytic methods, such as variational methods (Kantorovich and Krylov, 1958) and the hypercircle approach of Synge (1957). These permit the solution of more extensive classes of problems, but again they have strict limitations. The third group is that of numerical methods. A standard procedure is to replace the differential equation by a system of finite difference equations referring to a set of nodal points spaced throughout the appropriate domain. These may be solved by digital computer techniques, but complications arise in associating rectangular nets with curved boundaries. Further, the large number of nodal points normally required renders the method uneconomical from the point of view of computer time and storage space, particularly for exterior problems.

This thesis makes use of a numerical approach based upon the theory of boundary integral equations. Here ϕ is represented within B by a simple-layer potential or double-layer potential generated by source distributions over the boundary ∂B of B. Since these potentials are harmonic functions in B, their identity with ϕ is assured by imposing upon them the boundary conditions prescribed for ϕ . This procedure leads to the formulation of Fredholm integral equations to determine the source densities Once these are known, they may be utilised to generate the potential and hence ϕ , throughout B.

The integral equation formulation of potential theory yields the following equations of Fredholm type :-

$$\int_{\partial B} \ln |\underline{p} - \underline{q}| \, \sigma(\underline{q}) \, dq = \phi(\underline{p}), \qquad (2.1)$$

$$\int_{\partial B} \ln' |\underline{p} - \underline{q}| \, \sigma(\underline{q}) dq + \pi \sigma(\underline{p}) = \Psi(\underline{p}), \qquad (2.2)$$

$$\int_{\partial B} \ln |\underline{p} - \underline{q}|' \, \mu(\underline{q}) dq - \pi \mu(\underline{p}) = \phi(\underline{p}), \qquad (2.3)$$

where $\underline{p}$, $\underline{q}$ are vector variables specifying points on a given contour ∂B , dq denotes the arc differential

at $\underline{q}$ directed so as to keep B on the left; ϕ and ψ are prescribed continuous functions on ∂B, and σ or μ are the unknown source densities to be determined; $\ln'|\underline{P}-\underline{q}|$ denotes the normal derivative of $\ln|\underline{P}-\underline{q}|$ at $\underline{P}$ keeping $\underline{q}$ fixed, and reciprocally for $\ln|\underline{P}-\underline{q}|'$. For our purposes we may assume ∂B to be a single, simple, smooth contour, although generalisation to multiply-connected domains is possible (Symm, 1963). It will be found convenient for the positive normal to have two distinct directions at each point of ∂B depending on the context: it will always point into the domain B. Accordingly the direction relevant when differentiating exterior functions is opposite to that for interior functions. With an obvious suffix notation we have

$$\ln|\underline{P}-\underline{q}|'_i = -\ln|\underline{P}-\underline{q}|'_e \quad ; \qquad \underline{q}\neq\underline{P}, \qquad (2.4)$$

and after applying the Cauchy-Riemann equations we obtain the integral relation

$$\int_{\partial B} \ln|\underline{P}-\underline{q}|'_i \, dq = -\int_{\partial B} \ln|\underline{P}-\underline{q}|'_e \, dq = -\pi . \qquad (2.5)$$

This sign convention has the advantage that either interior or exterior problems are formulated by (2.2) and (2.3).

Equation (2.1) arises if a simple source distribution is adopted, and this representation is intuitively the most obvious for Dirichlet problems. If a solution exists it generates an interior harmonic function

$$\phi_i(\underline{P}) = \int_{\partial B} \ln|\underline{P}-\underline{q}|\sigma(\underline{q})dq \; ; \quad \underline{P}\in B_i+\partial B, \qquad (2.6)$$

and an exterior harmonic function

$$\phi_e(\underline{P}) = \int_{\partial B} \ln|\underline{P}-\underline{q}|\sigma(\underline{q})dq \; ; \quad \underline{P}\in B_i+\partial B, \qquad (2.7)$$

each of which reduces to $\phi(\underline{P})$ on ∂B. However in classical potential theory this formulation was not used because of analytical difficulties; little work having been done on existence theorems for Fredholm's first equation. It was customary instead to represent potentials by means of double layer distributions resulting in equation (2.3), a Fredholm integral equation of the second kind, for which the theory has been well developed. For a Neumann problem equation (2.2) is relevant and this, also being of Fredholm's second kind, presents no great difficulties.

Neumann problems

The interior Neumann problem is solved satisfactorily by Fredholm's second equation. Here we assume a simple-source distribution

$$\phi_i(\underline{P}) = \int_{\partial B} \ln |\underline{P} - \underline{q}| \, \sigma(\underline{q}) \, dq; \qquad \underline{P} \in B + \partial B, \tag{2.8}$$

yielding (Kellogg, 1929)

$$\phi_i'(\underline{P}) = \int_{\partial B} \ln_i' |\underline{P} - \underline{q}| \, \sigma(\underline{q}) \, dq + \pi \sigma(\underline{P}); \quad \underline{P} \in \partial B. \tag{2.9}$$

We identify the prescribed $\phi'(\underline{P})$ with $\Psi(\underline{P})$ in (2.2): $\underline{P} \in \partial B$. The transposed homogeneous form of (2.9) is

$$\int_{\partial B} \ln_i' |\underline{q} - \underline{P}| \, \sigma(\underline{q}) \, dq + \pi \sigma(\underline{P}) = 0; \qquad \underline{P} \in \partial B, \tag{2.10}$$

which possesses the obvious non-trivial solution σ = constant by (2.5). From the general theory of Fredholm integral equations (Mikhlin, 1957) the necessary and sufficient condition for (2.9) to exhibit a solution is that $\phi'(\underline{P})$ be orthogonal to the solution of (2.10), i.e. to a constant. Thus (2.9) has a solution if and only if

$$\int_{\partial B} \phi'(\underline{P}) \, dP = 0. \tag{2.11}$$

This we recognize as the Gauss condition which is necessary for any interior harmonic. The solution of (2.2), then, is unique and yields an interior harmonic function unique but for an arbitrary additive constant.

The exterior Neumann problem has a unique solution in all cases, since the homogeneous equation and its transpose have only trivial solutions; whence the orthogonality condition places no restriction on $\Psi(\underline{P}) = \phi_e'(\underline{P})$. We find that Gauss's theorem applied to the exterior domain gives

$$\int_{\partial B} \phi_e'(\underline{P}) \, dP = 2\pi \int_{\partial B} \sigma(\underline{q}) \, dq \tag{2.12}$$

by virtue of (2.5).

Interior Dirichlet problems

Jaswon (1963) drew attention to the advantages of Fredholm's first equation and showed that the analytical difficulties can be overcome by careful consideration of the boundary contour and by a resolution of the potential into constant and variable parts. The argument may be summarized as follows. We first show that either

$$\int_{\partial B} \ln |\underline{p} - \underline{q}| \, \lambda(\underline{q}) \, dq = 1 \tag{2.13}$$

or

$$\int_{\partial B} \ln |\underline{p} - \underline{q}| \, \lambda(\underline{q}) \, dq = 0 \tag{2.14}$$

has a non-trivial solution for any regular contour. Consider the Fredholm integral equation of the second kind

$$\int_{\partial B} \ln |\underline{p} - \underline{q}|'_e \, \mu(\underline{q}) \, dq - \pi \mu(\underline{p}) = 0. \tag{2.15}$$

This possesses the effectively unique non-trivial solution μ = constant, by virtue of (2.5), and therefore, by general theory, the transpose (adjoint) equation

$$\int_{\partial B} \ln'_e |\underline{p} - \underline{q}| \, \lambda(\underline{q}) \, dq - \pi \lambda(\underline{p}) = 0 \tag{2.16}$$

or, by (2.4),

$$\int_{\partial B} \ln'_i |\underline{p} - \underline{q}| \, \lambda(\underline{q}) \, dq + \pi \lambda(\underline{p}) = 0 \tag{2.17}$$

also possesses an effectively unique non-trivial solution. However, by comparison with (2.2), equation (2.17) is obviously the expression for the potential of a simple layer of density $\lambda(\underline{p})$ differentiated along the inward normal. Since a harmonic function is constant along ∂B if the inward normal derivative is zero along ∂B, this result implies

$$\int_{\partial B} \ln |\underline{p} - \underline{q}| \, \lambda(\underline{q}) \, dq = \text{constant}; \qquad \underline{p} \in \partial B, \tag{2.18}$$

whence it is evident that either (2.13) or (2.14) possesses an effectively unique solution for any given contour. It can be shown (Appendix 1) that given a family of similar contours there exists one - and only one - member of the family for which the constant in (2.18) is zero. This has been termed the Γ-contour. Accordingly equation (2.13) has no solution for Γ, whilst (2.14) has a non-trivial solution. For any other member of the family equation (2.13) has a solution, which must be unique, whilst (2.14) has only a trivial solution.

We can avoid the Γ-contour simply by changing the scale. We shall assume that this has been done in the subsequent theory. Turning our attention to equation (2.1), we note at the outset that a demonstration of the existence of a solution will imply uniqueness, for suppose σ_1 and σ_2 are two distinct solutions, subtraction will yield

$$\int_{\partial B} \left[\sigma_1(\underline{q}) - \sigma_2(\underline{q}) \right] \ln |\underline{p} - \underline{q}| \, dq = 0 \qquad (2.19)$$

but as $\left[\sigma_1(\underline{q}) - \sigma_2(\underline{q})\right]$ is assumed not to be identically zero, (2.19) shows that ∂B must be a Γ-contour contrary to hypothesis.

To show now that (2.1) exhibits a solution we consider the equation

$$\int_{\partial B} \ln_i |\underline{q} - \underline{p}|' \rho(\underline{q}) dq + \pi \rho(\underline{p}) = \phi_i'(\underline{p}). \qquad (2.20)$$

From general theory (Mikhlin, 1957) the necessary and sufficient condition for (2.20) to exhibit a solution is that $\phi_i'(\underline{p})$ be orthogonal to the solution μ of the adjoint homogeneous equation

$$\int_{\partial B} \ln_i' |\underline{q} - \underline{p}| \mu(\underline{q}) dq + \pi \mu(\underline{p}) = 0. \qquad (2.21)$$

This has a solution μ = constant by (2.5), so the orthogonality condition

$$\int_{\partial B} \mu(\underline{p}) \phi_i'(\underline{p}) \, dp = 0 \qquad (2.22)$$

becomes

$$\int_{\partial B} \phi_i'(\underline{p}) \, dp = 0. \qquad (2.23)$$

This, being the Gauss condition, is satisfied because ϕ_i is a harmonic function. Therefore equation (2.20) has a solution. Integration of (2.20) yields

$$\int_{\partial B} \ln|\underline{p}-\underline{q}|\,\rho(\underline{q})\,dq = \phi_i(\underline{p}) + A \tag{2.24}$$

where A is a constant. Thus, because of (2.13),

$$\int_{\partial B} \ln|\underline{p}-\underline{q}|\left\{\rho(\underline{q}) - A\,\lambda(\underline{q})\right\} dq = \phi_i(\underline{p}). \tag{2.25}$$

We have shown that ρ exists so $\rho - A\lambda$ is now displayed as the solution to (2.1). The apparent non-uniqueness arising from A may be eliminated upon observing (Appendix 1) that σ satisfies

$$\int_{\partial B} \sigma(\underline{q})\,dq = \int_{\partial B} \phi(\underline{p})\,\lambda(\underline{p})\,dp \tag{2.26}$$

or

$$\int_{\partial B} \rho(\underline{q})\,dq = A\int_{\partial B} \lambda(\underline{q})\,dq + \int_{\partial B} \phi(\underline{p})\,\lambda(\underline{p})\,dp, \tag{2.27}$$

which fixes A when ρ is known, as expected by our uniqueness result.

Exterior Dirichlet problems

As with interior Dirichlet problems, the theory of Fredholm integral equations of the first kind may be applied to equation (2.1) and its solution used to generate an exterior harmonic function (2.7). An important observation concerning the asymptotic behaviour of (2.7) is that

$$\left.\begin{aligned} &\phi_e(\underline{p}) \to \ln r \int_{\partial B} \sigma(\underline{q})\,dq + O\left(\tfrac{1}{r}\right) \\ &\text{as} \quad r \equiv |\underline{p}| \to \infty. \end{aligned}\right\} \tag{2.28}$$

Hence no constant harmonic function can be represented in an exterior domain by a simple source potential (although it may be so represented in an interior domain). This encourages us to make the resolution

$$\phi(\underline{p}) = \phi_e(\underline{p}) + k \tag{2.29}$$

where k is a constant which we shall specify completely by requiring

$$\int_{\partial B} \phi(\underline{p})\,\lambda(\underline{p})\,dp = k\int_{\partial B}\lambda(\underline{p})\,dp. \tag{2.30}$$

Equations (2.29) and (2.30) imply

$$\int_{\partial B} \phi_0(\underline{p})\,\lambda(\underline{p})\,dp = 0. \tag{2.31}$$

The corresponding resolution for $\sigma(\underline{q})$ is

$$\sigma(\underline{q}) = \sigma_0(\underline{q}) + k\lambda \tag{2.32}$$

since this will automatically satisfy the "constant" part of the potential and gives as the equation for $\sigma_0(\underline{q})$

$$\int_{\partial B} \ln|\underline{p}-\underline{q}|\,\sigma_0(\underline{q})\,dq = \phi_0(\underline{p}). \tag{2.33}$$

Thus the problem of solving (2.1) for $\sigma(\underline{q})$ has become the problem of solving for $\sigma_0(\underline{q})$ in (2.33).

The demonstration of the existence and uniqueness of the solution $\sigma_0(\underline{q})$ is practically identical to that given above for $\sigma(\underline{q})$. (Equations (2.19) to (2.27)). We note, however, that (2.26) is replaced by

$$\int_{\partial B} \sigma_0(\underline{q})\,dq = 0 \tag{2.34}$$

because of (2.31). Thus there exists a unique exterior harmonic function bounded at infinity: this may be identified as

$$\phi(\underline{P}) = \phi_0(\underline{P}) + k = \int_{\partial B} \ln|\underline{P}-\underline{q}|\,\sigma_0(\underline{q})\,dq + k. \tag{2.35}$$

We note from (2.34) that $\phi_0(\underline{P}) \to O\left(\frac{1}{r}\right)$ as $r\to\infty$, whereas by (2.28) $\phi_e(\underline{P})$ exhibits logarithmic behaviour at infinity.

Our method of solving the Dirichlet problem by Fredholm's first equation has three advantages over the conventional formulation in terms of Fredholm's second equation (2.3). In the latter the harmonic $\phi(\underline{P})$, for

which boundary values $\phi(\underline{P})$ are prescribed, is identified with the double-layer potential

$$W = W(\underline{P}) = \int_{\partial B} \mu(\underline{q}) \ln'|\underline{q} - \underline{P}| dq ; \quad \underline{P} \in B. \quad (2.36)$$

As $\underline{P} \to \underline{p}$ on ∂B this becomes

$$W(\underline{p}) = \int_{\partial B} \mu(\underline{q}) \ln'|\underline{q} - \underline{p}| dq - \pi\mu(\underline{p}). \quad (2.37)$$

We note the discontinuity at the boundary which does not arise with

$$\phi(\underline{P}) = \int_{\partial B} \sigma(\underline{q}) \ln|\underline{P} - \underline{q}| dq ; \quad \underline{P} \in B + \partial B. \quad (2.38)$$

Other disadvantages with W are that $\ln'|\underline{q} - \underline{p}|$ is more difficult to compute than $\ln|\underline{q} - \underline{p}|$ and that μ usually has much less physical significance than σ.

Green's formula

We have now laid sound theoretical foundations on which to build the numerical work of the next two chapters in which Dirichlet and Neumann problems are solved using simple-layer potentials only. It would be appropriate, however, to conclude a chapter on two-dimensional harmonic function analysis by referring to Green's boundary formula. This important identity can form the basis of an attack on mixed boundary value problems, and like the previous formulations by integral equation methods, admits generalisation to three dimensions (Laskar, 1972).

Green's formula, adapted to two-dimensional potential theory, takes the form

$$\frac{1}{2\pi} \int_{\partial B} \ln|\underline{P} - \underline{q}| \phi'(\underline{q}) dq - \frac{1}{2\pi} \int_{\partial B} \ln|\underline{P} - \underline{q}|' \phi(\underline{q}) dq = \phi(\underline{P}) ; \quad \underline{P} \in B, \quad (2.39)$$

its significance being as follows:- if there exists a harmonic function $\phi(\underline{P})$ throughout a simply connected domain B, admitting boundary values $\phi(\underline{q})$ and boundary normal derivatives $\phi'(\underline{q})$ on ∂B, the left-hand side of (2.39) is identical with $\phi(\underline{P})$. For a field point $\underline{P}$ outside B, it gives zero identically. For a field point $\underline{p}$ on ∂B itself, it equals $\frac{1}{2}\phi(\underline{p})$ owing to the jump in the double-layer integral at ∂B, and so $\phi(\underline{q}), \phi'(\underline{q})$ satisfy the

linear functional relation

$$\int_{\partial B} \ln|\underline{P}-\underline{q}|\,\phi'(\underline{q})\,dq - \int_{\partial B} \ln|\underline{P}-\underline{q}|'\,\phi(\underline{q})\,dq = \pi\,\phi(\underline{P}), \qquad (2.40)$$

known as Green's boundary formula. Thus for the third boundary value problem of potential theory with boundary relation

$$\alpha(\underline{q})\phi'(\underline{q}) + \beta(\underline{q})\phi(\underline{q}) = \gamma(\underline{q}) \qquad (2.41)$$

where α, β, γ are known functions, Green's boundary formula (2.40) becomes a Fredholm equation of the

(a) second kind for ϕ if ϕ' is eliminated in favour of ϕ and γ,

(b) second kind for ϕ' if ϕ is eliminated in favour of ϕ' and γ,

(c) first kind for ϕ' if only ϕ is prescribed. (Dirichlet problem),

(d) second kind for ϕ if only ϕ' is prescribed. (Neumann problem).

With $\phi(\underline{q})$ or $\phi'(\underline{q})$ computed, as the case may be, $\phi(\underline{P})$ can be generated at any interior point by means of Green's formula (2.39). These considerations can be adapted without difficulty to the case of exterior and multiply connected domains.

CHAPTER 3

NUMERICAL POTENTIAL THEORY: DIRICHLET PROBLEM

Discretisation procedure

To effect a numerical solution of integral equations associated with boundary value problems in two-dimensional potential theory (e.g.(2.1) to (2.3)) we divide the boundary ∂B into n intervals, the m^{th} being of length $2h_m$ and centred at a pivotal point $\underline{q}_m$ approximately midway between the interval points $\underline{q}_{m\pm\frac{1}{2}}$. The boundary ∂B must be "Kellogg regular" to ensure the existence of solutions but a finite number of corners is permissible (Kellogg,1929). If ∂B has corner points, we identify each of the corners as interval points, thus ensuring that the individual intervals themselves are smooth arcs so that (2.4) and (2.5) are still valid almost everywhere. The fundamental approximation is that σ remains constant in each interval, whereupon the integral equation may be approximated by a set of simultaneous linear equations.

As a trial Dirichlet problem we generate numerically the interior potential $\phi(\underline{P})$ given that $\phi(\underline{p}) = 1$ on the boundary ∂B of an ellipse. We know that the analytic solution is $\phi(\underline{P}) = 1$ everywhere in B. The relevant integral equation (2.1) becomes

$$\int_{\partial B} \ln|\underline{P} - \underline{q}|\,\sigma(\underline{q})\,dq = 1 \qquad (3.1)$$

which is replaced by the discrete system

$$\sum_{m=1}^{n} \sigma_m \int_m \ln|\underline{q} - \underline{P}|\,dq = 1\,; \qquad \underline{P} = \underline{q}_1, \underline{q}_2, \ldots, \underline{q}_n, \qquad (3.2)$$

where $\int_m \ldots dq$ denotes integration over the m^{th} interval and σ_m denotes the assumed constant value of σ in this interval. The algebraic system (3.2) may be written

$$\sum_{m=1}^{n} \sigma_m A_{rm} = 1\,; \qquad r = 1, 2, 3, \ldots, n. \qquad (3.3)$$

The simplest approximation for A_{rm} is obtained by assuming that the value of each kernel at the mid point of an interval is applicable throughout that interval.

Thus

$$A_{rm} = 2h_m \ln|\underline{q}_m - \underline{q}_r| \; ; \qquad m \neq r \, , \qquad (3.4)$$

which is equivalent to using the trapezoidal rule for integration. Generally, however, we find that results are improved by using an approximation based on Simpson's rule where

$$A_{rm} = \frac{h_m}{3}\left[\ln|\underline{q}_r - \underline{q}_{m-\frac{1}{2}}| + 4\ln|\underline{q}_r - \underline{q}_m| + \ln|\underline{q}_r - \underline{q}_{m+\frac{1}{2}}|\right] ; \quad m \neq r. \qquad (3.5)$$

In either case modifications are needed when $m=r$, because of the singular kernel in (3.2). Here we approximate the boundary by two chords joining $\underline{q}_m$ to $\underline{q}_{m\pm\frac{1}{2}}$ and use the result

$$\int_0^h \ln x \, dx = h(\ln h - 1)$$

to obtain

$$A_{mm} = |\underline{q}_m - \underline{q}_{m-\frac{1}{2}}|\left[\ln|\underline{q}_m - \underline{q}_{m-\frac{1}{2}}| - 1\right] + |\underline{q}_m - \underline{q}_{m+\frac{1}{2}}|\left[\ln|\underline{q}_m - \underline{q}_{m+\frac{1}{2}}| - 1\right] . \qquad (3.6)$$

All the numerical operations of assembling the coefficients can be effected by feeding appropriate subroutines into a digital computer working with the coordinates of $\underline{q}_m$ and $\underline{q}_{m\pm\frac{1}{2}}$ as input data. The individual subroutines may be combined into a single program that assembles and solves the system of equations (3.3) and then generates the discretised simple-layer potential

$$\phi_i(\underline{P}) = \sum_{m=1}^{n} \sigma_m \int_m \ln|\underline{P} - \underline{q}| \, dq \qquad (3.7)$$

throughout B and on ∂B itself.

The set of equations (3.3) is solved using a subroutine based on matrix inversion by Gaussian elimination. It is worth noting that the Gauss-Seidel method fails because, although for each r

$$|A_{rr}| > |A_{rm}| \; ; \qquad m = 1,2,\ldots,n, \quad (n \neq r)$$

the necessary condition for convergence

$$|A_{rr}| > \sum_{r \neq m} |A_{rm}| \; ; \qquad r = 1,2,\ldots,n,$$

is <u>not</u> satisfied. It is interesting that in three-dimensions the Gauss-Seidel method converges for corresponding problems because of the stronger singularity at the origin of r^{-1} in comparison with $\ln r$.

Error Analysis

The potential (3.7) generated throughout $B + \partial B$ has the property

$$\phi_i(\underline{P}) \to 1 \qquad \text{as} \quad \underline{P} \to \underline{p} = \underline{q}_1, \underline{q}_2, \ldots, \underline{q}_n . \qquad (3.8)$$

From the maximum modulus principle a measure of the error associated with $\phi_i(\underline{P})$ is provided by the maximum value of $|\phi_i(\underline{p}) - 1|$, which may be readily computed at boundary interval points.

A sound procedure in numerical analysis is to start with n small and examine how the computed data behave as n increases. It can be seen from (3.4) to (3.6) that as $n \to \infty$,

$$A_{rm} \to 0 \qquad \text{for all } r, m, \quad \text{since } h_m \to 0.$$

Thus $\det.|A_{rm}| \to 0 \qquad \text{as } n \to \infty.$

This is the phenomenon of inherent ill-conditioning which generally appears unless there exists a constant c such that

$$|A_{mm}| > c > 0 \qquad \text{for } m = 1, 2, \ldots, n$$

as happens with Fredholm integral equations of the second kind. So for Dirichlet problems solved by means of Fredholm integral equations of the first kind we have to balance two opposing factors :-

(i) n large: accurate numerical approximation but poor conditioning;

(ii) n small: poor numerical approximation but good conditioning.

We find that optimum conditioning occurs near $n = 32$. For a given n, best results are obtained with intervals as nearly as possible of constant length along ∂B. An ellipse may be divided into n equal intervals by means of elliptic integrals (Hancock, 1958).

Elliptic Boundary

In the first instance, we followed these procedures for the ellipse

$$\frac{x^2}{a^2} + \frac{y^2}{b^2} = 1 \qquad (3.9)$$

choosing various axial ratios $a:b$. The perimeter of the ellipse has a length given by

$$L = 4\int_0^a \sqrt{1 + \left(\frac{dy}{dx}\right)^2}\, dx \qquad (3.10)$$

and after substituting for $\frac{dy}{dx}$ and setting

$$x = a\sin\theta \quad , \qquad \frac{a^2-b^2}{a^2} = k^2 , \tag{3.11}$$

we find

$$L = 4a\int_0^{\pi/2} \sqrt{1-k^2\sin^2\theta}\ d\theta . \tag{3.12}$$

Comparison with the definition of the elliptic integral of the second kind,

$$E(k;\phi) = \int_0^{\phi} \sqrt{1-k^2\sin^2\theta}\ d\theta , \tag{3.13}$$

gives

$$L = 4a\,E(k;\tfrac{\pi}{2}) . \tag{3.14}$$

Division by $2n$ gives the constant h_m , whence the eccentric angles of every interval and nodal point are determined by repeated use of tables of elliptic integrals of the second kind.

Our initial choice of axial ratios for the test problem included those for which comparison could be made for the biharmonic problem with the earlier results of E.Jaswon(1969). No doubt he had found it more convenient to use the tables when $\sin^{-1}k$ is an integral number of degrees although by equation (3.11) the ratio $a:b$ is then sometimes irrational. For comparison with Symm (1964) we placed nodal points at the ends of the major and minor axes, but subsequently found that greater accuracy could be obtained if, instead, interval points were so placed. This also affords greater symmetry. We further improved accuracy by defining interval points by equal eccentric angles instead of equal arc length. This obviated the need to use elliptic integral tables with the associated laborious interpolations introducing inaccuracies and the possibility of mistakes; in fact a few errors were found in the tables themselves. With the use of equal eccentric angles the construction of all the input data can be automated by the computer program, and the number of nodal points systematically increased without extra effort. Although interval lengths are not now exactly equal, they may be made much smaller by increasing n , yielding results which, as far as we know, are more accurate than any previously obtained.

Our numerical results for σ may be compared with the analytic solutions which are readily obtained using confocal elliptic coordinates (Appendix 5), in which

$$\xi = \xi_0 = \cosh^{-1}\left(\frac{a}{c}\right) \tag{3.15}$$

defines the ellipse (3.8) where

$$c^2 = a^2 - b^2. \tag{3.16}$$

The simple source distribution which satisfies (3.1) generates the interior harmonic function $V_i(\underline{P}) = 1$ and the exterior harmonic function

$$V_e(\underline{P}) = \frac{\xi - \ln\frac{z}{c}}{\xi_0 - \ln\frac{z}{c}}. \tag{3.17}$$

Clearly $V_e(\underline{P})$ is harmonic in ξ (and therefore in x and y) and exhibits the required properties

$$V_e(\underline{P}) = V_e(\underline{p}) = 1 \qquad \text{on } \xi = \xi_0. \tag{3.18}$$

Since

$$\xi \to \ln\frac{2r}{c} \qquad \text{as } r \to \infty, \tag{3.19}$$

$V_e(\underline{P})$ possesses logarithmic potential behaviour at infinity, i.e. $V_e(\underline{P})$ is of the form

$$V_e(\underline{P}) = s \ln r + O\left(\frac{1}{r}\right) \quad \text{as } r \to \infty \tag{3.20}$$

where

$$s = \int_{\partial B} \sigma(\underline{q})\, dq = \frac{1}{\xi_0 - \ln\left(\frac{z}{c}\right)} = \frac{1}{\ln\left(\frac{a+b}{c}\right)}. \tag{3.21}$$

This result provides a check on the numerical estimate of S, which from (3.21) is given by

$$S = 2\sum_{m=1}^{n} \sigma_m h_m. \tag{3.22}$$

The result

$$2\pi\sigma(\underline{q}) = V_e'(\underline{q}) + V_i'(\underline{q}), \tag{3.23}$$

which arises from (2.2) and (2.4), yields

$$\sigma(\underline{q}) = \frac{V_e'(\underline{q})}{2\pi} \tag{3.24}$$

and the appropriate form of normal differentiation (A5.15) gives

$$\sigma(\underline{q}) = \frac{1}{\sqrt{2}\,\pi c}\left[\cosh 2\xi_0 - \cos 2\eta\right]^{-1/2}\left[\xi_0 - \ln\frac{2}{c}\right]^{-1}\frac{d}{d\xi}\left[\xi - \ln\frac{2}{c}\right] \qquad (3.25)$$

where η is the eccentric angle of $\underline{q}$, whence in terms of $x = x(\underline{q}) = a\cos\eta$ we have by equation (A5.6),

$$\sigma(\underline{q}) = \frac{a}{2\pi \ln\left(\frac{a+b}{2}\right)\sqrt{a^2 - x^2c^2}} \cdot \qquad (3.26)$$

Numerical results

Tables 1 - 10, pp.36-40, refer to the ellipses with $a = 2$; $b = \sqrt{3}, \sqrt{2}, 1, 0.684, 0.347$, with pivotal points distributed as in figure 1, i.e. with nodal points at the ends of axes and with equal arc lengths. Tables 1 - 5 show how the accuracy of the computed σ improves on passing from $n = 16$ to $n = 32$. (In the $n = 16$ column, the results for $i = 1,2,3,4,5$ are placed in positions $i = 1,3,5,7,9$ for comparison with $n = 32$). A corresponding improvement is found in the generated values of $\phi_i(\underline{P})$ as n increases. Tables 6 - 10 show the numerical value of $\phi_i(\underline{P})$ along the major axis when $n = 32$, and demonstrate the superiority of Simpson's rule (3.5) over (3.4). Since we are interested in how the numerical solution deteriorates near nodal points, the tables show more values of $\phi_i(\underline{P})$ near the end of the major axis than near the centre.

Tables 11 - 20, pp. 41 - 44, refer to the previous ellipses but with the interval points placed at the ends of the axes (as in figure 2, p.35). The overall accuracy of σ_i is marginally improved, and an appreciable improvement is found in the values of $\phi_i(\underline{P})$. Equation (3.5) has been used for numerical integration and $n = 32$. As expected, accuracy deteriorates as the axial ratio a/b increases.
Tables 11 - 15 refer to σ_i. Tables 16 - 20 refer to $\phi_i(\underline{P})$ generated along the major axis. The sharp drop in $\phi_i(\underline{P})$ near the end of the major axis (shown in tables 6 - 10) is eliminated since we are no longer approaching a singularity.

Tables 21 - 30 show the computed σ_i and $\phi_i(\underline{P})$ when equal eccentric angles are used to define interval and nodal points. Here, with $n = 32$ and (3.5) used, the

analysis is easily extended to a new range of axial ratios, and the results are favourable. The analytical "capacity" s of (3.21) and the numerical counterpart S of (3.22) are shown in table 30 with the corresponding error $|S-s|$. The values of $\phi_i(P)$, $i = 1,2,\ldots\ldots,8$ shown in table 30 correspond to field points on the major axis defined by $x = \frac{a_j}{2}$ where $j = 0.0, 1.0, 1.5, 1.75, 1.80, 1.85, 1.90, 1.95,$ so that direct comparison can be made with tables 16 - 20.

It proved possible to improve the accuracy of $\phi(P)$ near the boundary by using linear interpolation or Newton's backward difference formula involving the given boundary value of $\phi(P)$. These results are not recorded here since they are irrelevant to biharmonic problems where $\phi(P)$ is not prescribed.

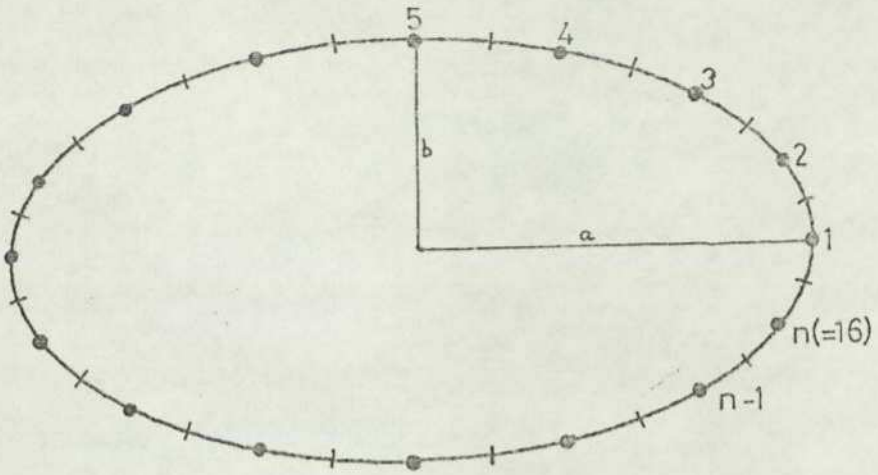


FIG. 1

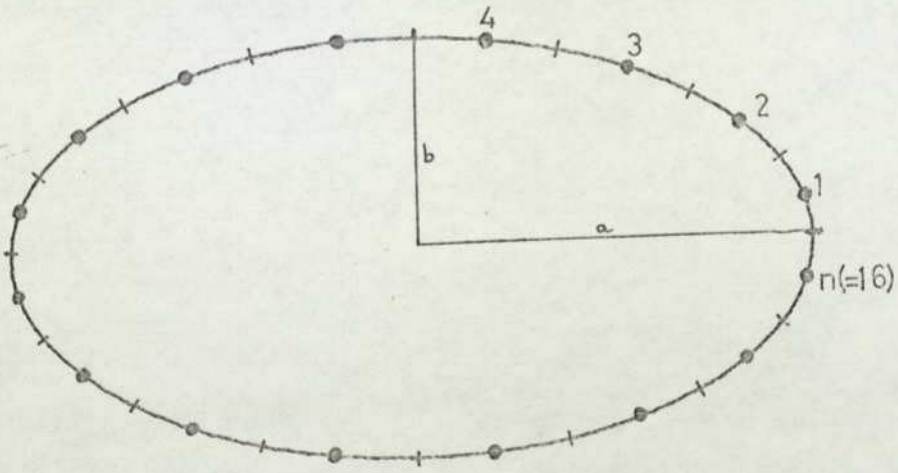


FIG. 2

TABLE 1

i	COMPUTED n = 16	COMPUTED n = 32	ANALYTIC	ERROR n = 32
1	0.1476	0.1474	0.1473	0.0001
2		0.1463	0.1462	0.0001
3	0.1436	0.1435	0.1434	0.0001
4		0.1396	0.1396	0.0000
5	0.1357	0.1357	0.1357	0.0000
6		0.1323	0.1323	0.0000
7	0.1296	0.1297	0.1297	0.0000
8		0.1281	0.1281	0.0000
9	0.1274	0.1276	0.1276	0.0000

Values of σ_i for $a = 2$, $b = \sqrt{3}$

TABLE 2

i	COMPUTED n = 16	COMPUTED n = 32	ANALYTIC	ERROR n = 32
1	0.2115	0.2109	0.2104	0.0005
2		0.2052	0.2049	0.0003
3	0.1927	0.1923	0.1922	0.0001
4		0.1786	0.1786	0.0000
5	0.1669	0.1672	0.1673	0.0001
6		0.1588	0.1588	0.0000
7	0.1528	0.1531	0.1531	0.0000
8		0.1498	0.1499	0.0001
9	0.1485	0.1488	0.1488	0.0000

Values of σ_i for $a = 2$, $b = \sqrt{2}$

TABLE 3

i	COMPUTED n = 16	COMPUTED n = 32	ANALYTIC	ERROR n = 32
1	0.3936	0.3928	0.3925	0.0003
2		0.3542	0.3515	0.0027
3	0.2941	0.2925	0.2934	0.0009
4		0.2534	0.2539	0.0005
5	0.2270	0.2287	0.2289	0.0002
6		0.2129	0.2131	0.0002
7	0.2024	0.2032	0.2033	0.0001
8		0.1979	0.1980	0.0001
9	0.1955	0.1962	0.1963	0.0001

Values of σ_i for $a = 2$, $b = 1$

TABLE 4

i	COMPUTED n = 16	COMPUTED n = 32	ANALYTIC	ERROR n = 32
1	0.7519	0.7948	0.7909	0.0039
2		0.5704	0.5695	0.0009
3	0.4123	0.4200	0.4242	0.0042
4		0.3537	0.3553	0.0016
5	0.3098	0.3161	0.3171	0.0010
6		0.2936	0.2941	0.0005
7	0.2761	0.2799	0.2803	0.0004
8		0.2725	0.2729	0.0004
9	0.2666	0.2703	0.2705	0.0002

Values of σ_i for $a = 2$, $b = 0.684$

TABLE 5

i	COMPUTED $n = 16$	COMPUTED $n = 32$	ANALYTIC	ERROR $n = 32$
1	1.8729	2.4480	2.8621	0.4141
2		0.9650	1.0800	0.1150
3	0.6047	0.7365	0.7709	0.0344
4		0.6217	0.6457	0.0240
5	0.5137	0.5591	0.5783	0.0192
6		0.5222	0.5382	0.0170
7	0.4581	0.4984	0.5141	0.0157
8		0.4859	0.5011	0.0152
9	0.4441	0.4820	0.4970	0.0150

Values for σ_i for $a = 2$, $b = 0.347$

TABLE 6

x	ϕ by (3.4)	ϕ by (3.5)
0.0	1.0003	1.0002
1.0	1.0002	1.0003
1.5	1.0002	1.0003
1.75	0.9996	1.0001
1.80	0.9987	0.9998
1.85	0.9964	0.9989
1.90	0.9900	0.9964
1.95	0.9707	0.9870

Values of $\phi_i(\underline{P})$ generated by (3.7) for $a = 2$, $b = \sqrt{3}$.

TABLE 7

x	ϕ by (3.4)	ϕ by (3.5)
0.0	1.0004	1.0003
1.0	1.0003	1.0003
1.5	1.0001	1.0003
1.75	0.9995	1.0002
1.80	0.9987	1.0000
1.85	0.9962	0.9991
1.90	0.9888	0.9963
1.95	0.9649	0.9849

Values of $\phi_i(\underline{P})$ generated by (3.7) for $a = 2$, $b = \sqrt{2}$.

TABLE 8

x	ϕ by (3.4)	ϕ by (3.5)
0.0	1.0011	1.0003
1.0	1.0008	1.0003
1.5	0.9999	1.0003
1.75	0.9991	1.0006
1.80	0.9983	1.0006
1.85	0.9956	0.9999
1.90	0.9858	0.9966
1.95	0.9492	0.9802

Values of $\phi_i(\underline{P})$ generated by (3.7) for $a = 2$, $b = 1$.

TABLE 9

x	ϕ by (3.4)	ϕ by (3.5)
0.0	1.0030	1.0004
1.0	1.0026	1.0002
1.5	1.0008	0.9997
1.75	0.9977	0.9996
1.80	0.9968	0.9997
1.85	0.9936	0.9991
1.90	0.9782	0.9941
1.95	0.9120	0.9659

Values of $\phi_i(\underline{P})$ generated by (3.7) for $a = 2$, $b = 0.684$

TABLE 10

x	ϕ by (3.4)	ϕ by (3.5)
0.0	1.0161	1.0006
1.0	1.0193	1.0004
1.5	1.0231	0.9979
1.75	1.0123	0.9840
1.80	1.0124	0.9786
1.85	1.0189	0.9735
1.90	0.9850	0.9589
1.95	0.7788	0.8901

Values of $\phi_i(\underline{P})$ generated by (3.7) for $a = 2$, $b = 0.347$

TABLE 11

c	COMPUTED	ANALYTIC	ERROR
1	0.1471	0.1470	0.0001
2	0.1451	0.1450	0.0001
3	0.1416	0.1416	
4	0.1376	0.1376	
5	0.1339	0.1339	0.0000
6	0.1309	0.1309	
7	0.1288	0.1288	
8	0.1277	0.1277	

$a = 2$, $b = \sqrt{3}$

TABLE 12

c	COMPUTED	ANALYTIC	ERROR
1	0.2094	0.2090	0.0004
2	0.1992	0.1990	0.0002
3	0.1853	0.1852	0.0001
4	0.1725	0.1726	0.0001
5	0.1626	0.1627	0.0001
6	0.1556	0.1557	0.0001
7	0.1512	0.1512	0.0000
8	0.1490	0.1491	0.0001

$a = 2$, $b = \sqrt{2}$

TABLE 13

c	COMPUTED	ANALYTIC	ERROR
1	0.3827	0.3799	0.0028
2	0.3201	0.3205	0.0004
3	0.2708	0.2714	0.0006
4	0.2396	0.2400	0.0004
5	0.2199	0.2201	0.0002
6	0.2075	0.2076	0.0001
7	0.2004	0.2002	0.0002
8	0.1966	0.1967	0.0001

$a = 2, \quad b = 1$

TABLE 14

c	COMPUTED	ANALYTIC	ERROR
1	0.7134	0.6978	0.0156
2	0.4758	0.4819	0.0061
3	0.3823	0.3842	0.0019
4	0.3327	0.3336	0.0009
5	0.3038	0.3042	0.0004
6	0.2860	0.2863	0.0003
7	0.2760	0.2759	0.0001
8	0.2709	0.2710	0.0001

$a = 2, \quad b = 0.684$

TABLE 15

i	COMPUTED	ANALYTIC	ERROR
1	1.8139	1.5334	0.2805
2	0.8437	0.8833	0.0396
3	0.7083	0.6975	0.0108
4	0.6174	0.6074	0.0100
5	0.5657	0.5558	0.0099
6	0.5342	0.5246	0.0096
7	0.5158	0.5064	0.0094
8	0.5073	0.4980	0.0093

$a = 2, \quad b = 0.347$

TABLE 16

x	ϕ
0.0	1.0002
1.0	1.0003
1.5	1.0003
1.75	1.0004
1.80	1.0007
1.85	1.0014
1.90	1.0026
1.95	1.0031

$a = 2, \quad b = \sqrt{3}$

TABLE 17

x	ϕ
0.0	1.0003
1.0	1.0003
1.5	1.0003
1.75	1.0005
1.80	1.0007
1.85	1.0015
1.90	1.0031
1.95	1.0044

$a = 2, \quad b = \sqrt{2}$

TABLE 18

x	ϕ
0.0	1.0003
1.0	1.0003
1.5	1.0003
1.75	1.0006
1.80	1.0009
1.85	1.0020
1.90	1.0049
1.95	1.0091

$a = 2, \quad b = 1$

TABLE 19

x	ϕ
0.0	1.0004
1.0	1.0002
1.5	0.9997
1.75	0.9997
1.80	1.0001
1.85	1.0017
1.90	1.0080
1.95	1.0217

$a = 2, \quad b = 0.684$

TABLE 20

x	ϕ
0.0	1.0007
1.0	1.0005
1.5	0.9970
1.75	0.9805
1.80	0.9766
1.85	0.9760
1.90	1.0104
1.95	1.1345

$a = 2, \quad b = 0.347$

TABLE 21

i	COMPUTED	ANALYTIC	ERROR
1	0.3861	0.3870	0.0009
2	0.3504	0.3507	0.0003
3	0.3042	0.3041	0.0001
4	0.2645	0.2642	0.0003
5	0.2352	0.2349	0.0003
6	0.2153	0.2150	0.0003
7	0.2031	0.2028	0.0003
8	0.1973	0.1970	0.0003

Values of σ_i for $a = 2, \quad b = 1$

TABLE 22

c	COMPUTED	ANALYTIC	ERROR
1	0.2198	0.2213	0.0015
2	0.1772	0.1775	0.0003
3	0.1378	0.1378	0.0000
4	0.1119	0.1118	0.0001
5	0.0956	0.0956	0.0000
6	0.0856	0.0854	0.0002
7	0.0797	0.0796	0.0001
8	0.0770	0.0769	0.0003

Values of σ_i for $a = 3,\ b = 1$

TABLE 23

c	COMPUTED	ANALYTIC	ERROR
1	0.1606	0.1624	0.0018
2	0.1152	0.1154	0.0002
3	0.0835	0.0834	0.0001
4	0.0655	0.0655	0.0000
5	0.0551	0.0550	0.0001
6	0.0489	0.0488	0.0001
7	0.0453	0.0453	0.0000
8	0.0437	0.0436	0.0001

Values of σ_i for $a = 4,\ b = 1$

TABLE 24

c	COMPUTED	ANALYTIC	ERROR
1	0.1286	0.1306	0.0020
2	0.0832	0.0833	0.0001
3	0.0576	0.0576	0.0000
4	0.0444	0.0444	0.0000
5	0.0370	0.0370	0.0000
6	0.0327	0.0327	0.0000
7	0.0303	0.0302	0.0001
8	0.0291	0.0291	0.0000

Values of σ_i for $a = 5,\ b = 1$

TABLE 25

c	COMPUTED	ANALYTIC	ERROR
1	0.1079	0.1099	0.0020
2	0.0638	0.0639	0.0001
3	0.0429	0.0429	0.0000
4	0.0327	0.0327	0.0000
5	0.0272	0.0271	0.0001
6	0.0239	0.0239	0.0000
7	0.0221	0.0221	0.0000
8	0.0213	0.0213	0.0000

Values of σ_i for $a=6$, $b = 1$

TABLE 26

c	COMPUTED	ANALYTIC	ERROR
1	0.0931	0.0950	0.0019
2	0.0510	0.0511	0.0001
3	0.0336	0.0336	0.0000
4	0.0255	0.0255	0.0000
5	0.0211	0.0211	0.0000
6	0.0186	0.0185	0.0001
7	0.0171	0.0171	0.0000
8	0.0165	0.0165	0.0000

Values of σ_i for $a = 7$, $b = 1$

TABLE 27

c	COMPUTED	ANALYTIC	ERROR
1	0.0818	0.0835	0.0017
2	0.0420	0.0421	0.0001
3	0.0273	0.0273	0.0000
4	0.0206	0.0206	0.0000
5	0.0170	0.0170	0.0000
6	0.0150	0.0150	0.0000
7	0.0138	0.0138	0.0000
8	0.0133	0.0133	0.0000

Values of σ_i for $a = 8$, $b = 1$

TABLE 28

c	COMPUTED	ANALYTIC	ERROR
1	0.0728	0.0744	0.0016
2	0.0354	0.0355	0.0001
3	0.0228	0.0228	0.0000
4	0.0172	0.0172	0.0000
5	0.0142	0.0142	0.0000
6	0.0125	0.0124	0.0001
7	0.0115	0.0115	0.0000
8	0.0111	0.0110	0.0001

Values of σ_i for $a = 9$, $b = 1$

TABLE 29

c	COMPUTED	ANALYTIC	ERROR
1	0.0655	0.0668	0.0013
2	0.0304	0.0305	0.0001
3	0.0195	0.0195	0.0000
4	0.0146	0.0146	0.0000
5	0.0120	0.0120	0.0000
6	0.0106	0.0106	0.0000
7	0.0098	0.0098	0.0000
8	0.0094	0.0094	0.0000

Values of σ_i for $a = 10$, $b = 1$

TABLE 30

ϕ	2 : 1	3 : 1	4 : 1	5 : 1	6 : 1	7 : 1	8 : 1	9 : 1	10 : 1
1	1.00048	1.00030	1.00023	1.00022	1.00025	1.00030	1.00039	1.00049	1.00060
2	1.00045	1.00026	1.00020	1.00017	1.00013	1.00009	1.00005	0.99999	0.99994
3	1.00039	1.00020	1.00013	1.00009	1.00004	0.99999	0.99993	0.99987	0.99982
4	1.00034	1.00012	1.00005	1.00000	0.99994	0.99986	0.99976	0.99964	0.99951
5	1.00034	1.00010	1.00002	1.00001	1.00001	1.00002	1.00003	1.00004	1.00004
6	1.00040	1.00008	0.99997	0.99992	0.99993	0.99999	1.00009	1.00021	1.00035
7	1.00099	1.00006	0.99994	0.99986	0.99998	0.99965	0.99953	0.99941	0.99929
8	1.00376	1.00089	1.00001	0.99973	0.99968	0.99972	0.99979	0.99987	0.99995
ANALYTICAL s	2.4663	1.4427	1.0914	0.9102	0.7982	0.7213	0.6649	0.6213	0.5866
COMPUTED S	2.4673	1.4430	1.0915	0.9103	0.7983	0.7213	0.6648	0.6213	0.5866
ERROR |S-s|	0.0010	0.0003	0.0001	0.0001	0.0001	0.0000	0.0001	0.0000	0.0000

CHAPTER 4

NUMERICAL POTENTIAL THEORY: NEUMANN PROBLEM

Discretisation procedure

We now turn our attention to the Neumann problem and seek to find a function $\phi(\underline{P})$ harmonic within an ellipse B given that $\phi'(\underline{P}) = 0$ on ∂B. The 'capacity' s of the ellipse is also prescribed to ensure uniqueness. The relevant equation (2.9) becomes

$$\int_{\partial B} \ln' |\underline{P} - \underline{q}| \sigma(\underline{q}) \, dq + \pi \sigma(\underline{P}) = 0 \qquad (4.1)$$

which, formulated numerically with the same notation as (3.2), takes the form

$$\sum_{i=1}^{n} \sigma_i \int_i \ln |\underline{q} - \underline{q}_r|' \, dq + \pi \sigma_r = 0 ; \qquad r = 1, 2, \ldots, n. \qquad (4.2)$$

To compute $\int_i \ln |\underline{q} - \underline{q}_r|' dq$ we use

$$\int_i \ln |\underline{q} - \underline{q}_r|' dq = 2h_i \ln |\underline{q}_i - \underline{q}_r|' \quad \text{if} \quad i \neq r \qquad (4.3)$$

where

$$\ln |\underline{q}_i - \underline{q}_r|' = \frac{[(x_r - x_i) x_r' + (y_r - y_i) y_r']}{|\underline{q}_i - \underline{q}_r|^2}, \qquad (4.4)$$

where $x_r = x(\underline{q}_r)$, $y_r = y(\underline{q}_r)$ and a dash denotes differentiation along the inward normal. For $i = r$ we use

$$\int_r \ln |\underline{q} - \underline{q}_r|' dq = -\pi - \sum_{\substack{i=1 \\ i \neq r}}^{n} \int_i \ln' |\underline{q} - \underline{q}_r| \, dq \qquad (4.5)$$

which is justified for interior problems by (2.5), and is computed from

$$\int_i \ln' |\underline{q} - \underline{q}_r| \, dq = 2h_i \frac{[(x_i - x_r) x_i' + (y_i - y_r) y_i']}{|\underline{q}_i - \underline{q}_r|^2} . \qquad (4.6)$$

We have now ensured that (4.2) is characterized by a singular matrix. The n equations of (4.2) in n unknowns have a relation of linear dependence so we can ignore one

equation of the homogeneous set, say the n^{th}, and solve for the ratios $\sigma_i^* = (\sigma_i/\sigma_n)$, $i = 1,2,\ldots,n-1$. Thus a set of equations of the form

$$\sum_{m=1}^{n} a_{rm}\sigma_m = 0, \qquad r = 1,2,\ldots,n, \tag{4.7}$$

is replaced by

$$\sum_{m=1}^{n-1} a_{rm}\sigma_m^* = -a_{rn} \qquad r = 1,2,\ldots,n-1. \tag{4.8}$$

The ratios $\sigma_1^* : \sigma_2^* : \ldots : \sigma_{n-1}^* : 1$

equal $\sigma_1 : \sigma_2 : \ldots : \sigma_{n-1} : \sigma_n$

and the values of σ_i can be found from

$$\left.\begin{aligned} \sigma_i &= \frac{\sigma_i^*}{Z}; \qquad i = 1,2,\ldots,n, \\ \sigma_n^* &= 1, \end{aligned}\right\} \tag{4.9}$$

where

$$sZ = \sum_{i=1}^{n} 2h_i\sigma_i^*. \tag{4.10}$$

The required values of σ and the generated potential ϕ are obtained from a single computer program using as input data nodal points again defined as in figure 2, p.35 using equal eccentric angles. The interval lengths are computed from the expression

$$2h_i = |\underline{q}_{i+\frac{1}{2}} - \underline{q}_i| + |\underline{q}_i - \underline{q}_{i-\frac{1}{2}}| \tag{4.11}$$

which replaces the arc by two chords and produces more accurate results than the more crude approximation

$$2h_i = |\underline{q}_{i+\frac{1}{2}} - \underline{q}_{i-\frac{1}{2}}|. \tag{4.12}$$

This remark applies equally to the foregoing Dirichlet problem and to the biharmonic problems tackled later.

Comparison with Dirichlet problem

In contrast with the corresponding Dirichlet problem, the system of equations for σ can be solved by the

Gauss-Seidel method, the derivative of the logarithm providing a more highly singular kernel. Good convergence was obtained when the problem was solved for $n = 32$ using this method; iterations were continued until values of σ improved by less than $\varepsilon = 0.00001$. No further improvement was obtained when the program was lengthened by taking $\varepsilon = 0.000001$. The equations were also solved using the matrix inversion subroutine employed previously and the results for σ differed only trivially in the fifth decimal place from those displayed in tables 31 - 39 obtained by the Gauss-Seidel method. Table 40 shows ϕ generated along the major axis. The results shown are for the axial ratios $a : b$ with $b = 1$; $a = 2,3,4,\ldots,10$, but the irrational axial ratios considered earlier, and the effects of changes of scale were also investigated. Generally the errors in σ are of the order of ten times less than for the corresponding Dirichlet problem, as is to be expected since we are now solving a Fredholm equation of the second kind. A notable feature is that the results of both Dirichlet and Neumann problems do not deteriorate as the axial ratio increases provided that equal eccentric angles are used to define nodal points. Instead of being equally spaced the latter are automatically more densely accumulated where they are needed, i.e. near the sharpening vertices at the ends of the major axes. The author believes these results to be more accurate than any previously obtained and that the numerical techniques developed in these harmonic problems provide a platform from which numerical biharmonic analysis can be confidently attacked.

Results

TABLE 31

i	COMPUTED	ANALYTIC	ERROR
1	0.38703	0.38699	0.00004
2	0.35073	0.35069	0.00004
3	0.30408	0.30405	0.00003
4	0.26422	0.26420	0.00002
5	0.23491	0.23489	0.00002
6	0.21501	0.21499	0.00002
7	0.20279	0.20277	0.00002
8	0.19699	0.19697	0.00002

Values of σ_i for $a = 2$, $b = 1$

TABLE 32

i	COMPUTED	ANALYTIC	ERROR
1	0.22118	0.22127	0.00009
2	0.17739	0.17746	0.00007
3	0.13771	0.13777	0.00006
4	0.11173	0.11178	0.00005
5	0.09546	0.09550	0.00004
6	0.08540	0.08544	0.00004
7	0.07954	0.07958	0.00004
8	0.07683	0.07687	0.00004

Values of σ_i for $a = 3$, $b = 1$

TABLE 33

i	COMPUTED	ANALYTIC	ERROR
1	0.16224	0.16239	0.00015
2	0.11533	0.11544	0.00011
3	0.08336	0.08344	0.00008
4	0.06542	0.06548	0.00006
5	0.05498	0.05503	0.00005
6	0.04876	0.04880	0.00004
7	0.04520	0.04525	0.00005
8	0.04358	0.04362	0.00004

Values of σ_i for $a = 4$, $b = 1$

TABLE 34

i	COMPUTED	ANALYTIC	ERROR
1	0.13041	0.13059	0.00018
2	0.08321	0.08333	0.00012
3	0.05748	0.05757	0.00009
4	0.04431	0.04437	0.00006
5	0.03693	0.03699	0.00006
6	0.03262	0.03267	0.00005
7	0.03018	0.03022	0.00004
8	0.02907	0.02911	0.00004

Values of σ_i for $a = 5$, $b = 1$

TABLE 35

i	COMPUTED	ANALYTIC	ERROR
1	0.10970	0.10990	0.00020
2	0.06381	0.06393	0.00012
3	0.04280	0.04288	0.00008
4	0.03265	0.03271	0.00006
5	0.02709	0.02714	0.00005
6	0.02387	0.02391	0.00004
7	0.02206	0.02210	0.00004
8	0.02123	0.02127	0.00004

Values of σ_i for $a = 6$, $b = 1$

TABLE 36

i	COMPUTED	ANALYTIC	ERROR
1	0.09477	0.09498	0.00021
2	0.05100	0.05111	0.00011
3	0.03354	0.03361	0.00007
4	0.02541	0.02547	0.00006
5	0.02102	0.02107	0.00005
6	0.01850	0.01854	0.00004
7	0.01708	0.01712	0.00004
8	0.01644	0.01648	0.00004

Values of σ_i for $a = 7$, $b = 1$

TABLE 37

i	COMPUTED	ANALYTIC	ERROR
1	0.08331	0.08352	0.00021
2	0.04202	0.04213	0.00011
3	0.02725	0.02732	0.00007
4	0.02056	0.02061	0.00005
5	0.01698	0.01702	0.00004
6	0.01493	0.01496	0.00003
7	0.01378	0.01381	0.00003
8	0.01326	0.01329	0.00003

Values of σ_i for $a = 8$, $b = 1$

TABLE 38

i	COMPUTED	ANALYTIC	ERROR
1	0.07417	0.07436	0.00019
2	0.03545	0.03554	0.00009
3	0.02276	0.02282	0.00006
4	0.01712	0.01716	0.00004
5	0.01412	0.01416	0.00004
6	0.01240	0.01244	0.00004
7	0.01144	0.01148	0.00004
8	0.01101	0.01104	0.00003

Values of σ_i for $a = 9$, $b = 1$

TABLE 39

i	COMPUTED	ANALYTIC	ERROR
1	0.06666	0.06684	0.00018
2	0.03046	0.03054	0.00008
3	0.01941	0.01947	0.00006
4	0.01457	0.01461	0.00004
5	0.01200	0.01204	0.00004
6	0.01054	0.01057	0.00003
7	0.00972	0.00975	0.00003
8	0.00935	0.00938	0.00003

Values of σ_i for $a = 10$, $b = 1$

TABLE 40

ζ	a = 2	a = 3	a = 4	a = 5	a = 6
1	1.0007	1.0010	1.0012	1.0014	1.0015
2	1.0003	1.0006	1.0008	1.0009	1.0010
3	0.9997	0.9999	1.0000	1.0001	1.0002
4	0.9991	0.9992	0.9992	0.9993	0.9993
5	0.9990	0.9990	0.9990	0.9991	0.9991
6	0.9990	0.9988	0.9987	0.9987	0.9987
7	0.9994	0.9985	0.9984	0.9983	0.9982
8	1.0020	0.9991	0.9981	0.9977	0.9976

ζ	a = 7	a = 8	a = 9	a = 10
1	1.0017	1.0018	1.0019	1.0020
2	1.0010	1.0010	1.0010	1.0009
3	1.0002	1.0002	1.0002	1.0001
4	0.9993	0.9992	0.9991	0.9990
5	0.9992	0.9992	0.9993	0.9993
6	0.9988	0.9990	0.9991	0.9993
7	0.9981	0.9980	0.9979	0.9979
8	0.9976	0.9977	0.9978	0.9980

b = 1 throughout.

Values of $\phi_i(\underline{P})$ generated on the major axis at $x = 0, \frac{a}{2}, (1.5)\frac{a}{2}, (1.75)\frac{a}{2}, (1.80)\frac{a}{2}, (1.85)\frac{a}{2}, (1.90)\frac{a}{2}, (1.95)\frac{a}{2}$.

CHAPTER 5

BIHARMONIC BOUNDARY VALUE PROBLEMS

Introduction

There are two areas of classical elasticity in which the biharmonic equation

$$\nabla^2(\nabla^2\chi) \equiv \nabla^4\chi = 0 \tag{5.1}$$

plays a fundamental role:

(i) plane strain or generalized plane stress conditions where (5.1) is satisfied by the Airy stress function χ.

(ii) the theory of thin elastic plates in which (5.1) is satisfied by the complementary function of the deflection ω.

An analytic and numerical study of case (i) for certain exterior problems of plane strain will be undertaken in part II of this thesis and applied in the elasto-plastic analysis of part III. The investigation of the Garabedian problem, which is the main aim of part I, falls within case (ii). Here we have an interior problem where the boundary ∂B is the ellipse (3.9). The previous analysis of harmonic boundary value problems enables us to solve biharmonic problems by representing the required function in terms of two harmonic functions and applying appropriate boundary conditions.

It is known (Hadamard, 1908) that a function χ which is continuous, and has continuous derivatives up to the fourth order throughout a finite domain B, and which satisfies the biharmonic equation (5.1) in B, exists and is uniquely defined in B if χ and χ' have prescribed continuous values on ∂B. We shall be concerned with the problem of actually constructing χ within B subject to these boundary conditions.

Representation of biharmonic functions

An arbitrary biharmonic function χ may be written in the form

$$\chi = x\phi + \psi \tag{5.2}$$

where ϕ, ψ are harmonic functions of the Cartesian coordinate variables x, y. First we note that the right hand side of (5.2) is certainly a biharmonic function since

$$\nabla^2 \chi = 2\frac{\partial \phi}{\partial x},$$

$$\nabla^2(\nabla^2 \chi) = 2\nabla^2 \frac{\partial \phi}{\partial x} = 2\frac{\partial}{\partial x}\nabla^2 \phi = 0.$$

Reversing these steps (Appendix 4), we can prove the validity of (5.2). Similarly we can write

$$\chi = y\phi + \psi. \tag{5.3}$$

A disadvantage of (5.2) and (5.3) is that ϕ and ψ are not unique for a given χ. For any given ϕ and ψ in (5.2), for example, we may replace ϕ by $\phi + a + by$ and ψ by $\psi - ax - bxy$, where a and b are constants, without altering χ.

A superior alternative to (5.2) and (5.3) is

$$\chi = r^2\phi + \psi \tag{5.4}$$

which is valid since

$$\nabla^2 \chi = 4\left(\phi + x\frac{\partial \phi}{\partial x} + y\frac{\partial \phi}{\partial y}\right) \tag{5.5}$$

is harmonic. The representation (5.4) <u>is</u> unique for if ϕ is replaced by $\phi + h$ where h is harmonic, ψ must be replaced by $\psi - r^2 h$. This requires

$$4\left(h + x\frac{\partial h}{\partial x} + y\frac{\partial h}{\partial y}\right) = 0 \tag{5.6}$$

and if $h = S_n$, a plane harmonic function of degree n, Euler's theorem on homogeneity then demands

$$(n+1)S_n = 0 \tag{5.7}$$

i.e.

$$n = -1, \quad h = \frac{\cos\theta}{r} \text{ or } \frac{\sin\theta}{r}$$

and this is impossible for an interior domain (containing the origin $r = 0$). The formulation would also be invalid in an exterior region in the context of logarithmic potential behaviour at infinity, since $r^2 h$ would be $O(r)$.

If χ, χ' are given on ∂B, then the boundary values of ϕ, ψ and their boundary normal derivatives ϕ', ψ' satisfy

$$\chi(\underline{p}) = r^2\phi(\underline{p}) + \psi(\underline{p}), \tag{5.8}$$

$$\chi'(\underline{p}) = 2rr'\phi(\underline{p}) + r^2\phi'(\underline{p}) + \psi'(\underline{p}). \tag{5.9}$$

These form two functional relations between four unknowns ϕ , ψ , ϕ' , ψ' . Nevertheless ϕ , ϕ' are coupled by Green's boundary formula

$$\int_{\partial B} \ln|\underline{p}-\underline{q}|\,\phi'(\underline{q})\,dq - \int_{\partial B} \ln|\underline{p}-\underline{q}|'\,\phi(\underline{q})\,dq = 0,$$

and similarly for ψ , ψ' . This shows that ϕ , ψ may in principle be determined from (5.8) and (5.9). We now show how they may be computed in practice.

Utilisation of simple-layer potentials

To make further progress we identify ϕ and ψ of (5.4) as logarithmic potentials generated by simple source distributions on ∂B with densities $\sigma(\underline{q})$, $\mu(\underline{q})$ to be determined. Thus we write

$$\phi(\underline{P}) = \int_{\partial B} \ln|\underline{P}-\underline{q}|\,\sigma(\underline{q})\,dq, \tag{5.10}$$

$$\psi(\underline{P}) = \int_{\partial B} \ln|\underline{P}-\underline{q}|\,\mu(\underline{q})\,dq. \tag{5.11}$$

These potentials remain continuous as $\underline{P}$ approaches any point $\underline{p}$ of ∂B and so on ∂B we have

$$\phi(\underline{p}) = \int_{\partial B} \ln|\underline{p}-\underline{q}|\,\sigma(\underline{q})\,dq, \tag{5.12}$$

$$\psi(\underline{p}) = \int_{\partial B} \ln|\underline{p}-\underline{q}|\,\mu(\underline{q})\,dq. \tag{5.13}$$

It is a known result (Kellogg, 1929) that

$$\phi'(\underline{p}) = \int_{\partial B} \ln'|\underline{p}-\underline{q}|\,\sigma(\underline{q})\,dq + \pi\sigma(\underline{p}), \tag{5.14}$$

$$\psi'(\underline{p}) = \int_{\partial B} \ln'|\underline{p}-\underline{q}|\,\mu(\underline{q})\,dq + \pi\mu(\underline{p}), \tag{5.15}$$

whence it follows that

$$\int_{\partial B} \phi'(\underline{P})\, dp = \int_{\partial B} \psi'(\underline{P})\, dp = 0 \qquad (5.16)$$

as expected.

Substitution from (5.12) to (5.15) into (5.8) and (5.9) gives

$$r^2 \int_{\partial B} \ln|\underline{P}-\underline{q}|\, \sigma(\underline{q})\, dq + \int_{\partial B} \ln|\underline{P}-\underline{q}|\, \mu(\underline{q})\, dq = \chi(\underline{P}), \qquad (5.17)$$

$$2rr' \int_{\partial B} \ln|\underline{P}-\underline{q}|\, \sigma(\underline{q})\, dq + r^2 \int_{\partial B} \ln'|\underline{P}-\underline{q}|\, \sigma(\underline{q})\, dq + r^2 \pi \sigma(\underline{P})$$

$$+ \int_{\partial B} \ln'|\underline{P}-\underline{q}|\, \mu(\underline{q})\, dq + \pi \mu(\underline{P}) = \chi'(\underline{P}). \qquad (5.18)$$

Equations (5.17) and (5.18) form a pair of coupled linear integral equations which exhibits a unique solution for the densities σ and μ. With these known, the harmonic functions ϕ and ψ, and hence also χ, can be generated at any point $\underline{P}$ of B using (5.10), (5.11) and (5.4).

To effect a numerical treatment of (5.17) and (5.18) we employ the assumptions, techniques and notation developed in chapters 3 & 4 so that the equations become

$$r^2 \sum_{i=1}^{n} \sigma_i \int_i \ln|\underline{P}-\underline{q}|\, dq + \sum_{i=1}^{n} \mu_i \int_i \ln|\underline{P}-\underline{q}|\, dq = -\chi(\underline{P}), \qquad (5.19)$$

$$\left.\begin{aligned} &2rr' \sum_{i=1}^{n} \sigma_i \int_i \ln|\underline{P}-\underline{q}|\, dq + r^2 \sum_{i=1}^{n} \sigma_i \int_i \ln'|\underline{P}-\underline{q}|\, dq + r^2 \pi \sigma(\underline{P}) \\ &+ \sum_{i=1}^{n} \mu_i \int_i \ln'|\underline{P}-\underline{q}|\, dq + \pi \mu(\underline{P}) = -\chi'(\underline{P}), \end{aligned}\right\} \qquad (5.20)$$

where subscripts on σ and μ refer to values at nodal points. These are defined on ∂B using equal eccentric angles and the integrals are computed using (3.5) and (3.6).

Trial Problem

As a basic trial problem we generate numerically $\chi = r^2$ in B from the boundary data $\chi = r^2$, $\chi' = 2rr'$ on ∂B and compare with its theoretically expected value. Since this problem only differs trivially from the actual

Garabedian problem i.e. the right hand sides of (5.19) and (5.20) will be different, it enables any errors of formulation, discretisation, or programming at once to be detected. If

$$\chi(\underline{P}) = \left[r(\underline{P})\right]^2 = r^2\phi(\underline{P}) + \Psi(\underline{P}) \; ; \qquad \underline{P} \in B, \quad (5.21)$$

clearly we have theoretically

$$\phi(\underline{P}) = 1, \qquad \Psi(\underline{P}) = 0 \; ; \qquad \underline{P} \in B \quad (5.22)$$

and σ and μ may be identified as solutions of

$$\int_{\partial B} \sigma(\underline{q}) \ln|\underline{P} - \underline{q}| \, dq = 1, \qquad \underline{P} \in \partial B, \quad (5.23)$$

$$\int_{\partial B} \mu(\underline{q}) \ln|\underline{P} - \underline{q}| \, dq = 0, \qquad \underline{P} \in \partial B. \quad (5.24)$$

Except on the Γ-contour (chapter 2), $\mu(\underline{q}) = 0$, and $\sigma(\underline{q})$ of (5.23) has been found numerically and analytically in chapter 3. It will be enlightening to compare these values of σ and μ with those obtained from (5.19) and (5.20). After the construction of $\phi(\underline{P})$ and $\Psi(\underline{P})$ from (5.10) and (5.11), equation (5.21) completes the biharmonic solution which may be compared with its analytic value $\chi = r^2$.

Our procedure again is successively to halve intervals and the final results shown in tables 41 to 50 are for $n = 32$. We considered ellipses with a range of axial ratios (a/b) on various scales. The tables show results obtained with $b = 1$; $a = 2, 3, 4, \ldots, 10$. In table 41, column (i) is the axial ratio, columns (ii) to (iv) are values of $\chi(\underline{P})$ generated along the major axis at the points $x = 0$, $x = (0.5)a$, $x = (0.975)a$ respectively; columns (v) and (vi) are the maximum and minimum values of the order of $|\mu(\underline{P})|$. In columns (ii), (v), and (vi) the analytic value is zero. In columns (iii) and (iv) the upper figures are the computed values, the middle figures the analytic values, and the lower figures are the errors. Tables 42 to 50 show numerical values of $\sigma(\underline{P})$ in comparison with the analytic values. As before

$$\sigma_1 = \sigma_{16} = \sigma_{17} = \sigma_{32},$$

$$\sigma_2 = \sigma_{15} = \sigma_{18} = \sigma_{31}, \qquad \text{etc.}$$

by symmetry. As might be expected, numerical results for biharmonic problems are not as accurate as in harmonic analysis. Nevertheless the generated χ, even very near the boundary (column (iv)), and the values of $\sigma(\underline{P})$ are all within 1% of their analytic values for the 2 : 1 ellipse; whilst $\mu = O(10^{-2})$ is a good numerical counterpart to the analytic solution $\mu = 0$. We may now confidently proceed to the Garabedian problem itself.

Thin Plate Theory.

The deflection w of a thin isotropic plate under a transverse load f per unit area satisfies the biharmonic equation

$$\nabla^4 w = \frac{f}{D} \qquad \text{in } B \tag{5.25}$$

where D is the flexural rigidity, i.e.

$$D = \frac{2h^3 E}{3(1-\nu^2)}$$

where E is Young's modulus, ν is Poisson's ratio, and $2h$ is the thickness. The boundary condition for a clamped plate is

$$w = w' = 0 \qquad \text{on } \partial B. \tag{5.26}$$

A single concentrated transverse load is represented mathematically by

$$f = k\delta(\underline{P}-\underline{S}) \tag{5.27}$$

where k is a constant and δ is Dirac's delta function. The vector $\underline{S}$ specifies the point of application of the load (source point) and the vector variable $\underline{P}$ specifies points in B (field points). The required deflection, therefore, is the biharmonic Green's function G which satisfies

$$\nabla^4 G = \frac{k}{D}\delta(\underline{P}-\underline{S}). \tag{5.28}$$

This equation admits a particular integral

$$g = \frac{k}{8\pi D} R^2 \ln R \tag{5.29}$$

where $R = |\underline{P}-\underline{S}|$. The textbooks (e.g. Love, 1952) provide formal proof of this, but give no general solution except in the special case of a circular domain.

Equation (5.29) is, in fact, the fundamental solution of (5.28) or, alternatively, the Green's function for an infinite domain. Since $R^2\phi$ is biharmonic if ϕ is harmonic we may regard $R^2 \ln R$ to be the biharmonic singularity corresponding to the harmonic singularity $\ln R$. It is clear that g and g' can be determined on ∂B for any $\underline{S}$. Thus to solve (5.28) subject to the boundary conditions

$$G = G' = 0 \qquad \text{on } \partial B, \tag{5.30}$$

we write

$$G = g + \chi \tag{5.31}$$

where

$$\nabla^4 \chi = 0 \qquad \text{in } B \tag{5.32}$$

subject to

$$\chi = -g, \quad \chi' = -g' \qquad \text{on } \partial B. \tag{5.33}$$

The biharmonic equation (5.32) may now be solved subject to the canonical boundary conditions (5.33) using the methods described in this chapter. Results and discussion are contained in chapter 6.

TABLE 41

(i)	(ii)	(iii)	(iv)	(v)	(vi)
$a/b (b = 1)$	$\chi(o)$	$\chi(\frac{a}{2})$	$\chi(\frac{a}{2}\ 1.95)$	Order max/μl	Order min/μl
2/1	- 0.0003	1.0004 1.0000 0.0004	3.8173 3.8025 0.0158	10^{-2}	10^{-4}
3/1	- 0.0002	2.2501 2.2500 0.0001	8.5649 8.5556 0.0093	10^{-2}	10^{-4}
4/1	- 0.0001	4.0003 4.0000 0.0003	15.2139 15.2100 0.0039	10^{-1}	10^{-4}
5/1	- 0.0001	6.2509 6.2500 0.0009	23.7659 23.7656 0.0003	10^{-1}	10^{-3}
6/1	- 0.0004	9.0020 9.0000 0.0020	34.2217 34.2225 0.0008	10^{-1}	10^{-3}
7/1	- 0.0010	12.2535 12.2500 0.0035	46.5814 46.5806 0.0008	10^{-1}	10^{-3}
8/1	- 0.0019	16.0050 16.0000 0.0050	60.8447 60.8400 0.0047	1	10^{-3}
9/1	- 0.0029	20.2560 20.2500 0.0060	77.0114 77.0006 0.0108	1	10^{-3}
10/1	- 0.0037	25.0060 25.0000 0.0060	95.0813 95.0625 0.0188	1	10^{-3}

TABLE 42

i	COMPUTED	ANALYTIC	ERROR
1	0.3905	0.3870	0.0035
2	0.3491	0.3507	0.0016
3	0.3026	0.3041	0.0015
4	0.2638	0.2642	0.0004
5	0.2350	0.2349	0.0001
6	0.2153	0.2150	0.0003
7	0.2031	0.2028	0.0003
8	0.1973	0.1970	0.0003

Values of σ_i for $a=2$, $b=1$

TABLE 43

i	COMPUTED	ANALYTIC	ERROR
1	0.2293	0.2213	0.0080
2	0.1703	0.1775	0.0072
3	0.1373	0.1378	0.0005
4	0.1115	0.1118	0.0003
5	0.0957	0.0955	0.0002
6	0.0855	0.0854	0.0001
7	0.0797	0.0796	0.0001
8	0.0770	0.0769	0.0001

Values of σ_i for $a=3$, $b=1$

TABLE 44

i	COMPUTED	ANALYTIC	ERROR
1	0.1743	0.1624	0.0119
2	0.1035	0.1154	0.0119
3	0.0854	0.0834	0.0020
4	0.0646	0.0655	0.0009
5	0.0557	0.0550	0.0007
6	0.0486	0.0488	0.0002
7	0.0455	0.0453	0.0002
8	0.0436	0.0436	0.0000

Values of σ_i for $a=4$, $b=1$

TABLE 45

c	COMPUTED	ANALYTIC	ERROR
1	0.1446	0.1306	0.0140
2	0.0693	0.0833	0.0140
3	0.0613	0.0576	0.0037
4	0.0426	0.0444	0.0018
5	0.0381	0.0370	0.0011
6	0.0320	0.0327	0.0007
7	0.0307	0.0302	0.0005
8	0.0290	0.0291	0.0001

Values of σ_i for $a = 5$, $b = 1$

TABLE 46

c	COMPUTED	ANALYTIC	ERROR
1	0.1244	0.1099	0.0145
2	0.0499	0.0639	0.0140
3	0.0473	0.0429	0.0044
4	0.0305	0.0327	0.0022
5	0.0286	0.0271	0.0015
6	0.0229	0.0239	0.0010
7	0.0229	0.0221	0.0008
8	0.0210	0.0213	0.0003

Values of σ_i for $a = 6$, $b = 1$

TABLE 47

c	COMPUTED	ANALYTIC	ERROR
1	0.1088	0.0950	0.0138
2	0.0384	0.0511	0.0127
3	0.0379	0.0336	0.0043
4	0.0232	0.0255	0.0023
5	0.0226	0.0211	0.0015
6	0.0174	0.0185	0.0011
7	0.0181	0.0171	0.0010
8	0.0160	0.0165	0.0005

Values of σ_i for $a = 7$, $b = 1$

TABLE 48

C	COMPUTED	ANALYTIC	ERROR
1	0.0959	0.0835	0.0124
2	0.0313	0.0421	0.0108
3	0.0311	0.0273	0.0038
4	0.0185	0.0206	0.0021
5	0.0185	0.0170	0.0015
6	0.0139	0.0150	0.0011
7	0.0148	0.0138	0.0010
8	0.0128	0.0133	0.0005

Values of σ_i for $a = 8$, $b = 1$

TABLE 49

C	COMPUTED	ANALYTIC	ERROR
1	0.0850	0.0744	0.0106
2	0.0267	0.0355	0.0088
3	0.0258	0.0228	0.0030
4	0.0154	0.0172	0.0018
5	0.0154	0.0142	0.0012
6	0.0115	0.0124	0.0009
7	0.0124	0.0115	0.0009
8	0.0106	0.0110	0.0004

Values of σ_i for $a = 9$, $b = 1$

TABLE 50

C	COMPUTED	ANALYTIC	ERROR
1	0.0758	0.0668	0.0090
2	0.0235	0.0305	0.0070
3	0.0218	0.0195	0.0022
4	0.0132	0.0146	0.0014
5	0.0130	0.0120	0.0010
6	0.0098	0.0106	0.0008
7	0.0105	0.0098	0.0007
8	0.0090	0.0094	0.0004

Values of σ_i for $a = 10$, $b = 1$

CHAPTER 6

STUDY OF THE GARABEDIAN PROBLEM

Introduction

In chapter I we gave an account of the Garabedian problem. This concerns the deflection of a thin clamped elastic plate under concentrated transverse loading. Translated into mathematical terms the problem is that of determining a biharmonic Green's function G throughout the domain B of the plate subject to the appropriate conditions on the boundary ∂B. Hadamard (1908) conjectured that G has the same sign throughout B, i.e. the deflection has everywhere the same direction as the applied load. Garabedian (1951) demonstrated that the conjecture fails if B is an ellipse of axial ratio 5/3 if the load is located sufficiently near an extremity.

It has been established that the transverse deflection of a thin clamped elliptic plate can be computed numerically using boundary integral equations. On the basis of the formulation and numerical analysis described earlier, the author has written a computer program which yields the deflection $G(\underline{P}, \underline{S})$ for any location of the source point $\underline{S}$ and of the field point $\underline{P}$ within the ellipse.

We recall that the required deflection is the solution of the equation

$$\nabla^4 G = \frac{k}{D} \delta(\underline{P}-\underline{S}) \qquad (6.1)$$

subject to the boundary condition

$$G = G' = 0 \qquad (6.2)$$

on the boundary ∂B given by

$$\frac{x^2}{a^2} + \frac{y^2}{b^2} = 1. \qquad (6.3)$$

Choice of ellipses

Results have been obtained for several ellipses on various scales, and we select for discussion in this thesis the following axial ratios:-

$$2/2, \quad 2/\sqrt{3}, \quad 2/\sqrt{2}, \quad 2/1 \quad 2/\tfrac{2}{3}, \quad 2/\tfrac{2}{5}.$$

Our choice was motivated by the following four considerations:

(i) The circle (2/2) should obviously be included since this is the only "ellipse" for which an exact analytical solution is available. This provides a valuable check on accuracy.

(ii) The $2/\sqrt{3}$, $2/\sqrt{2}$, 2/1 ellipses were considered by E. Jaswon (1969), and comparison with his earlier numerical work is possible if these axial ratios are included.

(iii) It seems advantageous to extend the analysis to ellipses of higher axial ratios than any previously considered. Thus we include $2/\frac{2}{3} = 3/1$ and $2/\frac{2}{5} = 5/1$.

(iv) Garabedian considered the axial ratio 2/1.2. We believe that, in the neighbourhood of this value, there exists a critical axial ratio from the point of view of the failure of Hadamard's conjecture. Accordingly we consider three axial ratios which are greater and three which are less than the one considered by Garabedian.

To facilitate comparisons we take $a = 2$ throughout. This also ensures that the Γ-contour (Appendix 1) is avoided for all $b > 0$.

In each ellipse, source points $\underline{S}$ were taken successively at

$x = 0,\ 1.0,\ 1.5,\ 1.75,\ 1.80,\ 1.85,\ 1.90,\ 1.95$

and the deflection $G(\underline{P}, \underline{S})$ was generated at field points along the major axis separated by intervals of 0.125. Additional field points $\underline{P}$ were inserted near the vertices at

$x = \pm 1.80, \quad \pm 1.85, \quad \pm 1.90, \quad \pm 1.95$

so that close attention could be paid to the generated deflection and its normal derivative near the boundary. From these results the profiles were drawn after critical examination. Abbreviated results are shown in tables 52 - 57.

Assessment of Accuracy

Careful scrutiny of the results is important since Hadamard's conjecture is disproved by very small negative deflections. These are $O(10^{-3})$ in units of $ka/32\pi D$. It is interesting to note that in Garabedian's example the result depended on the sign of a certain infinite sum. This also proved to be $O(10^{-3})$. To ensure the reliability

of our conclusions, we must distinguish between deflections that are inherently negative and those that are in fact small and positive but are made negative by numerical inaccuracies. As a check on the validity of our numerical solutions we adopted the following procedures:-

(1) The number of nodal points was successively increased, i.e. n = 4, 8, 16, 32, so enabling numerical conditioning to be examined. It was found that deflections steadily approached their values shown in the tables, which refer to n = 32.

(2) The biharmonic trial function r^2 was generated numerically throughout B and compared with its theoretically expected value (chapter 5). Reliable results were obtained in this trial problem which differs only trivially from the Garabedian problem. Errors of formulation, discretisation or programming are thus detected and eliminated.

(3) An exact analytical solution is available for the circle against which our numerical solution can be tested. Reference to table 52 shows that the latter provides a reliable picture of the deflection profile.

(4) The theoretically expected symmetry property $G(\underline{P},\underline{S}) = G(\underline{S},\underline{P})$ is fulfilled to an excellent degree of accuracy by the numerical solutions. Furthermore, by virtue of the symmetry of the problem with respect to the minor axis $G(\underline{P},\underline{S}) = G(-\underline{P},-\underline{S})$ i.e. $G(\underline{P},\underline{S}) = G(-\underline{S},-\underline{P})$, so providing an additional check on accuracy. Examples are indicated in the tables by underlining quantities which are theoretically equal.

(5) The generated profile must approximate towards $G = G' = 0$ as the boundary $x = \pm 2.00$ is approached.

Procedures (1) and (2) have been discussed earlier. Concerning (3) it suffices to quote the classical formula which yields the results shown in table 52. From Timoshenko and Woinowsky-Krieger (1959) we obtain an expression which reduces to

$$G(\underline{P},\underline{S}) = G(\underline{S},\underline{P}) = \frac{k}{16\pi D}\left|\frac{(a^2-r^2)(a^2-x^2)}{a^2} + (r-x)^2 \ln\frac{a^2(r-x)^2}{(a^2-rx)^2}\right|, \qquad (6.4)$$

where r and x are the Cartesian coordinates of $\underline{P}$, $\underline{S}$ respectively. In the preparation of the graphs and tables,

procedures (4) and (5) were used extensively. We did not accept the validity of a negative deflection $G(\underline{P}, \underline{S})$ unless $G(\underline{S}, \underline{P})$ was also negative. When only one of $G(\underline{P}, \underline{S})$, $G(\underline{S}, \underline{P})$ was negative, the symbol (-) is attached to that negative value to indicate that zero would be a more reliable result. Unreliable results only occur for field points very near the boundary. In such cases it was sometimes obvious that a better result could be obtained from interpolation using the boundary value $G = 0$. An asterisk in the tables indicates where this improvement has been made. The symbol - 0.000 denotes a value between zero and - 0.0005. Negative values were rejected according to procedure (5) if they did not return towards zero as $\underline{P} \rightarrow (\pm 2.0, 0)$. For example,

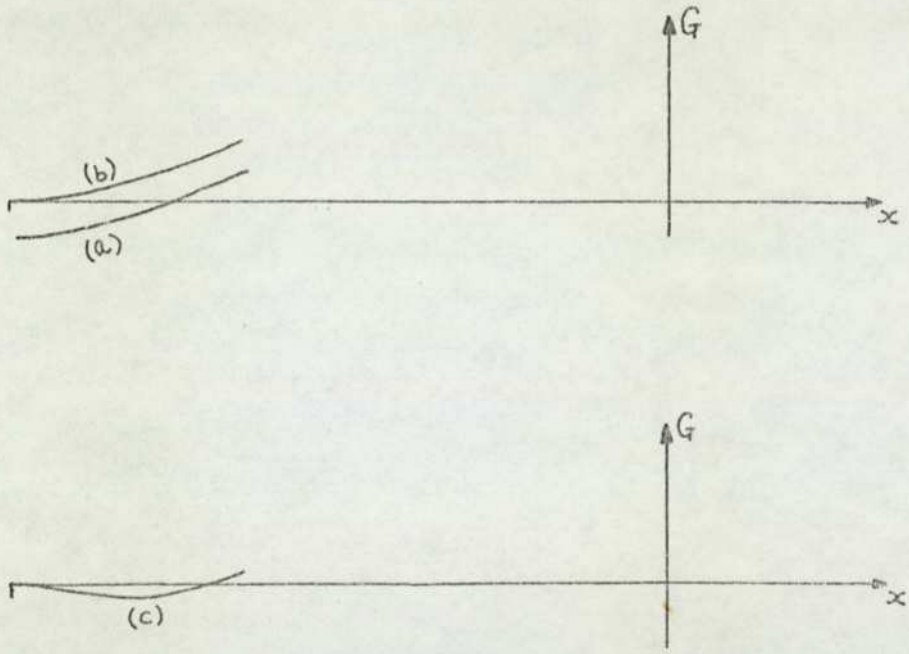


FIG. 3

the negative values in the profile (a) of figure 3 may be regarded as only numerical approximations for those of the true profile (b); whereas profile (c) suggests negative values should be accepted. This suggestion becomes a confident assertion if verified by the reciprocity relationship of (4). To illustrate behaviour of type (c) above, we include table 58 which gives extra decimal places and extra field points for the 2/1 ellipse.

When spurious results had been discarded on the basis

of the above considerations, the values of G were fed into a computer program which produced the profile as output on a graph plotter. An approximation based on cubic splines was used to draw the profile, and the program automatically constrained G and G' to take their assigned values on the boundary, i.e. $G = G' = 0$. This constraint assisted further in minimizing the effect of inaccurate data near the boundaries. Graph plotting by hand was also carried out as a check and showed that, in some cases, notably near the maxima of G, the cubic approximation was inadequate. Some manual overwriting was necessary; the profiles are shown in figures 4 to 27 for $\underline{S}$ given by

$$y = 0.00; \quad x = 0.00, \quad 1.00, \quad 1.75, \quad 1.90.$$

Exhibition of Results

We now display our results in the form of tables and graphs. In the graphs the horizontal axis is the major axis (x - axis) on which an arrow indicates the source point. The vertical axis measures the deflection and is marked in units of the dimensionless quantity

$$\frac{w}{a} = \frac{ka}{32\pi D}.$$

The tables also list units of this quantity.

An interesting effect of the clamping is that the maximum deflection deviates slightly from $\underline{S}$ towards the centre. Thus it is only when $\underline{S}$ is at the origin that the maximum deflection occurs exactly at $\underline{S}$. To illustrate this deviation, table 59 is included which shows extra field points for the $2/\sqrt{3}$ ellipse.

Conclusions

Some general conclusions clearly emerge from the results obtained. For any ellipse the maximum deflection always occurs when $\underline{S}$ and $\underline{P}$ are at the centre. The value of this maximum decreases as the minor axis decreases. As $\underline{S}$ approaches the end of the major axis, the deflection everywhere approaches zero as expected.

The deflection profile for the $2/\sqrt{3}$ ellipse follows broadly the same pattern as for the circle with $G > 0$ everywhere for each choice of $\underline{S}$. As the axial ratio increases to $2/\sqrt{2}$ the behaviour of G becomes marginal from the point of view of Hadamard's conjecture. Some negative

values are generated, but the procedures described earlier suggest that these are only spurious numerical effects. We differ here from E. Jaswon (1969) who concluded that negative deflections existed for any location of $\underline{S}$ in this ellipse.

For the 2/1 ellipse our analysis indicates that $G > 0$ everywhere if the load is at the centre, but negative deflections do arise as $\underline{S}$ moves towards an extremity. Our procedures confirm this as well established if $|\underline{P}| \geq 1$. (Table 58 supplies good supplementary evidence to support the results of table 55). Our profiles for the most part resemble those of E. Jaswon (1969). We disagree, however, with his conclusion that, if Hadamard's conjecture fails for an ellipse, it fails for any location of $\underline{S}$ on that ellipse.

When we compare the behaviour of G for the higher axial ratios given by $b = \frac{2}{3}$ and $b = \frac{2}{5}$ we find again that negative deflections exist. Two other interesting features are evident :

(a) negative deflections now arise for any $\underline{S}$ on the major axis;

(b) negative deflections arise between the source and the nearer vertex if $\underline{S}$ is sufficiently near the centre. (For the 2/1 ellipse negative deflections only exist between $\underline{S}$ and the farther vertex).

It must be admitted that the oscillatory behaviour of G in figures 26 and 27 is partly a numerical effect which becomes more pronounced as a/b increases to 10/1. However, for elongated ellipses, oscillations of this kind have been expected by engineers. As far as we are aware no attempt has been made to investigate this problem experimentally although interest has been expressed. The experimental errors in

(a) preparing a perfectly isotropic specimen,

(b) producing true clamping conditions,

(c) measuring elastic constants,

are no doubt likely to be of a higher order of magnitude than is found in our numerical analysis. Experiments have been carried out on some similar plate problems by Ligtenberg (1954). Using photographs of "Moiré" fringes. he claimed accuracy of about 5% except near the edges of the plate.

The most interesting conclusions suggested by our results are :

(i) there exists a critical axial ratio R in the neighbourhood of $2/\sqrt{2}$ below which Hadamard's

conjecture always holds and above which it fails for $\underline{S}$ sufficiently near a vertex;

(ii) there exists a higher axial ratio H satisfying $2 < H < 3$ such that if $a/b > H$ Hadamard's conjecture fails for any $\underline{S}$.

Garabedian's particular investigation for the case of $a/b = 2/1.2 = 5/3$ is in accordance with (i), and the result

$$1.414 < h < 1.667$$

is suggested. The following table displays the behaviour of G as the axial ratio increases, i.e. as b decreases while a is held equal to 2.

TABLE 51

b	Axial ratio	Result
2	1.0	$G(\underline{P}, \underline{S}) \geq 0$ for all $\underline{P}$ and all $\underline{S}$
$\sqrt{3}$	1.1547	$G(\underline{P}, \underline{S}) \geq 0$ for all $\underline{P}$ and all $\underline{S}$
$\sqrt{2}$	1.4142	$G(\underline{P}, \underline{S}) \geq 0$ for all $\underline{P}$ and all $\underline{S}$
$2/h$	h	
1.2	1.6667	$G(\underline{P}, \underline{S}) < 0$ for some $\underline{P}$ for some $\underline{S}$
1	2.0	$G(\underline{P}, \underline{S}) < 0$ for some $\underline{P}$ for some $\underline{S}$
$2/H$	H	
$2/3$	3.0	$G(\underline{P}, \underline{S}) < 0$ for some $\underline{P}$ for all $\underline{S}$
$2/5$	5.0	$G(\underline{P}, \underline{S}) < 0$ for some $\underline{P}$ for all $\underline{S}$

Summary

The preliminary analysis of Garabedian has thus been confirmed and extended. The originality of our present contribution to the problem consists chiefly of

(a) the presentation of profiles more accurate than any previously obtained. This has been made possible by refined numerical procedures, and the improvement is confirmed when our results are compared with the analytic solutions for the circle.

(b) the discussion of more elongated ellipses than have been previously considered and the conclusions concerning the critical axial ratios h and H in (i) and (ii) above.

TABLE 52 Circle (Ellipse 2/2)

P \ S	0.00	1.00	1.75	1.90
-1.90	0.010 0.004	0.002 0.012	0.000 * 0.002	0.000 * 0.002
-1.75	0.060 0.059	0.015 0.017	0.004 0.004	0.000 0.004
-1.00	0.807 0.807	0.232 0.232	0.015 0.014	0.002 0.001
0.00	2.000 2.001	0.807 0.807	0.060 0.060	0.010 0.010
1.00	0.807 0.807	1.125 1.125	0.123 0.123	0.021 0.023
1.75	0.060 0.059	0.123 0.120	0.110 0.111	0.027 0.037
1.90	0.010 0.004	0.021 0.001	0.027 0.010	0.019 0.013

The upper figures were obtained analytically.
The lower figures were obtained numerically.

TABLE 53 Ellipse $2/\sqrt{3}$

P \ S	0.00	1.00	1.75	1.90
-1.90	0.002	0.007	*0.001	*0.001
-1.75	0.043	0.010	0.002	0.002
-1.00	0.638	0.159	0.008	0.000
0.00	1.698	0.639	0.044	0.008
1.00	0.638	0.994	0.105	0.018
1.75	0.043	0.103	0.104	0.030
1.90	0.002	0.000	0.006	0.007

TABLE 54 Ellipse $2/\sqrt{2}$

P \ S	0.00	1.00	1.75	1.90
-1.90	(-)0.001	0.003	*0.000	*0.000
-1.75	0.022	0.003	0.000	0.000
-1.00	0.406	0.074	0.002	(-)0.001
0.00	1.266	0.407	0.024	0.004
1.00	0.406	0.792	0.078	0.012
1.75	0.022	0.076	0.094	0.022
1.90	(-)0.001	(-)0.001	0.005	0.003

TABLE 55 Ellipse 2/1

P \ S	0.00	1.00	1.75	1.90
-1.90	(-)0.001	-0.001	-0.001	-0.002
-1.75	0.002	-0.001	-0.002	-0.002
-1.00	0.131	0.007	-0.000	-0.001
0.00	0.689	0.133	0.004	0.001
1.00	0.131	0.474	0.034	0.003
1.75	0.002	0.030	0.072	0.012
1.90	(-)0.001	(-)0.002	0.007	0.004

TABLE 56 Ellipse $2/\frac{2}{3}$

P \ S	0.00	1.00	1.75	1.90
-1.90	-0.001	-0.002	-0.003	-0.004
-1.75	-0.001	-0.002	-0.003	-0.004
-1.00	0.017	-0.001	-0.001	-0.001
0.00	0.317	0.018	-0.001	-0.001
1.00	0.017	0.230	0.005	-0.001
1.75	-0.001	0.001	0.045	0.004
1.90	-0.001	-0.004	0.003	0.004

TABLE 57 Ellipse $2/\frac{2}{5}$

P \ S	0.00	1.00	1.75	1.90
-1.90	-0.000	-0.001	-0.003	-0.003
-1.75	0.000	0.001	0.003	0.003
-1.00	-0.000	-0.001	-0.003	-0.003
0.00	0.118	-0.002	-0.003	-0.004
1.00	-0.000	0.086	-0.005	-0.005
1.75	0.000	0.001	0.028	0.008
1.90	-0.000	-0.002	(-)0.001	0.003

TABLE 58 Ellipse 2/1

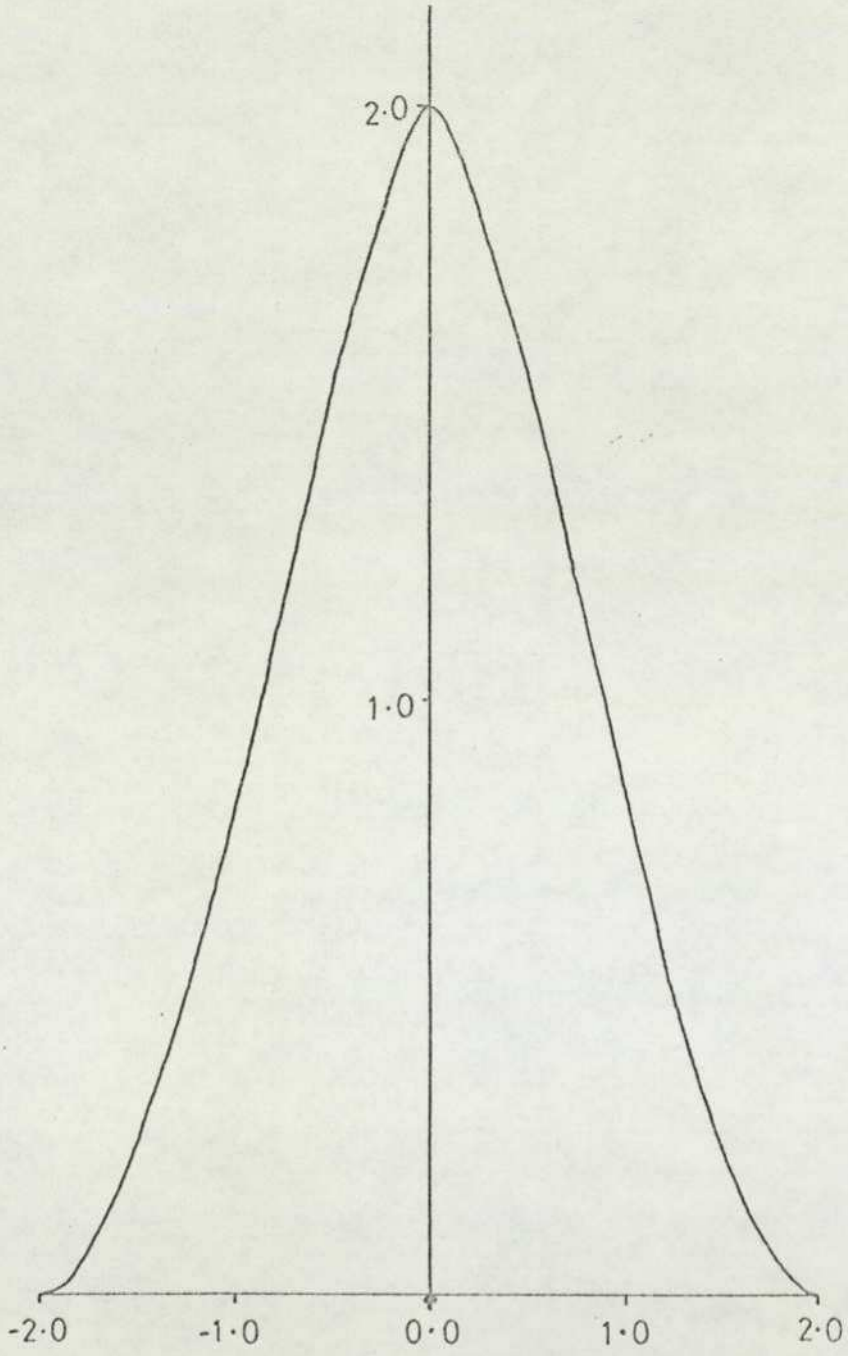
P \ S	1.5	1.75
-1.875	-0.0009	-0.0012
-1.750	-0.0013	-0.0017
-1.625	-0.0016	-0.0019
-1.500	-0.0016	-0.0019
-1.375	-0.0015	-0.0018
-1.250	-0.0012	-0.0016
-1.125	-0.0009	-0.0014
-1.000	-0.0004	-0.0011
-0.875	0.0003	-0.0008
-0.750	0.0013	-0.0004
-0.625	0.0026	-0.0000
-0.500	0.0045	0.0005

Behaviour of G in the neighbourhood of a minimum.

TABLE 59

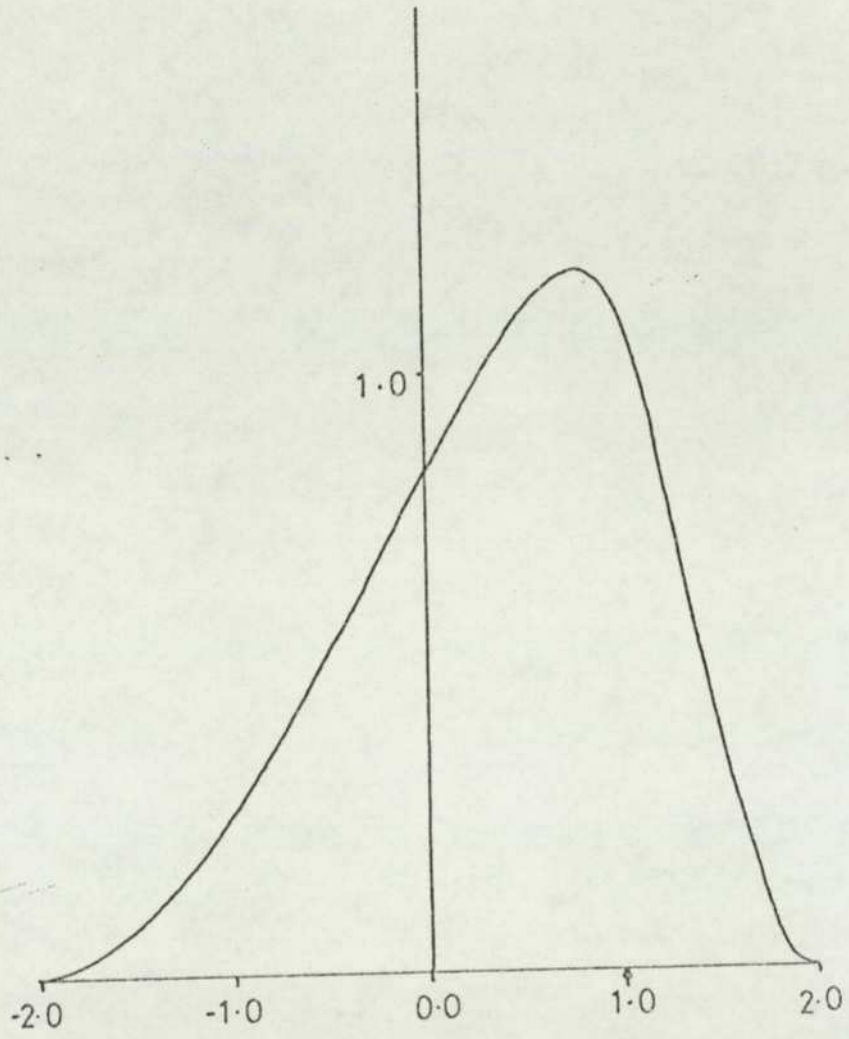
P\S	0	1.0	1.5	1.75
-1.875	0.007	0.007	*0.002	*0.000
-1.75	0.043	0.010	0.003	*0.001
-1.625	0.097	0.022	0.005	0.001
-1.5	0.171	0.038	0.009	0.002
-1.375	0.263	0.061	0.014	0.003
-1.25	0.373	0.088	0.020	0.004
-1.125	0.499	0.121	0.028	0.006
-1.0	0.638	0.159	0.038	0.008
-0.875	0.788	0.203	0.049	0.011
-0.75	0.945	0.252	0.062	0.014
-0.625	1.105	0.306	0.076	0.018
-0.5	1.263	0.365	0.092	0.022
-0.375	1.413	0.428	0.109	0.027
-0.25	1.546	0.496	0.128	0.032
-0.125	1.649	0.566	0.149	0.038
0	1.698	0.639	0.171	0.044
0.125	1.649	0.712	0.195	0.050
0.25	1.546	0.786	0.220	0.057
0.375	1.413	0.856	0.246	0.065
0.5	1.263	0.921	0.272	0.072
0.625	1.105	0.976	0.299	0.080
0.75	0.945	1.015	0.325	0.089
0.875	0.788	1.028	0.350	0.097
1.0	0.638	0.994	0.373	0.105
1.125	0.499	0.873	0.390	0.113
1.25	0.373	0.712	0.399	0.121
1.375	0.263	0.539	0.392	0.127
1.5	0.171	0.372	0.354	0.129
1.625	0.097	0.223	0.248	0.126
1.75	0.043	0.103	0.129	0.104
1.875	0.007	0.015	0.022	0.026

Ellipse $2/\sqrt{3}$



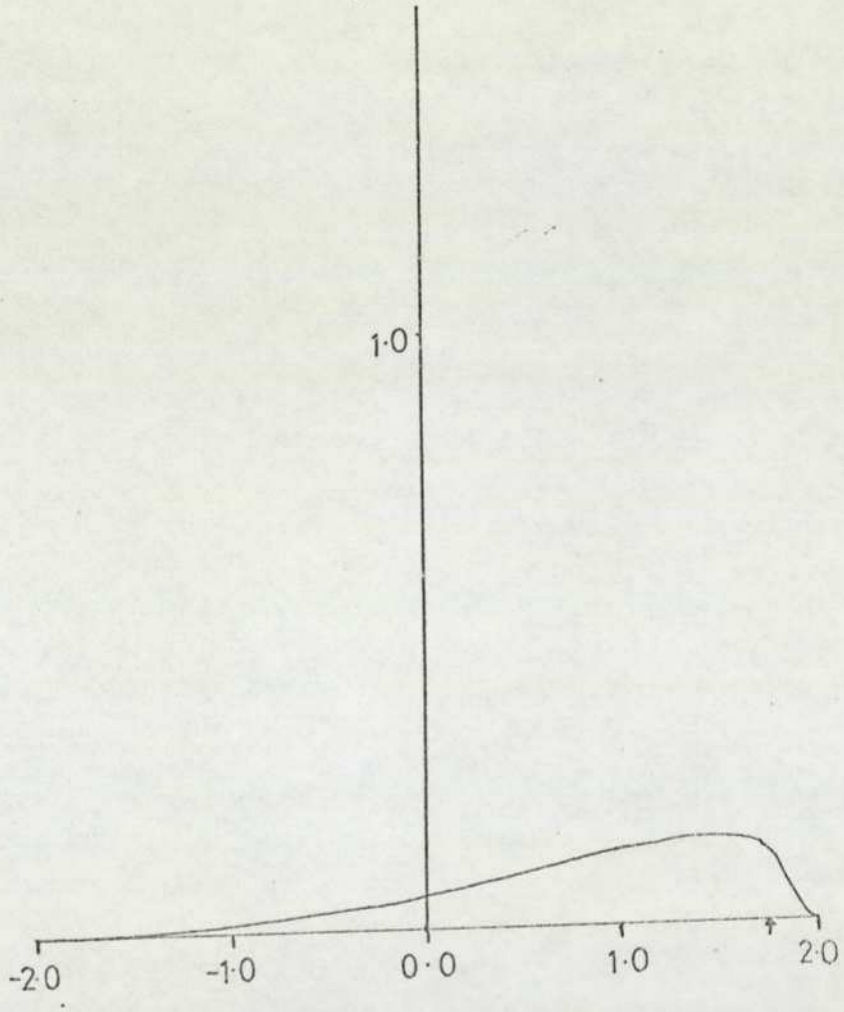
2:2 Ellipse. Load at 0.00

Figure 4.



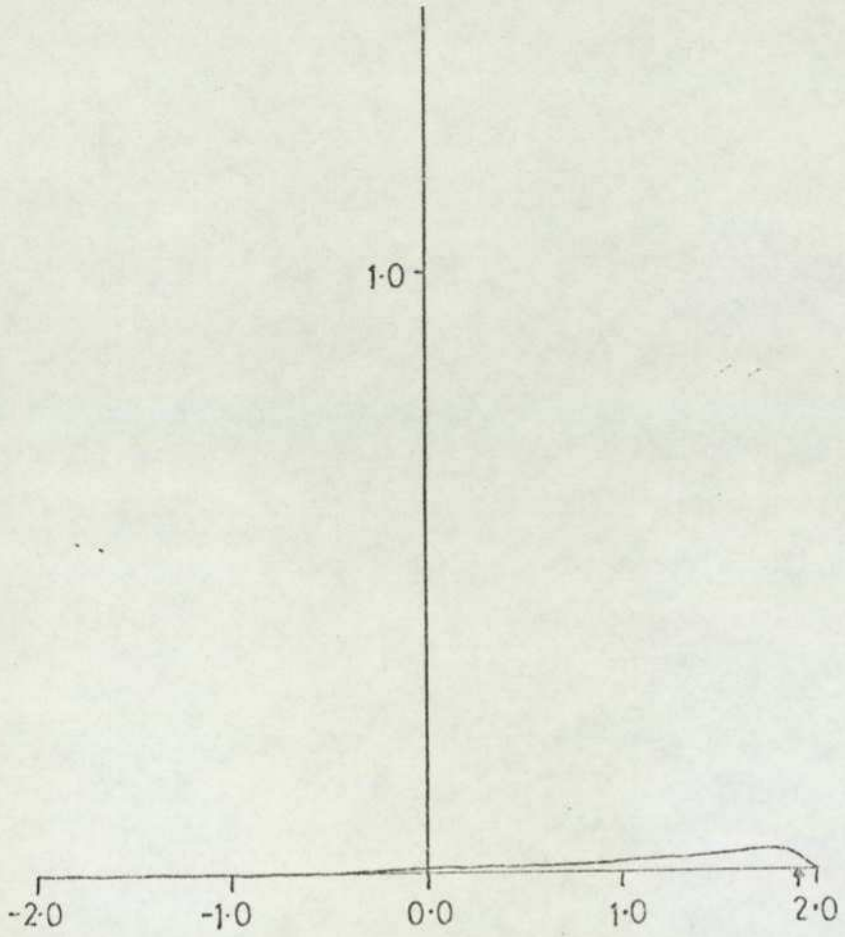
2:2 Ellipse. Load at 1.00

Figure 5.



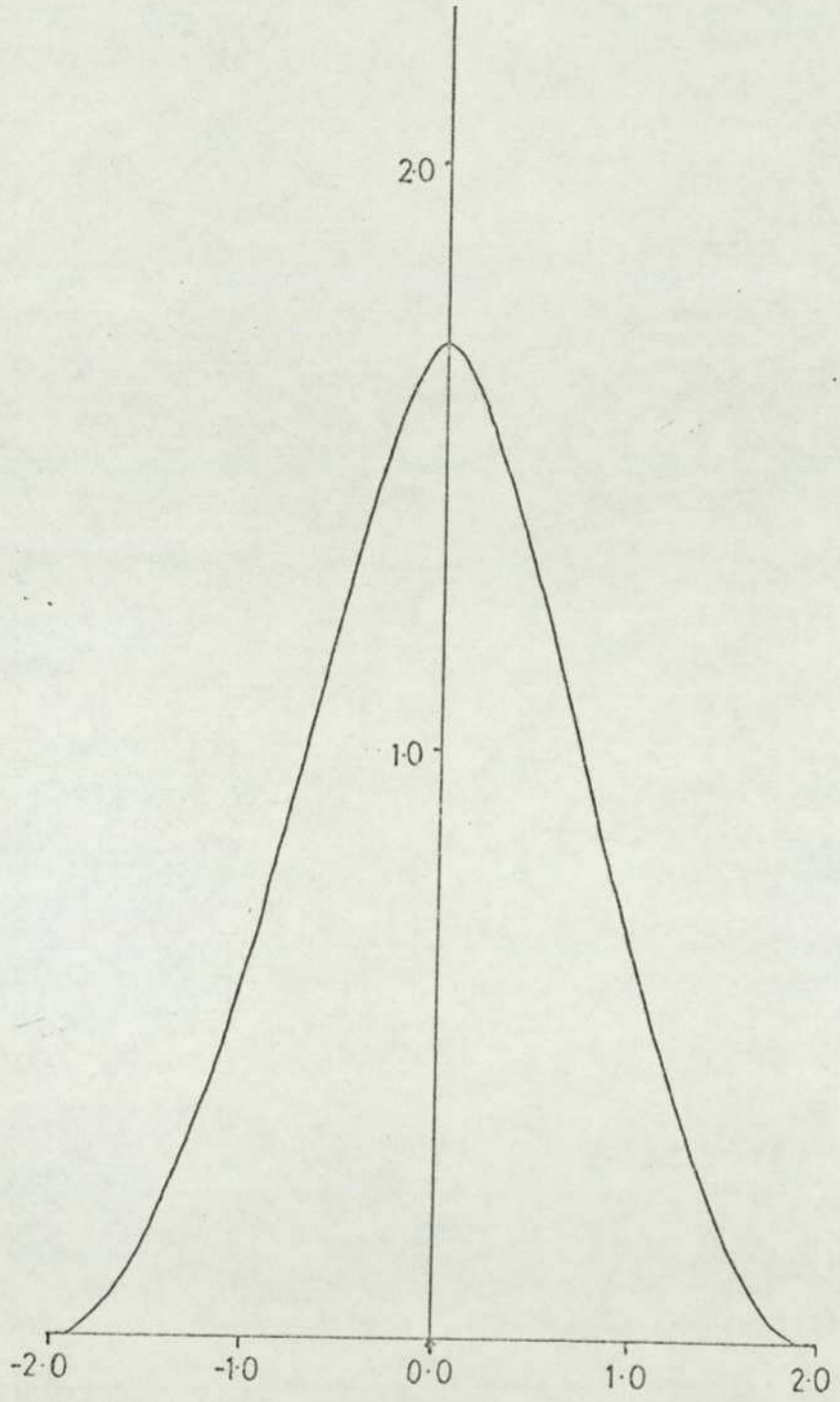
2:2 Ellipse. Load at 1.75

Figure 6.



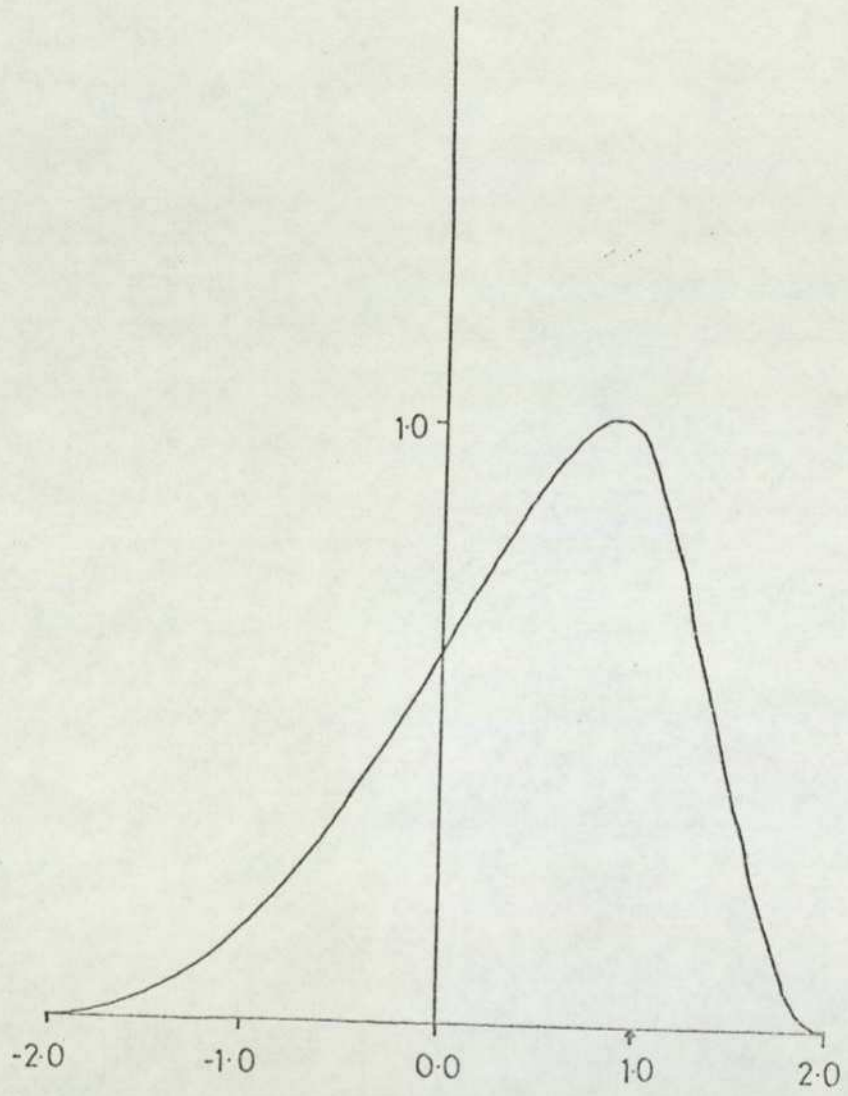
2:2 Ellipse. Load at 1.90

Figure 7.



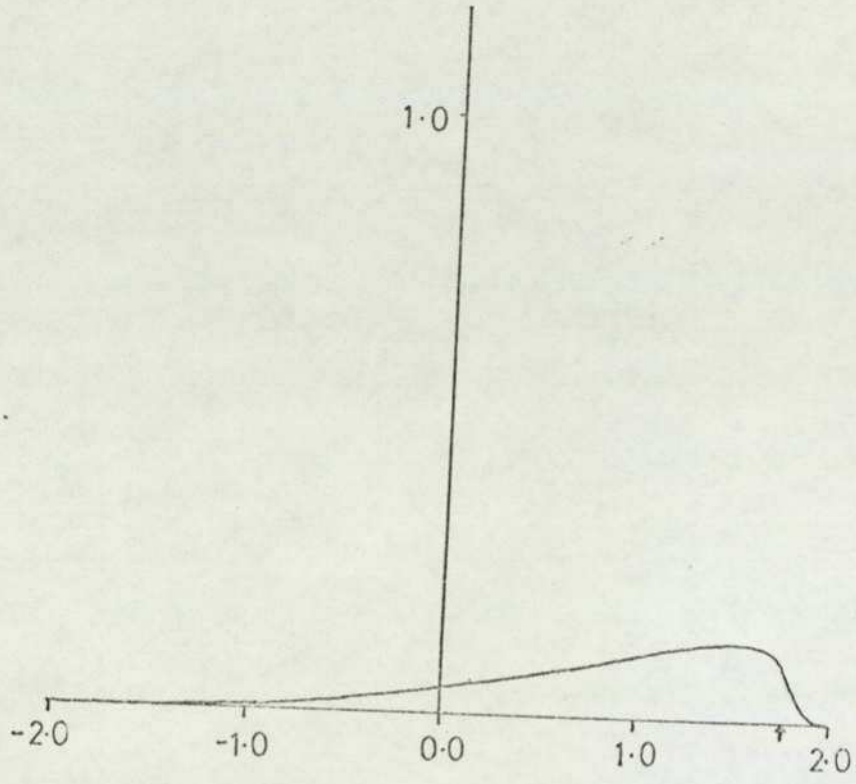
2:$\sqrt{3}$ Ellipse. Load at 0.00

Figure 8.



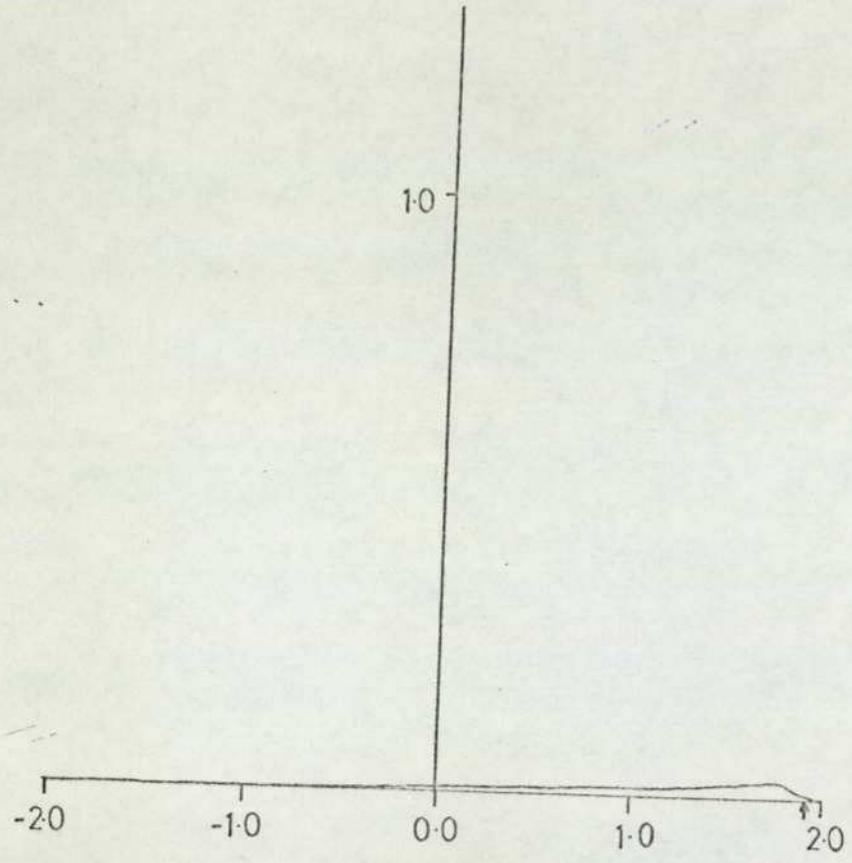
2:$\sqrt{3}$ Ellipse. Load at 1.00

Figure 9.



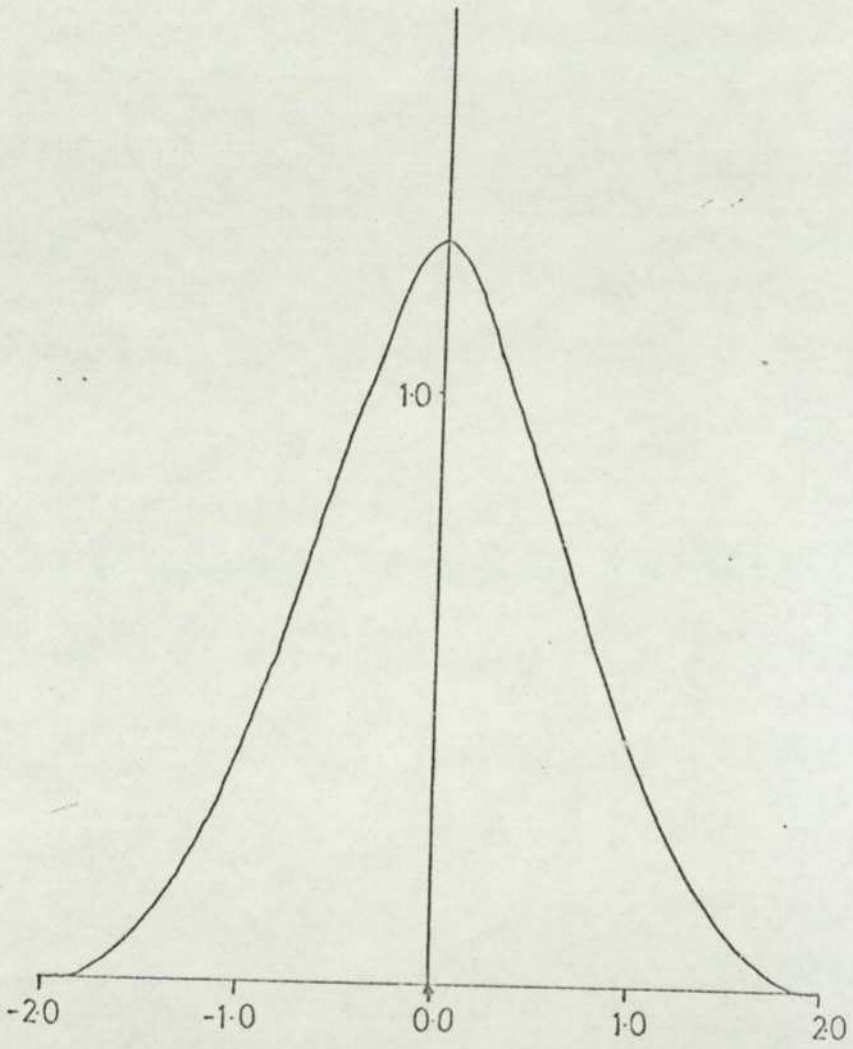
2:$\sqrt{3}$ Ellipse. Load at 1.75

Figure 10.



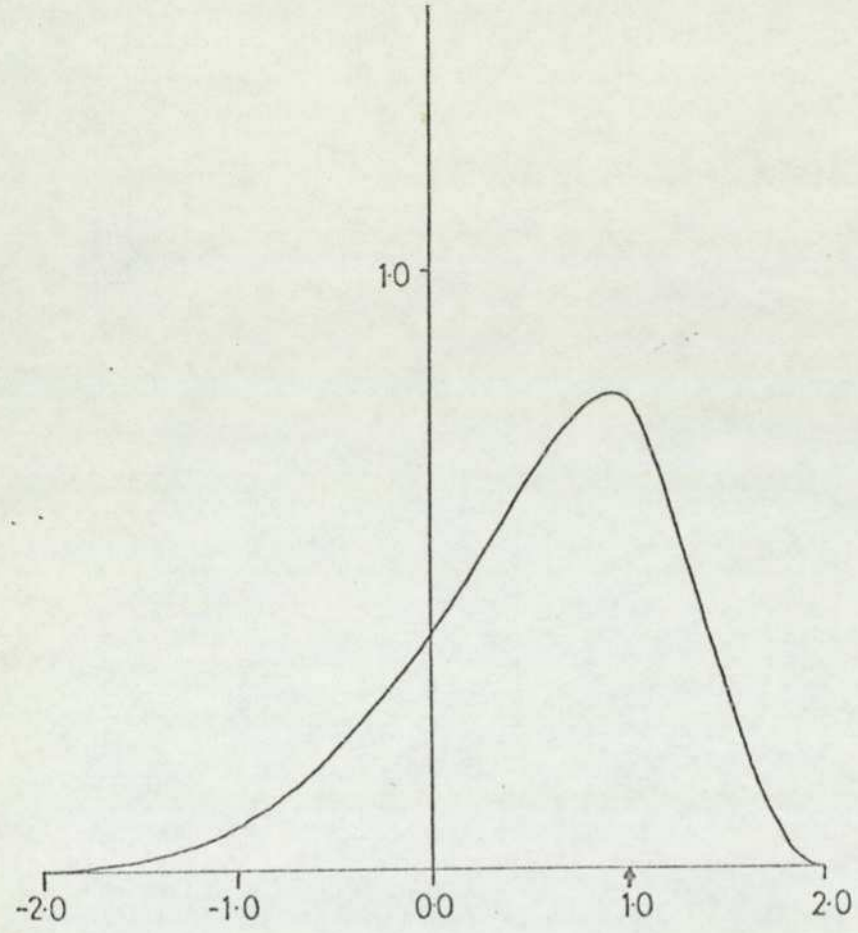
2:$\sqrt{3}$ Ellipse. Load at 1.90

Figure 11.



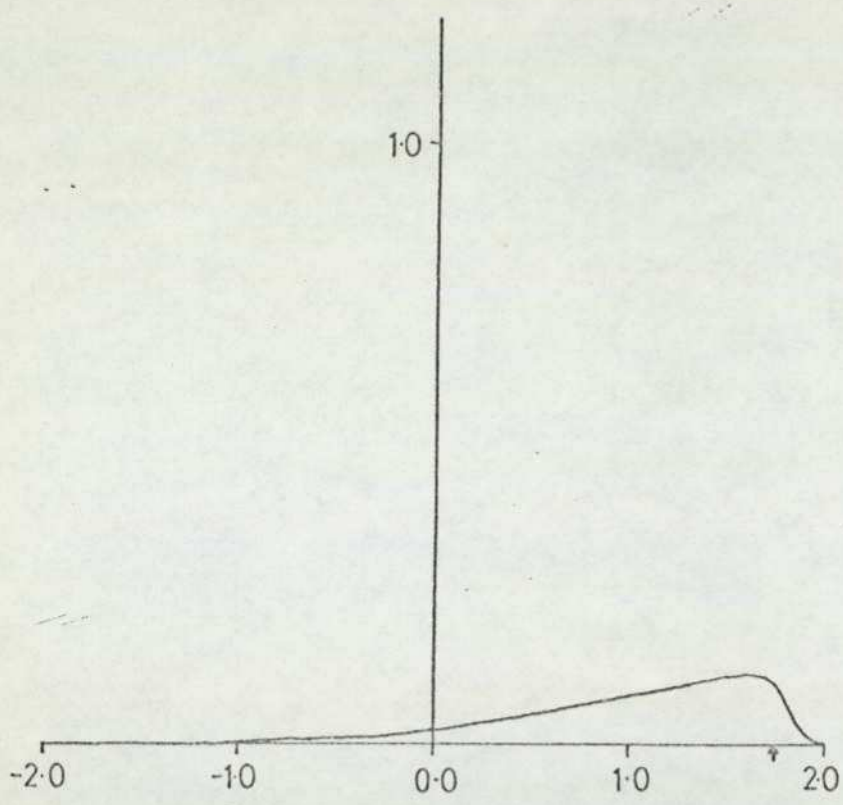
2:$\sqrt{2}$ Ellipse. Load at 0.00

Figure 12.



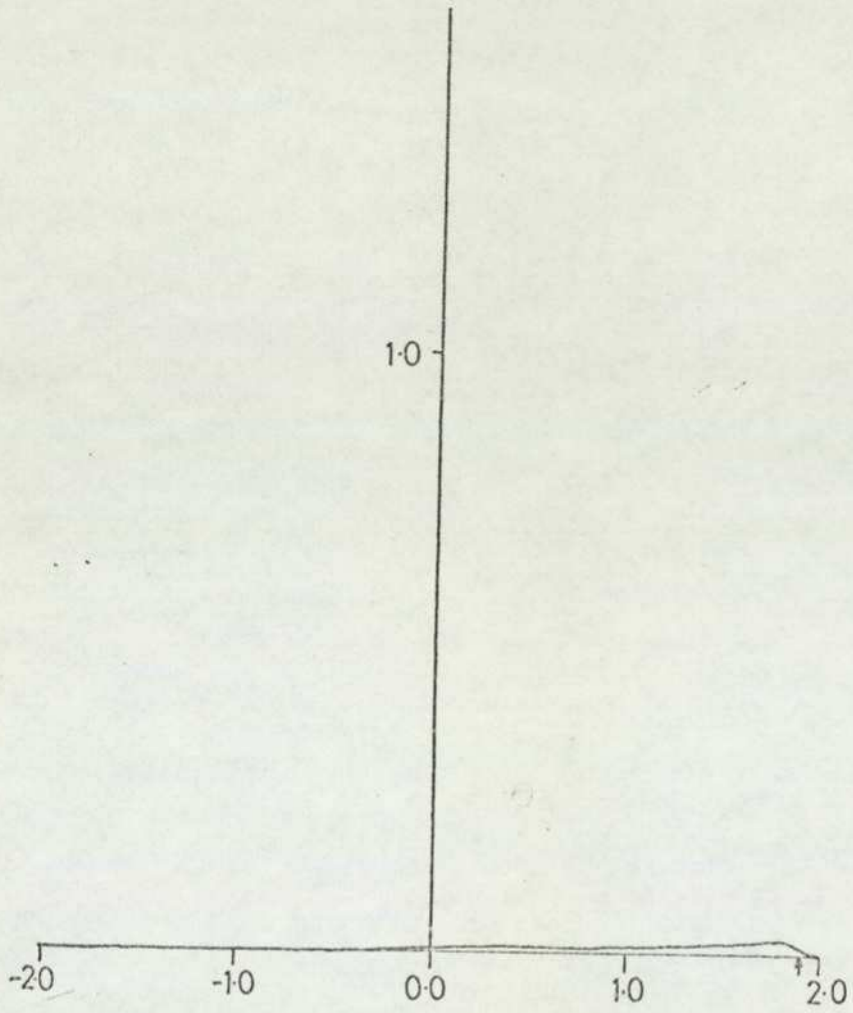
2:$\sqrt{2}$ Ellipse. Load at 1.00

Figure 13.



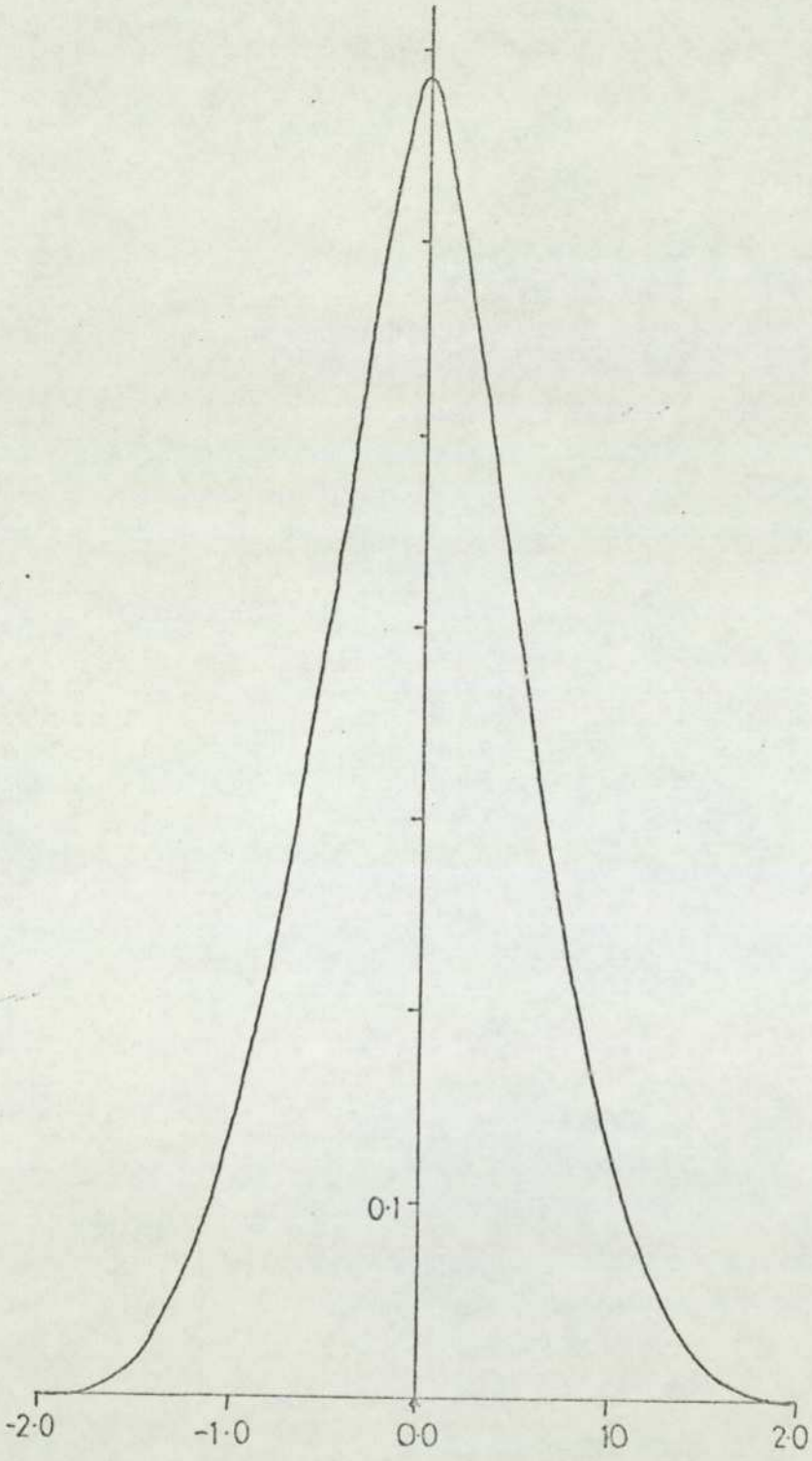
2:$\sqrt{2}$ Ellipse. Load at 1.75

Figure 14.



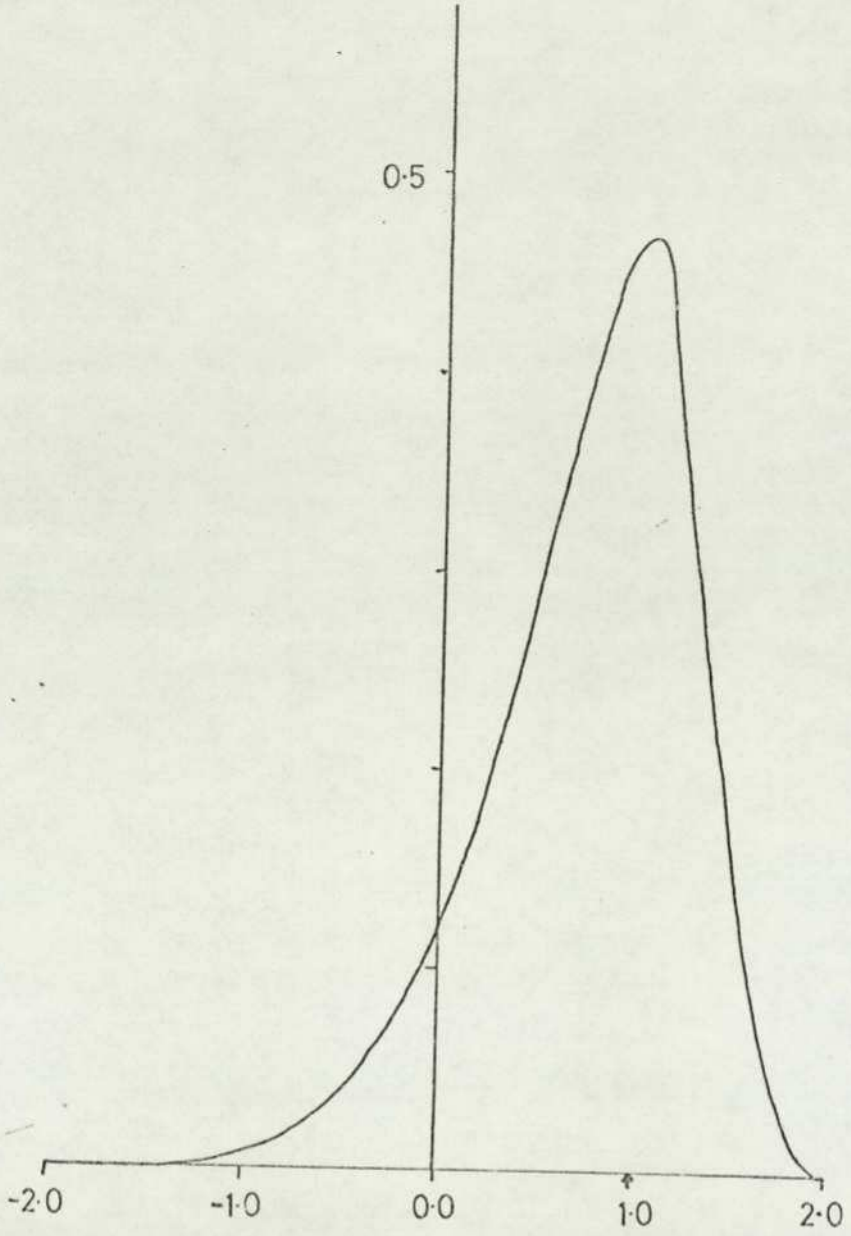
2:$\sqrt{2}$ Ellipse. Load at 1.90

Figure 15.



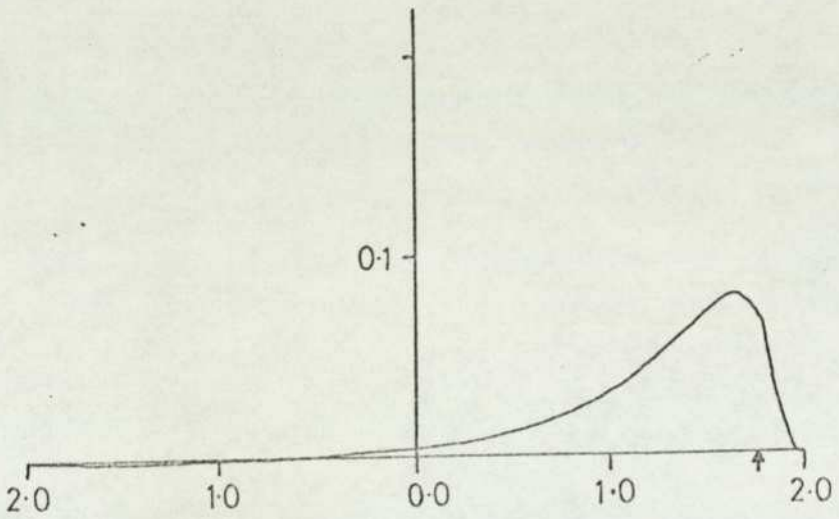
2:1 Ellipse. Load at 0.00

Figure 16.



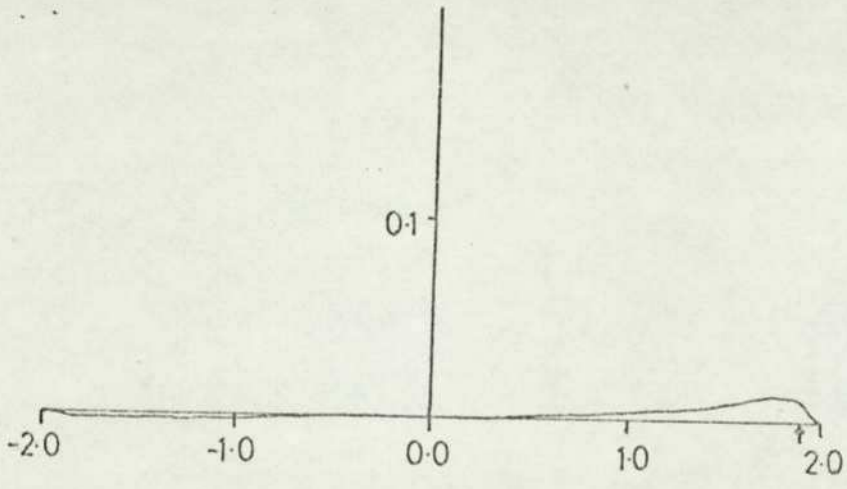
2:1 Ellipse. Load at 1.00

Figure 17.



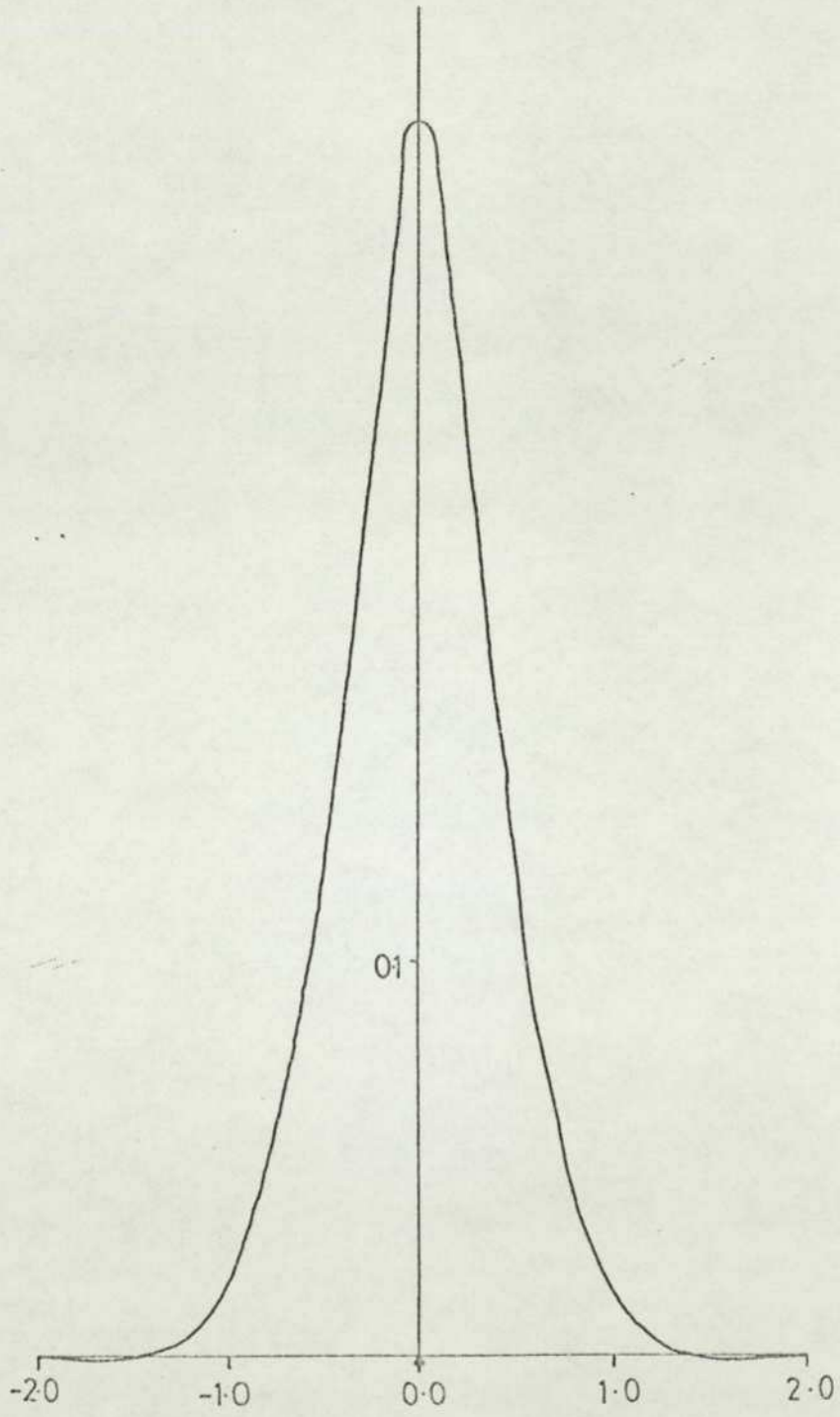
2:1 Ellipse. Load at 1.75

Figure 18.



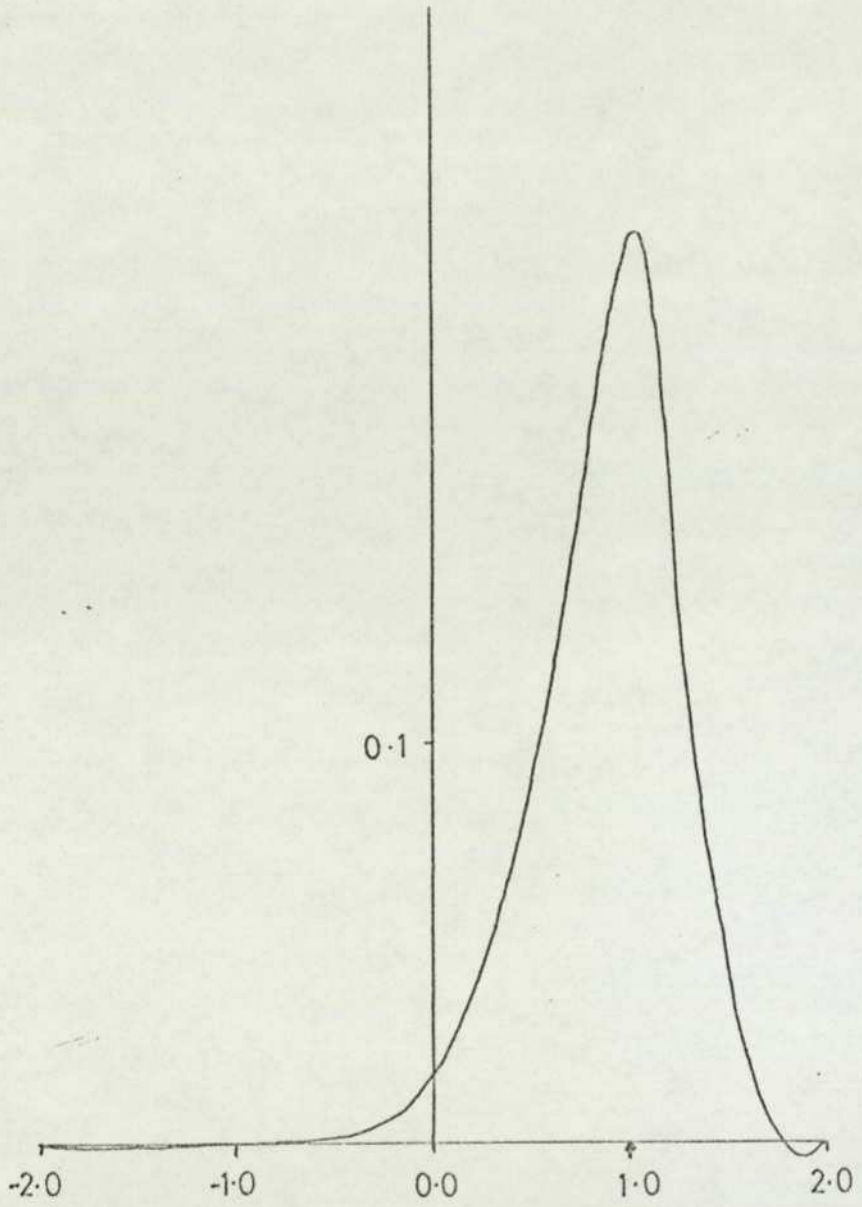
2:1 Ellipse. Load at 1.90

Figure 19.



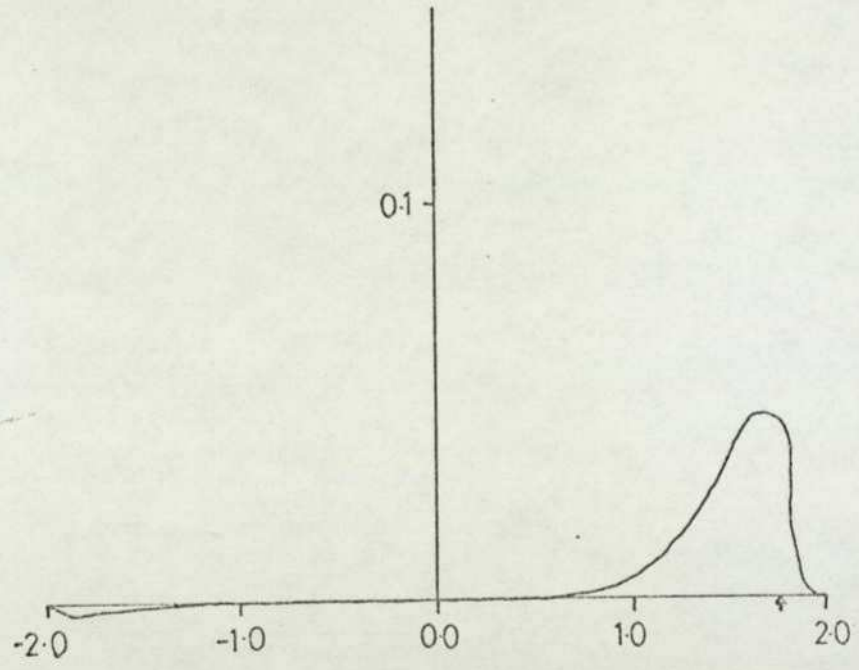
2:⅔ Ellipse. Load at 0.00

Figure 20.



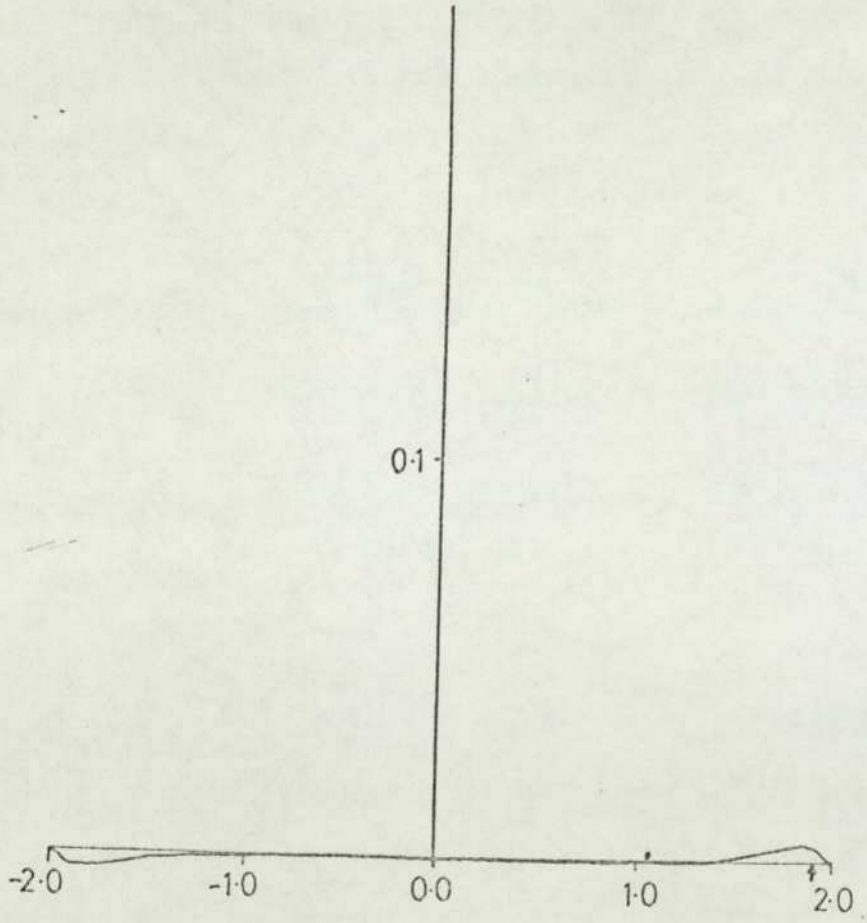
2:$\frac{2}{3}$ Ellipse. Load at 1.00

Figure 21.



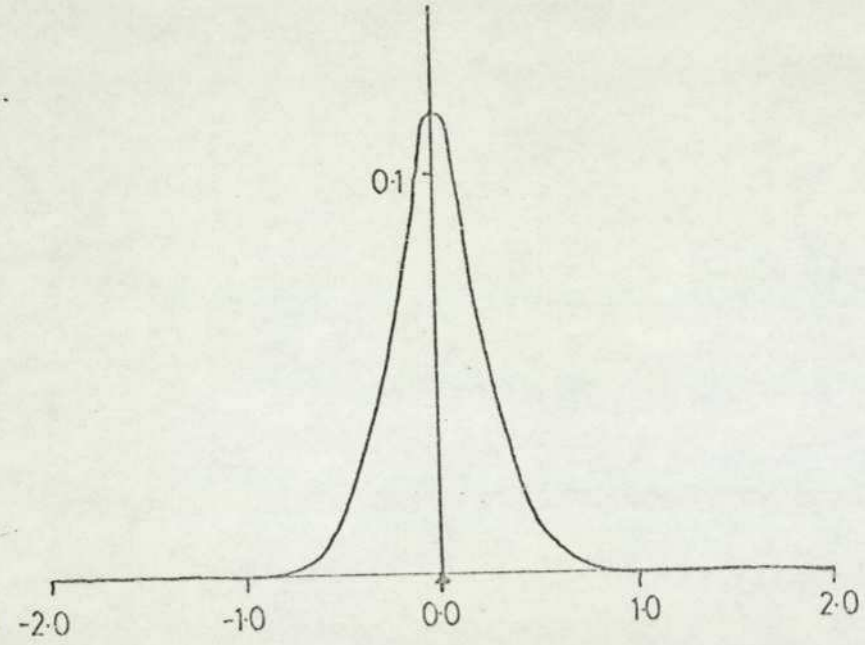
2:$\frac{2}{3}$ Ellipse. Load at 1.75

Figure 22.



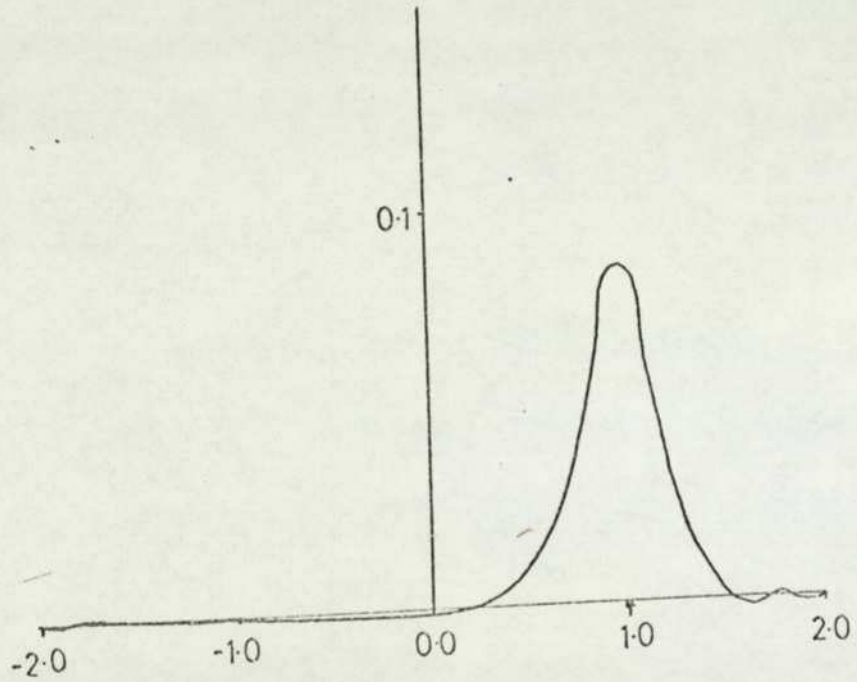
2:⅔ Ellipse. Load at 1.90

Figure 23.



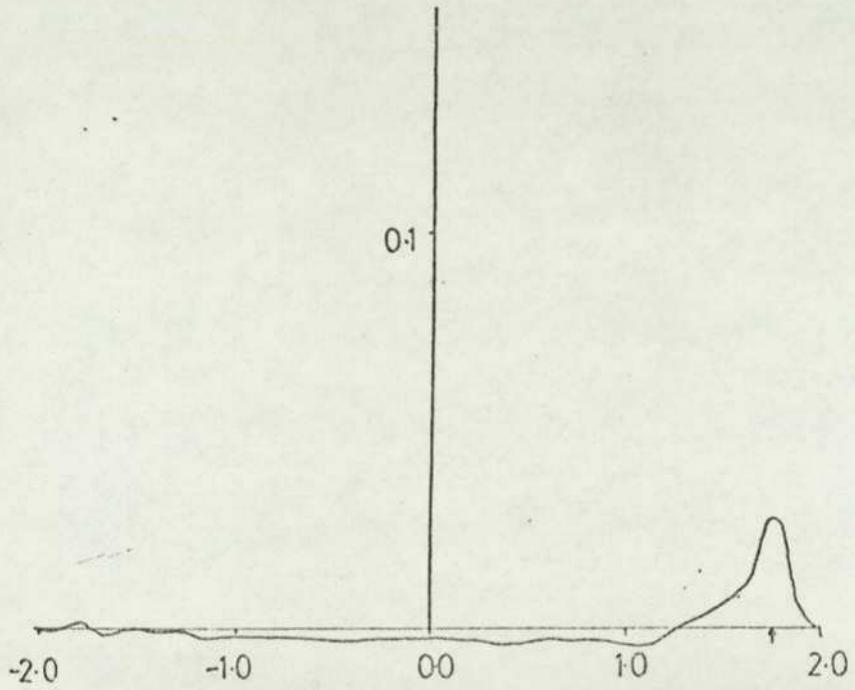
2:$\frac{2}{5}$ Ellipse. Load at 0.00

Figure 24.



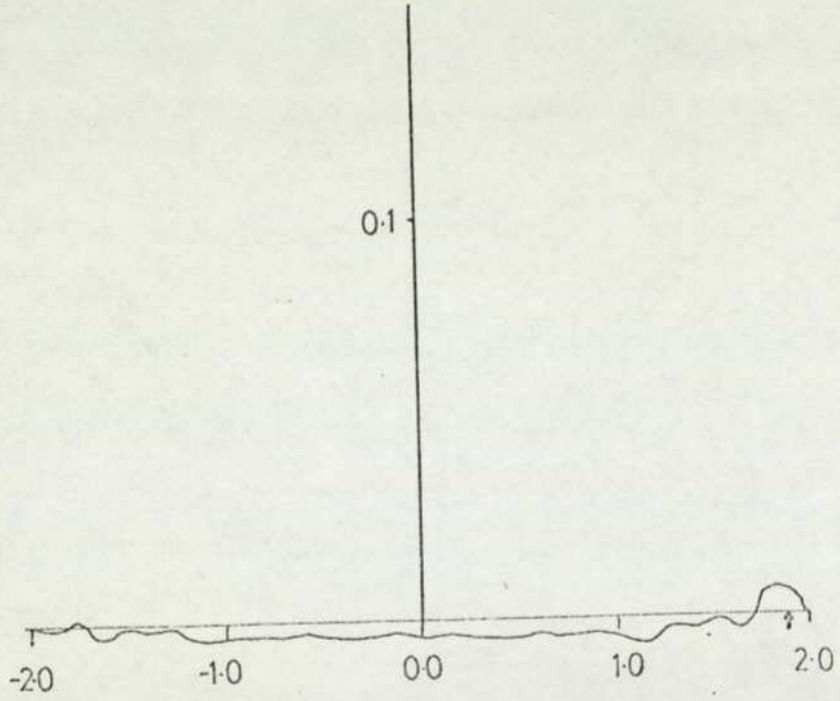
2:⅔ Ellipse. Load at 1.00

Figure 25.



2:$\frac{2}{5}$ Ellipse. Load at 1.75

Figure 26.



2:$\frac{2}{5}$ Ellipse. Load at 1.90

Figure 27.

P A R T II

ELLIPTIC CAVITY PROBLEMS

CHAPTER 7

INTRODUCTION

Introduction

In part II of this thesis we consider another type of biharmonic problem, that of determining the elastic stress field outside an elliptic cavity under plane strain conditions. These problems differ from that of part I in the following respects :-

(i) the biharmonic equation is satisfied by Airy's stress function, which has no direct physical significance

(ii) when the biharmonic function has been obtained, further operations are required to compute the stresses;

(iii) we now have an exterior problem;

(iv) progress can be made with analytical solutions in confocal elliptic coordinates.

Two main contributions are here made to the study of such problems. First, the formulation and techniques of part I are adapted to the plane strain of infinite exterior domains. Secondly, some exact analytical solutions are achieved utilising the representation $\chi = r^2\phi + \psi$, which agree with those previously obtained by Muskhelishvili (1963) on the basis of his complex variable formulation.

The present chapter is devoted to the theory of Airy stress functions and to the representation of these functions in terms of two-dimensional potentials.

Plane Strain

The equations of equilibrium for plane strain conditions in the absence of body forces are

$$\left.\begin{aligned} \frac{\partial \hat{xx}}{\partial x} + \frac{\partial \hat{xy}}{\partial y} &= 0, \\ \frac{\partial \hat{xy}}{\partial x} + \frac{\partial \hat{yy}}{\partial y} &= 0, \\ \frac{\partial \hat{zz}}{\partial z} &= 0, \end{aligned}\right\} \qquad (7.1)$$

where x, y, z are Cartesian coordinate variables and $\hat{xx}$, $\hat{xy}$, $\hat{yy}$, $\hat{zz}$ are the non-vanishing Cartesian stress components. The first two equations of (7.1) are automatically satisfied by writing

$$\hat{xx} = \frac{\partial^2 \chi}{\partial y^2}, \quad \hat{yy} = \frac{\partial^2 \chi}{\partial x^2}, \quad \hat{xy} = -\frac{\partial^2 \chi}{\partial x \partial y}, \qquad (7.2)$$

where $\chi = \chi(x, y)$ is termed the Airy stress function. The strain-stress relations for an isotropic material are

$$E\varepsilon_{pq} = (1+\nu)\hat{pq} - \nu\Theta\delta_{pq}\,; \tag{7.3}$$

where

$$\delta_{pq} = \begin{cases} 0 \text{ when } & p \neq q, \\ 1 \text{ when } & p = q, \end{cases}$$

$$p, q = x, y, z,$$

$$\Theta = x\hat{x} + y\hat{y} + z\hat{z},$$

E is Young's modulus and ν is Poisson's ratio.
The non-vanishing strain components are

$$\varepsilon_{xx} = \frac{\partial u}{\partial x}, \quad \varepsilon_{yy} = \frac{\partial v}{\partial y}, \quad \varepsilon_{xy} = \frac{1}{2}\left(\frac{\partial u}{\partial y} + \frac{\partial v}{\partial x}\right), \tag{7.4}$$

where u, v are the Cartesian components of the elastostatic displacement. Since $\varepsilon_{zz} = 0$ under conditions of plane strain, it follows from (7.3) that

$$z\hat{z} = \nu(x\hat{x} + y\hat{y}). \tag{7.5}$$

It can be seen from (7.4) that

$$\frac{\partial^2\varepsilon_{xx}}{\partial y^2} + \frac{\partial^2\varepsilon_{yy}}{\partial x^2} = 2\frac{\partial^2\varepsilon_{xy}}{\partial x \partial y} \tag{7.6}$$

which is the Saint-Venant compatibility condition between the strains. Arbitrary prescribed strains must satisfy (7.6) to ensure the existence of a displacement vector. Substituting (7.3) into (7.6) and utilising (7.1) we obtain

$$\nabla^2\Theta = 0 \tag{7.7}$$

where ∇^2 is the two-dimensional Laplacian operator, whence, by (7.5)

$$\nabla^2(x\hat{x} + y\hat{y}) = 0. \tag{7.8}$$

Since

$$x\hat{x} + y\hat{y} = \nabla^2\chi$$

by (7.2), we see that χ satisfies

$$\nabla^2(\nabla^2\chi) = \frac{\partial^4\chi}{\partial x^4} + 2\frac{\partial^4\chi}{\partial x^2\partial y^2} + \frac{\partial^4\chi}{\partial y^4} = 0,$$

i.e. the biharmonic equation

$$\nabla^4\chi = 0. \tag{7.9}$$

Thus a plane strain problem for a medium free from

body forces may be formulated as that of finding a solution of (7.9) subject to the appropriate boundary conditions. (An analogous equation can be obtained for generalized plane stress. In this case $\hat{zz} = 0$ everywhere and the derivation of equation (7.9) is therefore slightly different).

Boundary conditions for traction problems

We introduce $F_x(s)$, $F_y(s)$ to denote the traction components per unit length of boundary at the point $x(s)$, $y(s)$ of the boundary ∂B, where the tangent vector increases in such a way as to keep B on the left. The usual convention that $\underline{n}$ is the inward normal ensures that the "Cauchy-Riemann" equations

$$\frac{dx}{ds} = \frac{dy}{dn}, \qquad \frac{dx}{dn} = -\frac{dy}{ds} \tag{7.10}$$

are satisfied. Treating the expressions in (7.10) as direction cosines we have

$$\left.\begin{aligned} F_x &= -\hat{xx}\frac{dx}{dn} - \hat{yx}\frac{dy}{dn} = \hat{xx}\frac{dy}{ds} - \hat{xy}\frac{dx}{ds}, \\ F_y &= -\hat{xy}\frac{dx}{dn} - \hat{yy}\frac{dy}{dn} = \hat{xy}\frac{dy}{ds} - \hat{yy}\frac{dx}{ds}. \end{aligned}\right\} \tag{7.11}$$

By (7.2) these become

$$F_x = \frac{d}{ds}\left(\frac{\partial\chi}{\partial y}\right), \qquad F_y = -\frac{d}{ds}\left(\frac{\partial\chi}{\partial x}\right). \tag{7.12}$$

Integration of (7.12) yields

$$\left.\begin{aligned} \frac{\partial\chi}{\partial x} &= -\int_{s_0}^{s} F_y(s)\,ds + \alpha, \\ \frac{\partial\chi}{\partial y} &= -\int_{s_0}^{s} F_x(s)\,ds + \beta, \end{aligned}\right\} \tag{7.13}$$

where s_0 denotes an arbitrary origin on ∂B, and α, β are arbitrary constants of integration. Hence, given F_x, F_y, we may evalute the boundary quantities

$$\chi(s) = \int_{s_0}^{s} \frac{d\chi}{ds}\,ds = \int_{s_0}^{s}\left(\frac{\partial\chi}{\partial x}\frac{dx}{ds} + \frac{\partial\chi}{\partial y}\frac{dy}{ds}\right)ds + \gamma \tag{7.14}$$

where γ is a further constant of integration, and

$$\chi'(s) = \frac{d\chi}{dn} = \frac{\partial\chi}{\partial x}\frac{dx}{dn} + \frac{\partial\chi}{\partial y}\frac{dy}{dn}. \tag{7.15}$$

Thus the traction problem leads directly to the canonical boundary conditions for the biharmonic equation (7.9), i.e. the problem consists of finding χ in B when χ and χ' assume prescribed values on ∂B. We note that χ, χ' include arbitrary terms $\alpha x + \beta y + \gamma$, $\alpha x' + \beta y'$ respectively. These are the boundary values and boundary normal derivatives of a harmonic function $\alpha x + \beta y + \gamma$ existing in B. It arises from the constants of integration but makes no contribution to the stress field. Thus we may, for example, set $\alpha = \beta = \gamma = 0$ since s_0 is arbitrary.

From (7.13) we see that the x - component of resultant force on ∂B between s_0 and s is $\left[\frac{\partial \chi}{\partial y}\right]_{s_0}^{s}$. Thus for a simply-connected domain B in statical equilibrium, $\frac{\partial \chi}{\partial y}$ must be a single-valued function of s, and similarly for $\frac{\partial \chi}{\partial x}$. Further, the resultant positive couple on ∂B between s_0 and s is

$$\int_{s_0}^{s} (x F_y - y F_x)\, ds = -\int_{s_0}^{s} \left[x \frac{d}{ds}\left(\frac{\partial \chi}{\partial x}\right) + y \frac{d}{ds}\left(\frac{\partial \chi}{\partial y}\right)\right] ds$$

$$= \left[\chi - x\frac{\partial \chi}{\partial x} - y\frac{\partial \chi}{\partial y}\right]_{s_0}^{s} \qquad (7.16)$$

showing that $\chi - x\frac{\partial \chi}{\partial x} - y\frac{\partial \chi}{\partial y}$ is a single-valued function of s in statical equilibrium. This implies that χ itself is single-valued on ∂B and hence throughout B.

Exterior Domains

If ∂B is the internal boundary of an infinite domain then the resultant tractions and couples on ∂B need not be equilibrated, since they can be compensated by stresses applied at infinity. If the tractions are equilibrated, then $\frac{\partial \chi}{\partial x}$, $\frac{\partial \chi}{\partial y}$ are single-valued, but this does not necessarily imply that χ is single-valued. If, for example, $\chi = \theta$ we have

$$\frac{\partial \chi}{\partial x} = \frac{\partial \theta}{\partial x} = \frac{-y}{x^2+y^2}\,; \qquad \frac{\partial \chi}{\partial y} = \frac{\partial \theta}{\partial y} = \frac{x}{x^2+y^2}\,.$$

Single-valuedness of χ is ensured from (7.16) if the resultant couple is equilibrated. Multi-valued displacements corresponding to Volterra dislocations may exist in a ring-shaped domain or an infinite exterior domain, even if χ is single-valued (Love, 1952).

This analysis was discussed generally by Jaswon (private communication) and Symm (1964) who showed how to construct harmonic functions exhibiting given multi-valuedness

in χ, $\frac{\partial \chi}{\partial x}$, $\frac{\partial \chi}{\partial y}$ respectively, no dislocations (Love, 1952) being present.

We shall assume that all non-vanishing stresses at infinity can be eliminated by suitable superpositions and that no dislocations are present. Hence χ is always a single-valued function in our analysis. For example consider the problem of an infinite medium with an internal boundary subject to uniform normal pressure P. In this case no resultant force or couple is produced. By reference to figure 28

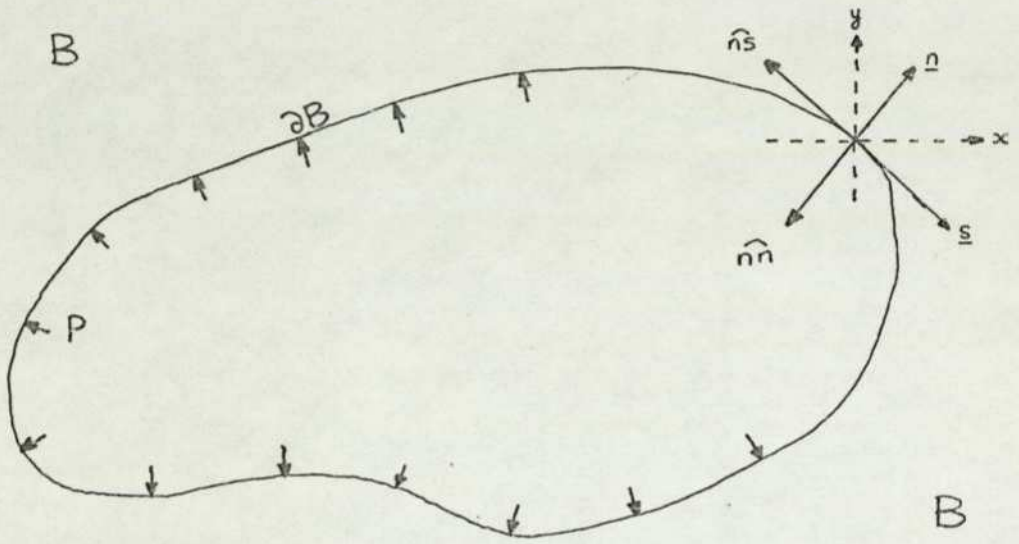


FIG. 28

and equations (7.10) we obtain convenient formulae for evaluating F_x, F_y. The normal and tangential stress components $\hat{nn}$, $\hat{ns}$, at s may be viewed as the components of stress in the $-\underline{n}$, $-\underline{s}$, directions on an element of boundary oriented in the $-\underline{n}$-direction. Thus there results

$$\left.\begin{aligned} F_x &= -\hat{nn}\frac{dx}{dn} - \hat{ns}\frac{dx}{ds} = \hat{nn}\frac{dy}{ds} - \hat{ns}\frac{dx}{ds}, \\ F_y &= -\hat{nn}\frac{dy}{dn} - \hat{ns}\frac{dy}{ds} = -\hat{nn}\frac{dx}{ds} - \hat{ns}\frac{dy}{ds}. \end{aligned}\right\} \qquad (7.17)$$

For uniform pressure P we have

$$\hat{nn} = -P, \qquad \hat{ns} = 0 \qquad \text{on } \partial B, \qquad (7.18)$$

whence the boundary quantities

$$F_x = -P\frac{dy}{ds}, \qquad F_y = P\frac{dx}{ds}, \qquad (7.19)$$

$$\chi = -\frac{P}{2}(x^2+y^2), \qquad \chi' = -P(xx'+yy') \quad \text{on } \partial B, \tag{7.20}$$

the constants of (7.13) and (7.14) being so chosen as to produce maximum symmetry.

Biharmonic Representations

We now discuss the solution of the biharmonic equation (7.9) subject to the boundary conditions (7.20). We note at the outset that the resolution $\chi = r^2\phi + \psi$ used in part I, where ϕ and ψ are simple source potentials, is inadequate to represent a biharmonic χ in an exterior domain. This is a consequence of the behaviour

$$\int_{\partial B} \sigma(\underline{q}) \ln |\underline{P}-\underline{q}|\, dq \to \ln r \int_{\partial B} \sigma(\underline{q})\, dq + O\left(\frac{1}{r}\right)$$

as $r \equiv |\underline{P}| \to \infty$, which implies that no constant harmonic function can be represented in an exterior domain B by a simple source potential (although it could be so represented in an interior region).

It is therefore necessary to modify the formulation (5.4) used for the interior problem and write

$$\chi = r^2\phi + \psi + \gamma, \tag{7.21}$$

where

$$\left.\begin{aligned} \phi &= \phi(\underline{P}) = \int_{\partial B} \sigma(\underline{q}) \ln |\underline{P}-\underline{q}|\, dq, \\ \psi &= \psi(\underline{P}) = \int_{\partial B} \mu(\underline{q}) \ln |\underline{P}-\underline{q}|\, dq, \end{aligned}\right\} \tag{7.22}$$

and γ is a constant to be determined from the physical condition that the stresses decay at infinity. To ensure this we must have

$$\phi = O\left(\frac{1}{r}\right) \tag{7.23}$$

since higher powers would either produce non-vanishing stresses at infinity, or in the case of $\phi = O(\ln r)$, $r^2\phi = O(r^2 \ln r)$, a radial fissure (Love, 1952).

Equation (7.23) is satisfied by imposing the condition

$$\int_{\partial B} \phi'(\underline{q})\, dq = 2\pi \int_{\partial B} \sigma(\underline{q})\, dq = 0. \tag{7.24}$$

We require, therefore, to solve for $\sigma(\underline{q})$, $\mu(\underline{q})$ and γ the coupled integral equations

$$\left.\begin{aligned} r^2\phi(\underline{p}) + \psi(\underline{p}) + \gamma &= \chi(\underline{p}), \\ 2rr'\phi(\underline{p}) + r^2\phi'(\underline{p}) + \psi'(\underline{p}) &= \chi'(\underline{p}), \end{aligned}\right\} \quad \underline{p} \in \partial B, \tag{7.25}$$

subject to the side condition

$$\int_{\partial B} \sigma(\underline{q})\, dq = 0 \qquad (7.26)$$

which compensates for the appearance of the unknown constant γ. The right hand sides of (7.25) are the known values of $\chi(\underline{P})$, $\chi'(\underline{P})$ given by (7.20). The terms $\phi(\underline{P})$, $\psi(\underline{P})$, $\phi'(\underline{P})$, $\psi'(\underline{P})$ are as in (5.12) to (5.15), i.e. they are obtained from the potentials in (7.22) and their normal derivatives by letting $\underline{P} \to \underline{P}$ on ∂B. Equations (7.25) and (7.26) may be solved numerically, whereupon χ can be generated throughout B using (7.21) and (7.22).

Stress Invariants

Stresses can be found either by numerical differentiation of χ or by using differentiated kernels. Thus to compute the stress invariant $\Theta = x\hat{x} + y\hat{y}$ in B we may write

$$\begin{aligned} \Theta &= \nabla^2 \chi && \text{by (7.2)} \\ &= \nabla^2 (r^2\phi + \psi + \gamma) && \text{by (7.21)} \\ &= \nabla^2 (r^2 \phi) \\ &= 4(\phi + x\phi_x + y\phi_y) && (7.27) \end{aligned}$$

where subscripts denote partial differentiations and ϕ_x, ϕ_y may be found from

$$\left.\begin{aligned} \phi_x &= \frac{\partial \phi(\underline{P})}{\partial x} = \int_{\partial B} \sigma(\underline{q}) \frac{\partial}{\partial x} \ln |\underline{P} - \underline{q}|\, dq, \\ \phi_y &= \frac{\partial \phi(\underline{P})}{\partial y} = \int_{\partial B} \sigma(\underline{q}) \frac{\partial}{\partial y} \ln |\underline{P} - \underline{q}|\, dq. \end{aligned}\right\} \qquad (7.28)$$

The quantity Θ is significant since it is proportional to the hydrostatic pressure. More precisely if

$$x\hat{x} = y\hat{y} = z\hat{z} = -p,$$

then

$$x\hat{x} + y\hat{y} + z\hat{z} = \Theta = -3p, \qquad (7.29)$$

and (7.5) yields

$$\Theta = \frac{-3p}{1+\nu}. \qquad (7.30)$$

Some writers speak of Θ as the hydrostatic pressure. Another stress combination of physical significance is the maximum shear stress s. This invariant is of importance

in elasto-plastic analysis (part III) and is given by

$$4s^2 = (\hat{x}\hat{x} - \hat{y}\hat{y})^2 + 4\hat{x}\hat{y}^2 \qquad (7.31)$$
$$= (\chi_{yy} - \chi_{xx})^2 + 4(\chi_{xy})^2 \qquad \text{by (7.2),}$$

where

$$\chi_{xx} = r^2\phi_{xx} + 4x\phi_x + 2\phi + \Psi_{xx}, \qquad (7.32)$$

$$\chi_{yy} = r^2\phi_{yy} + 4y\phi_y + 2\phi + \Psi_{yy}, \qquad (7.33)$$

$$\chi_{xy} = r^2\phi_{xy} + 2y\phi_x + 2x\phi_y + \Psi_{xy}. \qquad (7.34)$$

Thus

$$4s^2 = \left[r^2(\phi_{yy} - \phi_{xx})^2 + 4(y\phi_y - x\phi_x) + \Psi_{yy} - \Psi_{xx}\right]^2$$
$$+ 4\left[r^2\phi_{xy} + 2(x\phi_y + y\phi_x) + \Psi_{xy}\right]^2. \qquad (7.35)$$

The second order partial derivatives of ϕ and Ψ may be expressed in a form similar to (7.28) whereupon (7.35) may be used to compute $4s^2$ throughout B. Formulae for adapting equations such as (7.28) for numerical solution will be given in chapter 8.

CHAPTER 8

EXACT SOLUTIONS IN CONFOCAL ELLIPTIC COORDINATES

Introduction

In this chapter we develop analytical solutions of the plane strain problem of an infinite medium with a cavity of elliptic cross-section. Because of the similarity to the equations of generalized plane stress, our solutions are equally relevant to the case of an infinite plate with an elliptic hole. We consider the solution of the biharmonic equation in confocal elliptic coordinates subject to various boundary conditions, namely :

(i) uniform internal normal pressure on the elliptic boundary ∂B; zero stress at infinity,

(ii) uniaxial tension at infinity parallel to an axis of the ellipse; ∂B stress free,

(iii) uniaxial tension at an arbitrary angle β to the major axis; ∂B stress free. This problem may be attacked either directly or by two applications of case (ii) and a suitable superposition of case (iv)

(iv) simple shear at infinity; ∂B stress free.

These stress fields have been investigated by Muskhelishvili (1963) using complex variable techniques. Case (i) was considered by Bhargava (1965) and by Jaswon, Maiti and Symm (1967) using the representation of a biharmonic function in the form $\chi = r^2\phi + \Psi$. However this formulation has not been previously exploited for the more general problems (ii), (iii) and (iv).

Our aim is to construct suitable biharmonic functions in terms of confocal elliptic coordinates. Some of these are evident in the known solution of (i), but new ones have to be introduced in order to solve the less symmetric problems that follow.

Uniform Internal Pressure on Elliptic Cavity

For problem (i) we consider uniform normal pressure P on the internal elliptic boundary ∂B :

$$\frac{x^2}{a^2} + \frac{y^2}{b^2} = 1 \; ; \qquad a \neq b . \tag{8.1}$$

In terms of confocal elliptic coordinates (ξ, η) (Appendix 5), (8.1) may be replaced by

$$\xi = \xi_0 = \ln\left(\frac{a+b}{c}\right) \tag{8.2}$$

where $c^2 = a^2 - b^2$ and

$$x = c\cosh\xi_0\cos\eta\,, \qquad y = c\sinh\xi_0\sin\eta \qquad \text{on } \partial B.$$

The analytic solution is known to be (Bhargava, 1959)

$$\chi = -P\left[\frac{c^2}{4}\left(e^{-2\xi} + \cos 2\eta\right) + \frac{(a^2+b^2)}{2}\xi\right] + \text{constant}. \tag{8.3}$$

Taking $P \equiv -1$, we seek to identify (8.3) with the representation

$$\chi = r^2\phi + \psi + \gamma\,; \qquad \nabla^2\phi = \nabla^2\psi = 0, \tag{8.4}$$

where γ is a constant. Since $\xi \to \ln r - \ln\frac{c}{2}$ as $r \to \infty$, $\gamma = 0$ if in (8.3) we put

$$\text{constant} = \left(\frac{a^2+b^2}{2}\right)\ln\frac{c}{2}\,, \tag{8.5}$$

i.e.

$$\chi = \frac{c^2}{4}\left(e^{-2\xi} + \cos 2\eta\right) + \frac{a^2+b^2}{2}\left(\xi - \ln\frac{2}{c}\right). \tag{8.6}$$

It is clear from (8.6) that $\chi = O(\ln r)$ as $r \to \infty$ which ensures that the medium has no dislocations and no stresses at infinity. Comparison of (8.4) with (8.6) yields

$$\phi = \frac{1}{2}\left(\frac{e^{-2\xi} + \cos 2\eta}{\cosh 2\xi + \cos 2\eta}\right) = O\left(r^{-2}\right) \quad \text{as } r \to \infty, \tag{8.7}$$

$$\psi = \frac{a^2+b^2}{2}\left(\xi - \ln\frac{2}{c}\right) = O(\ln r) \quad \text{as } r \to \infty, \tag{8.8}$$

Since by (A5.9)

$$r^2 = \frac{c^2}{2}\left(\cosh 2\xi + \cos 2\eta\right). \tag{8.9}$$

It is interesting to note that (8.7) possesses the expansion

$$\phi = \sum_{n=1}^{\infty}(-1)^{n+1}\frac{\cos 2n\eta}{e^{2n\xi}} \tag{8.10}$$

which shows that ϕ is a harmonic function. On the boundary ∂B which is defined by (8.2), (8.6) reduces to

$$\chi = \frac{r^2}{2}\left(1 - \frac{ab}{r^2}\right) + \frac{a^2+b^2}{2}\ln\left(\frac{a+b}{2}\right) \tag{8.11}$$

showing that

$$\left.\begin{aligned} \phi &= \tfrac{1}{2}\left(1 - \frac{ab}{r^2}\right), \\ \psi &= \frac{a^2+b^2}{2}\ln\left(\frac{a+b}{2}\right), \end{aligned}\right\} \quad \text{on } \partial B. \tag{8.12}$$

To find the boundary normal derivative of (8.6) we use

$$\frac{\partial}{\partial n} = \frac{\sqrt{2}}{c\sqrt{\cosh 2\xi - \cos 2\eta}}\frac{\partial}{\partial \xi}, \tag{8.13}$$

$$\cosh 2\xi_0 = \frac{a^2+b^2}{c^2}, \qquad e^{\xi_0} = \frac{a+b}{c}, \tag{8.14}$$

and obtain after simplification

$$\chi' = \frac{\sqrt{2}\ ab}{(a^2+b^2-c^2\cos 2\eta)^{1/2}} \quad \text{on } \partial B, \tag{8.15}$$

$$\phi' = \frac{-\sqrt{2}\,c^2\left[c^2+(a^2+b^2)\cos 2\eta\right]}{(a^2+b^2+c^2\cos 2\eta)^{1/2}(a^2+b^2-c^2\cos 2\eta)^{1/2}} \quad \text{on } \partial B, \tag{8.16}$$

$$\psi' = \frac{\sqrt{2}\,(a^2+b^2)}{2(a^2+b^2-c^2\cos 2\eta)^{1/2}} \quad \text{on } \partial B. \tag{8.17}$$

Unstressed Elliptic Cavity: Uniaxial Tension at Infinity Parallel to Minor Axis.

We now consider an infinite medium with an unstressed infinite cavity of elliptic cross-section defined by (8.1). For uniaxial tension at infinity parallel to the minor axis we have

$$\hat{yy} = T, \qquad \hat{xy} = \hat{xx} = 0 \tag{8.18}$$

at infinity, whilst on ∂B

$$\hat{nn} = \hat{ns} = 0.$$

The problem may be regarded as the superposition of

(1) uniaxial tension throughout B given by (8.18),

(2) the stress field generated by a stress $\hat{yy} = -T$ applied everywhere on ∂B.

For the simple tension (1) the solution is

$$\chi_1 = \tfrac{1}{2}Tx^2 \quad \text{in B} \tag{8.19}$$

while (2) is characterized by a biharmonic function χ_2 satisfying

$$\left.\begin{aligned} \chi_2 &= -\tfrac{1}{2} T x^2, \\ \chi_2' &= -T x x', \end{aligned}\right\} \quad \text{on } \partial B. \qquad (8.20)$$

The conditions (8.20) imply $\chi = \chi' = 0$ on ∂B.

Thus for the appropriate biharmonic function χ, represented as $\chi_1 + \chi_2$ we have

$$\chi_1 = \frac{Tc^2}{4} \cosh^2\xi (\cos 2\eta + 1) \qquad \text{in } B, \qquad (8.21)$$

while χ_2 may be determined from its boundary properties:

$$\left.\begin{aligned} \chi_2 &= \frac{-Ta^2}{4}(1+\cos 2\eta) \\ \chi_2' &= \frac{-\lambda T a b}{2}(1+\cos 2\eta) \end{aligned}\right\} \quad \text{on } \partial B, \qquad (8.22)$$

where

$$\lambda = \frac{\sqrt{2}}{c}(\cosh 2\xi_0 - \cos 2\eta)^{-\frac{1}{2}}$$

arises from the normal derivative operator (8.13) in confocal elliptic coordinates (A5.15).

A suitable biharmonic function satisfying

$$\chi = O(\ln r) \text{ as } r \to \infty \qquad (8.23)$$

is

$$\chi_2 = A(e^{-2\xi} + \cos 2\eta) + B\xi + D + Ee^{-2\xi}\cos 2\eta, \qquad (8.24)$$

where the constants A, B, D, E are found by constraining (8.24) to obey the boundary conditions (8.22). Thus

$$\left.\begin{aligned} -\frac{Ta^2}{4}(1+\cos 2\eta) &= A\left(\frac{c^2}{(a+b)^2} + \cos 2\eta\right) + B\xi_0 + D + \frac{Ec^2}{(a+b)^2}\cos 2\eta, \\ -\frac{Tab}{2}(1+\cos 2\eta) &= \frac{-2Ac^2}{(a+b)^2} + B - \frac{2Ec^2}{(a+b)^2}\cos 2\eta. \end{aligned}\right\} \qquad (8.25)$$

Hence from 4 equations in the 4 unknown constants which arise from equating the coefficients of $\cos 2\eta$ and the constant terms, we deduce

$$A = \frac{-Ta(a+b)}{4}, \qquad B = \frac{-Ta^2}{2},$$

$$D = \frac{-Tab}{4} + \frac{Ta^2\xi_0}{2}, \qquad E = \frac{Tab(a+b)^2}{4c^2}.$$

Thus the complete solution is given by

$$\begin{aligned}\chi &= \chi_1 + \chi_2 \\ &= \frac{Tc^2}{4}\cosh^2\xi\,(\cos 2\eta + 1) - \frac{Ta(a+b)}{4}\left(e^{-2\xi} + \cos 2\eta\right) \\ &\quad - \frac{Ta^2\xi}{2} - \frac{Tab}{4} + \frac{Ta^2\xi_0}{2} + \frac{Tab(a+b)^2}{4c^2}\left(e^{-2\xi}\cos 2\eta\right).\end{aligned} \tag{8.26}$$

Comparing (8.26) with (8.4) we find

$$\left.\begin{aligned}\phi &= \frac{-Ta}{2(a-b)}\left(\frac{e^{-2\xi} + \cos 2\eta}{\cosh 2\xi + \cos 2\eta}\right), \\ \psi &= B\xi + Ee^{-2\xi}\cos 2\eta, \\ \gamma &= D\,.\end{aligned}\right\} \tag{8.27}$$

From (8.7), (8.9) and (8.10) we see that ϕ is harmonic and

$$\phi = O\left(\frac{1}{r^2}\right) \qquad \text{as} \qquad r \to \infty\,, \tag{8.28}$$

while ψ is clearly harmonic and has the required asymptotic behaviour

$$\psi \to B\ln r + O\left(\frac{1}{r^2}\right) \text{as} \qquad r \to \infty\,. \tag{8.29}$$

The hoop stress $\hat{\eta\eta}$ on ∂B may be found easily from the boundary conditions

$$\hat{\xi\eta} = \hat{\xi\xi} = 0 \qquad \text{on} \qquad \xi = \xi_0\,,$$

which, by virtue of (7.2) and the invariant property of $\mathcal{H}$, yields

$$\hat{\eta\eta} = \nabla^2\chi \qquad \text{on } \partial B. \tag{8.30}$$

Thus harmonic terms in (8.26) do not contribute to the hoop stress

$$\begin{aligned}\hat{\eta\eta} &= A\nabla^2\left(e^{-2\xi} + \cos 2\eta\right) + \frac{T}{2}\nabla^2 x^2 \\ &= T - \frac{2Ta(a+b)\left(e^{-2\xi_0} - \cos 2\eta\right)}{c^2\left(\cosh 2\xi_0 - \cos 2\eta\right)} \qquad \text{on } \partial B \end{aligned} \tag{8.31}$$

$$= Te^{2\xi_0}\left[\frac{\sinh 2\xi_0\,(1+e^{-2\xi_0})}{\cosh 2\xi_0 - \cos 2\eta} - 1\right] \qquad \text{on } \partial B, \tag{8.32}$$

which is in agreement with the classical result (Timoshenko

and Goodier, 1970) derived from complex potentials. Maximum and minimum values of $\hat{\eta\eta}$ are found by putting $\cos 2\eta = \pm 1$ so that

$$\left.\begin{aligned} \eta\eta_{max.} &= T\left(1+\frac{2a}{b}\right) \quad \text{at} \quad x = \pm a, y = 0; \\ \eta\eta_{min.} &= -T \qquad\qquad \text{at} \quad x = 0, y = \pm b. \end{aligned}\right\} \quad (8.33)$$

Unstressed Elliptic Cavity: Uniaxial Tension at Infinity Parallel to Major Axis.

By the same procedure we find a biharmonic function χ producing stresses

$$\hat{xx} = T, \qquad \hat{xy} = \hat{yy} = 0$$

at infinity, and

$$\hat{nn} = \hat{ns} = 0 \qquad \text{on } \partial B.$$

The results are

$$\chi = \chi_1 + \chi_2,$$

where

$$\chi_1 = \frac{Tc^2}{4}\sinh^2\xi\,(1-\cos 2\eta),$$

$$\chi_2 = A\left(e^{-2\xi}+\cos 2\eta\right) + B\xi + D + E\,e^{-2\xi}\cos 2\eta, \quad (8.34)$$

where

$$A = \frac{Tb(a+b)}{4}, \qquad B = -\frac{Tb^2}{2},$$

$$D = -\frac{Tab}{4} + \frac{Tb^2\xi_0}{2}, \qquad E = -\frac{Tab(a+b)^2}{4c^2}.$$

The hoop stress on ∂B (c.f. 8.31) is

$$\hat{\eta\eta} = T + \frac{2Tb(a+b)\left(e^{-2\xi_0}-\cos 2\eta\right)}{c^2\left(\cosh 2\xi_0 - \cos 2\eta\right)}, \quad (8.35)$$

which yields results comparable with equations (8.33):

$$\hat{\eta\eta}_{max.} = T\left(1+\frac{2b}{a}\right) \qquad \text{at} \quad x = 0, y = \pm b;$$

$$\hat{\eta\eta}_{min.} = -T \qquad\qquad \text{at} \quad x = \pm a, y = 0.$$

It is notable that $\hat{\eta\eta}_{max.} \to T$ as $\frac{a}{b} \to \infty$ whereas if the simple tension at infinity is parallel to the minor axis $\hat{\eta\eta}_{max.} \to \infty$ as $\frac{a}{b} \to \infty$.

Simple Tension at Infinity at an Angle β to the Major Axis of the Elliptic Cavity.

We consider now an infinite material in a state of simple tension at an angle β below the x - axis, disturbed by an elliptic cavity with its major axis along the x - axis (Figure 29).

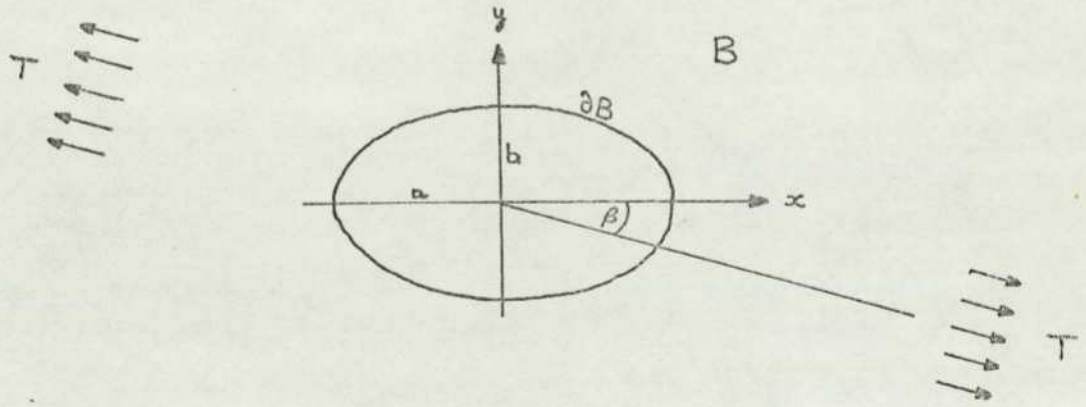


FIG. 29

The undisturbed stress field is given by

$$\left.\begin{aligned} \hat{xx} &= \frac{T}{2}(1+\cos 2\beta), \\ \hat{yy} &= \frac{T}{2}(1-\cos 2\beta), \\ \hat{xy} &= \frac{-T}{2}\sin 2\beta . \end{aligned}\right\} \qquad (8.36)$$

With a convenient choice of constants of integration, the corresponding Airy stress function is

$$\chi_1 = \frac{Ty^2}{4}(1+\cos 2\beta) + \frac{Tx^2}{4}(1-\cos 2\beta) + \frac{Txy}{2}\sin 2\beta . \qquad (8.37)$$

Our problem is to find $\chi = \chi_1 + \chi_2$ in B where χ_2 satisfies

$$\nabla^4 \chi_2 = 0 \qquad \text{in B,} \qquad (8.38)$$

$$\chi_2 = -\chi_1 , \quad \chi_2' = -\chi_1' \text{ on } \partial B. \qquad (8.39)$$

To this end we express χ_1 in confocal elliptic coordinates and note that ∂B is given by

$$\left.\begin{aligned} x &= c\cosh\xi_0\cos\eta, & y &= c\sinh\xi_0\sin\eta; \\ \cosh\xi_0 &= \frac{a}{c}, & \sinh\xi_0 &= \frac{b}{c} . \end{aligned}\right\} \qquad (8.40)$$

We also differentiate (8.37) along the normal to ∂B, drawn into B, using (8.13). Hence, after simplification,

the boundary conditions (8.39) become

$$\chi_2 = -\frac{T}{8}(a^2+b^2) + \frac{T}{8}(a^2-b^2)\cos 2\beta + \frac{T\cos 2\eta}{8}\left[b^2(1+\cos 2\beta) - a^2(1-\cos 2\beta)\right] - \frac{Tab}{4}\sin 2\eta \sin 2\beta , \tag{8.41}$$

$$\frac{\chi_2'}{\lambda} = -\frac{Tab}{2}\left[1-\cos 2\eta \cos 2\beta\right] - \frac{T(a^2+b^2)}{4}\sin 2\beta \sin 2\eta . \tag{8.42}$$

To proceed as before we must now construct a biharmonic function χ_2 which satisfies (8.41) and (8.42) and exhibits the required asymptotic behaviour, i.e.

$$\left.\begin{aligned} &\chi_2 = r^2\phi + \psi \quad \text{where} \quad \nabla^2\phi = \nabla^2\psi = 0 \quad \text{and} \\ &\phi = O\left(\tfrac{1}{r^2}\right), \\ &\psi \to B\ln r + D + O\left(\tfrac{1}{r}\right) \end{aligned}\right\} \tag{8.43}$$

as $r \to \infty$, where B and D are constants.

This problem exhibits less symmetry than any previously considered by this formulation and it is clear from the boundary conditions that χ_2 must depend on $\sin 2\eta$ as well as $\cos 2\eta$. At first sight there appears to be no problem. We merely require the sine term corresponding to the harmonic function

$$\phi = \frac{e^{-2\xi} + \cos 2\eta}{r^2} \tag{8.44}$$

employed previously. However $\frac{e^{-2\xi} + \sin 2\eta}{r^2}$ is not harmonic. This result is less surprising if r^2 is replaced by $\frac{c^2}{2}(\cosh 2\xi + \cos 2\eta)$ but there remains the problem of finding the harmonic function analogous to (8.44). To make progress we revert to the expansion in series (8.10):

$$\phi = \frac{1}{2}\left(\frac{e^{-2\xi} + \cos 2\eta}{\cosh 2\xi + \cos 2\eta}\right) = \sum_{n=1}^{\infty}(-1)^{n+1}\frac{\cos 2n\eta}{e^{2n\xi}} , \tag{8.45}$$

and consider the corresponding series

$$\phi = \sum_{n=1}^{\infty}(-1)^{n+1}\frac{\sin 2n\eta}{e^{2n\xi}} . \tag{8.46}$$

After expressing $\sin 2n\eta$ in terms of exponential functions we find the sum of this series to be

$$\phi = \frac{1}{2}\left(\frac{\sin 2\eta}{\cosh 2\xi + \cos 2\eta}\right) \tag{8.47}$$

so that $\frac{\sin 2\eta}{r^2}$ is the required harmonic function. Thus we have the most interesting result that $\sin 2\eta$ is biharmonic, the "conjugate" biharmonic function being not $\cos 2\eta$ but $e^{-2\xi} + \cos 2\eta$.

With this established we may express the required biharmonic function χ_2 in the form

$$\chi_2 = A(e^{-2\xi} + \cos 2\eta) + B\xi + D + Ee^{-2\xi}\cos 2\eta + Fe^{-2\xi}\sin 2\eta + G\sin 2\eta \qquad (8.48)$$

where A,B,D,E,F,G are constants to be determined. The component harmonic functions

$$\left.\begin{aligned} \phi &= A\left(\frac{e^{-2\xi} + \cos 2\eta}{r^2}\right) + G\,\frac{\sin 2\eta}{r^2}, \\ \psi &= B\xi + D + Ee^{-2\xi}\cos 2\eta + Fe^{-2\xi}\sin 2\eta, \end{aligned}\right\} \qquad (8.49)$$

possess the required asymptotic behaviour (8.43) since

$$\xi = O(\ln r), \qquad e^{-2\xi} = O\left(\frac{1}{r^2}\right) \quad \text{as } r \to \infty.$$

We now constrain (8.48) to satisfy the boundary conditions using (8.13) again for the normal derivative. Equating coefficients of $\cos 2\eta$, $\sin 2\eta$ and the constant term in each of equations (8.41) and (8.42) we have six equations in the six unknowns A,B,D,E,F,G yielding after simplification :

$$\left.\begin{aligned} A &= \frac{T}{4}(a+b)(b\cos^2\beta - a\sin^2\beta), \\ B &= -\frac{T}{2}(a^2\sin^2\beta + b^2\cos^2\beta), \\ D &= -\frac{Tab}{4} + \frac{T\xi_0}{2}(a^2\sin^2\beta + b^2\cos^2\beta), \\ E &= \frac{-Tab(a+b)^2\cos 2\beta}{4(a-b)^2}, \\ F &= \frac{T(a+b)^2(a^2+b^2)\sin 2\beta}{8(a-b)^2}, \\ G &= -\frac{T}{8}(a+b)^2\sin 2\beta. \end{aligned}\right\} \qquad (8.50)$$

The complete solution to the problem is given by

$$\left.\begin{aligned} \chi &= \chi_1 + \chi_2 \\ &= \frac{T}{2}(x^2\sin^2\beta + y^2\cos^2\beta + xy\sin 2\beta) \\ &\quad + A(e^{-2\xi} + \cos 2\eta) + G\sin 2\eta \\ &\quad + B\xi + D + Ee^{-2\xi}\cos 2\eta + Fe^{-2\xi}\sin 2\eta. \end{aligned}\right\} \qquad (8.51)$$

If $\beta = \frac{\pi}{2}$ we recover the result (8.26) as expected.

Unstressed Elliptic Cavity: Simple Shear at Infinity.

The undisturbed stress field for a simple shear

$$\hat{xy} = S, \qquad \hat{xx} = \hat{yy} = 0,$$

is generated by the Airy stress function

$$\chi_1 = -Sxy = -\frac{Sc^2}{4}\sinh 2\xi \sin 2\eta.$$

When the elliptic cavity $\xi = \xi_0$ is introduced the complete solution becomes

$$\chi = \chi_1 + \chi_2$$

where

$$\nabla^4 \chi_2 = 0 \qquad \text{in B,} \tag{8.52}$$

$$\left.\begin{aligned} \chi_2 &= \tfrac{1}{2} Sab \sin 2\eta, \\ \chi_2' &= \tfrac{1}{2}\lambda Sab(a^2+b^2)\sin 2\eta \end{aligned}\right\} \text{ on } \partial B. \tag{8.53}$$

The boundary conditions (8.53) can be satisfied by taking χ_2 in the form

$$\chi_2 = Fe^{-2\xi}\sin 2\eta + G \sin 2\eta, \tag{8.54}$$

where F and G are constants determined by substituting for the boundary values of (8.54) and its normal derivative in equations (8.53). Hence we find

$$\chi = -\tfrac{1}{4}Sc^2 \sinh 2\xi \sin 2\eta + \tfrac{1}{4}S(a+b)^2 \sin 2\eta \left[1 - \frac{(a^2+b^2)}{c^2} e^{-2\xi}\right]. \tag{8.55}$$

This solution possesses the required asymptotic behaviour since $\chi \to -Sxy + O(1)$ as $r \to \infty$.

The hoop stress $\hat{\eta\eta}$ on ∂B may be found from

$$\nabla^2 \chi = G \nabla^2 \sin 2\eta \tag{8.56}$$

which takes the value

$$\hat{\eta\eta} = \frac{-2Se^{2\xi_0}\sin 2\eta}{\cosh 2\xi_0 - \cos 2\eta} \qquad \text{on } \partial B \tag{8.57}$$

whence $\hat{\eta\eta} = 0$ at the ends of the minor axes and

$$\left.\begin{aligned} \hat{\eta\eta} = \hat{\eta\eta}_{\max.} &= \frac{S(a+b)^2}{ab} \qquad \text{if } \tan\eta = \frac{b}{a}, \\ \hat{\eta\eta} = \hat{\eta\eta}_{\min.} &= \frac{-S(a+b)^2}{ab} \qquad \text{if } \tan\eta = \frac{-b}{a}. \end{aligned}\right\} \tag{8.58}$$

As $\frac{a}{b} \to \infty$, $\left|\hat{\eta\eta}_{\max.}\right| = \left|\hat{\eta\eta}_{\min.}\right| \to \infty$

and the points at which these maxima and minima occur approach the ends of the major axis.

Conclusion

The derivation of χ for uniaxial tension at infinity at an arbitrary angle β to the major axis of the elliptic cavity may be viewed as the most general and original contribution of this chapter. We conclude by analyzing this χ as the resultant of three simple stress fields at infinity, each disturbed by the same elliptic cavity. According to (8.36) the fields are : uniaxial tensions $T\cos^2\beta$, $T\sin^2\beta$ parallel to the x and y axes respectively, together with a Cartesian shear stress $\widehat{xy} = -T\sin\beta\cos\beta$. It is evident that the new harmonic term (8.47) corresponding to the biharmonic $\sin 2\eta$ is required whenever shear stress is present with respect to the major and minor axes of the ellipse.

The result (8.51) is recovered by adding together

(a) (8.34) with T replaced by $T\cos^2\beta$,

(b) (8.26) with T replaced by $T\sin^2\beta$,

(c) (8.55) with S replaced by $-T\sin\beta\cos\beta$.

The terms of χ are displayed in table 60 which shows how the individual terms arise from (a), (b) or (c). Terms involving $\sin 2\eta$ appear only in column (c). The four lower rows are the harmonic terms.

	(a) Tension parallel to x - axis	(b) Tension parallel to y-axis	(c) Shear
χ, terms	$\frac{Tc^2}{2}\sinh^2\xi\sin^2\eta\cos^2\beta$	$\frac{Tc^2}{2}\cosh^2\xi\cos^2\eta\sin^2\beta$	$\frac{Tc^2}{8}\sinh 2\xi\sin 2\eta\sin 2\beta$
$r^2\phi$ terms	$\frac{Tb(a+b)}{4}\cos^2\beta\left(e^{-2\xi}+\cos 2\eta\right)$	$\frac{-Ta(a+b)}{4}\sin^2\beta\left(e^{-2\xi}+\cos 2\eta\right)$	$\frac{-T(a+b)^2}{8}\sin 2\eta\sin 2\beta$
Coefficients of ξ	$-\frac{Tb^2}{2}\cos^2\beta$	$-\frac{Ta^2}{2}\sin^2\beta$	0
Constant terms	$-\frac{Tab}{4}\cos^2\beta+\frac{Tb^2\xi_0\cos^2\beta}{2}$	$-\frac{Tab}{4}\sin^2\beta+\frac{Ta^2\xi_0\sin^2\beta}{2}$	0
Coefficients of $\frac{\cos 2\eta}{e^{2\xi}}$	$-\frac{Tab(a+b)^2}{4c^2}\cos^2\beta$	$\frac{Tab(a+b)^2}{4c^2}\sin^2\beta$	0
Coefficients of $\frac{\sin 2\eta}{e^{2\xi}}$	0	0	$\frac{T(a^2+b^2)(a+b)^2\sin 2\beta}{8c^2}$

TABLE 60

The hoop stress $\hat{\eta\eta}$ on ∂B may be found by making the substitutions of (a), (b), (c) in equations (8.35), (8.31), (8.57) respectively. Addition gives

$$\hat{\eta\eta} = \frac{T}{(\cosh 2\xi_0 - \cos 2\eta)}\left[\sinh 2\xi_0 + \cos 2\beta - e^{2\xi_0}\cos(\beta-\eta)\right] \quad \text{on } \partial B$$

which is in agreement with the classical result.

Addendum: Special Case of Circular Cavity

If $a = b$ in (8.1) we have a circle with radius $r = a$. The solutions (8.6), (8.26) are then obviously inappropriate since $c = 0$. However, for the pressure problem, a direct approach utilising (8.4) gives

$$\chi = -Pa^2(\ln r - \ln a + \tfrac{1}{2}). \qquad (8.59)$$

This is in agreement with the classical solution in which two complex potential functions are used. They lead to a corresponding Airy stress function $\chi = -Pa^2\ln r$ which differs from (8.59) only by an additive constant.

We now consider an infinite medium with an unstressed infinite cavity of circular cross section, subject to uniaxial tension T at infinity. The problem may be regarded as the superposition of

(1) uniaxial tension throughout B given by (8.18), i.e. $\chi_1 = -\frac{1}{2}Tr^2\cos 2\theta$;

(2) the stress field generated by a stress $\hat{yy} = -T$ applied everywhere on ∂B.

Accordingly χ_1, and χ_2 may be defined as in (8.19) and (8.20) and χ_2 put in the form (8.4). Suitable harmonic functions satisfying (8.28) and (8.29) are

$$\phi = \frac{A\cos 2\theta}{r^2} + \frac{B\sin 2\theta}{r^2},$$

$$\psi = C\ln r + \left(\frac{D\cos 2\theta}{r^2} + \frac{E\sin 2\theta}{r^2}\right),$$

where A,B,C,D,E are constants. Symmetry requires $B = E = 0$ so that

$$\chi_2 = A\cos 2\theta + C\ln r + \frac{D\cos 2\theta}{r^2} + \gamma. \qquad (8.60)$$

In the usual way we may now use the boundary conditions to obtain equations for the unknowns A,C,D,γ. The result

$$\chi = \chi_1 + \chi_2$$

$$= \frac{Tr^2}{4}(\cos 2\theta + 1) - \frac{Ta^2}{2}\ln r - \frac{Ta^2}{2}\cos 2\theta$$

$$+ \frac{Ta^4}{4}\frac{\cos 2\theta}{r^2} - \frac{Ta^2}{4}(1 - 2\ln a) \qquad (8.61)$$

also agrees with the classical complex variable result (Muskhelishvili, 1963) apart from an additive constant. We further note that the solution for χ in (8.26) is asymptotic to (8.61) if we let $\xi \to \infty$ ($\eta \to \theta$, $\cosh^2 \xi \to \frac{r^2}{c^2}$) and $b \to a$.

CHAPTER 9

EXTERIOR NUMERICAL SOLUTIONS

Numerical Analysis

In chapter 7 it was shown that the solution of an elliptic cavity problem can be obtained by solving a pair of coupled integral equations (7.25) and so generating the Airy stress function throughout B. The numerical procedures of part I were followed and n nodal points defined on ∂B using equal eccentric angles. Equations (7.25) and (7.26) have been solved as an algebraic system which may be expressed in matrix notation as

$$\underline{A}\,\underline{x} = \underline{B}\,, \tag{9.1}$$

where

$$\underline{A} = \left(\begin{array}{c|c|c} & & 1\ 1\ \cdots\ 1 \\ \hdashline & \underline{A}_1 & 0\ 0\ \cdots\ 0 \\ \hdashline h_1\ h_2\ \cdots\ h_n & 0\ 0\ \cdots\ 0 & 0 \end{array}\right), \tag{9.2}$$

$$\underline{x} = \begin{pmatrix} \sigma_1 \\ \sigma_2 \\ \vdots \\ \sigma_n \\ \mu_1 \\ \mu_2 \\ \vdots \\ \mu_n \\ \gamma \end{pmatrix}, \qquad \underline{B} = \begin{pmatrix} \chi_1 \\ \chi_2 \\ \vdots \\ \chi_n \\ \chi_1' \\ \chi_2' \\ \vdots \\ \chi_n' \\ 0 \end{pmatrix}. \tag{9.3}$$

The square matrix $\underline{A}$ has degree $2n + 1$ and is related to the corresponding matrix $\underline{A}_1$, which arises from the numerical solution of the Garabedian problem((5.19) and (5.20)). More precisely $\underline{A}$ consists of the coefficients of $\underline{A}_1$, augmented as shown in (9.2) with the following alteration. The matrix $\underline{A}_1$ is assembled from the coefficients of the $n \times n$ matrices used in the Dirichlet and Neumann problems, but whereas equation (4.5) was used in the interior Neumann problem for terms on the main diagonal, we must now use

$$\int_r \ln|\underline{q}-\underline{q}_r|'\,dq = \pi - \sum_{\substack{i=1\\ i\neq r}}^{n} \ln'|\underline{q}-\underline{q}_r|\,dq \qquad (9.4)$$

which is relevant to an exterior problem.

From the solution of (9.1), the functions ϕ, ψ and hence χ were generated in B by the methods of chapter 7. Stress combinations were then found by differentiation. The required functions (7.32) to (7.34) were computed from the formulae

$$\phi = \sum_{q=1}^{n} \sigma_q \ln|\underline{P}-\underline{q}|\,dq_q, \qquad (9.5)$$

where

$$|\underline{P}-\underline{q}| = \left[(x_p-x_q)^2+(y_p-y_q)\right]^{1/2}, \qquad (9.6)$$

$$\phi_x = \sum_{q=1}^{n} \sigma_q \frac{(x_p-x_q)}{|\underline{P}-\underline{q}|^2}\,dq_q, \qquad (9.7)$$

$$\phi_y = \sum_{q=1}^{n} \sigma_q \frac{(y_p-y_q)}{|\underline{P}-\underline{q}|^2}\,dq_q, \qquad (9.8)$$

$$\phi_{xx} = \sum_{q=1}^{n} \sigma_q \frac{|\underline{P}-\underline{q}|^2-2(x_p-x_q)^2}{|\underline{P}-\underline{q}|^4}\,dq_q, \qquad (9.9)$$

$$\phi_{yy} = \sum_{q=1}^{n} \sigma_q \frac{|\underline{P}-\underline{q}|^2-2(y_p-y_q)^2}{|\underline{P}-\underline{q}|^4}\,dq_q, \qquad (9.10)$$

$$\phi_{xy} = \sum_{q=1}^{n} \sigma_q \frac{(-2)(x_p-x_q)(y_p-y_q)}{|\underline{P}-\underline{q}|^4}\,dq_q. \qquad (9.11)$$

To find ψ_x, ψ_y, ψ_{xx}, ψ_{yy}, ψ_{xy} we simply use the above formulae replacing σ_q by μ_q. We note that all the differentiations are with regard to $\underline{P}$ as variable while $\underline{q}$ remains fixed.

Using (9.5) to (9.11) we substitute into (7.27) and (7.35) and thus compute Θ, $4s^2$ over a mesh of field

points in B. Equations (7.27) and (7.35) refer in particular to the uniform pressure problem. Other problems may be solved by the methods of chapter 8 using appropriate boundary conditions. It must be remembered that, if a superposition of stress states is employed, the resultant χ must be used. Thus, for example, in the case of the unstressed elliptic cavity, if there is uniaxial tension at infinity parallel to the minor axis, the solution is

$$\chi = \chi_1 + \chi_2 = r^2\phi + \Psi + \gamma + \tfrac{1}{2}Tx^2$$

in the notation of chapter 8. Accordingly for the hydrostatic stress we use

$$\textcircled{H} = 4\left(\phi + x\frac{\partial\phi}{\partial x} + y\frac{\partial\phi}{\partial y}\right) + 1 \qquad (9.12)$$

instead of (7.27); and (7.35) is replaced by

$$4s^2 = \left[r^2(\phi_{yy} - \phi_{xx})^2 + 4(y\phi_y - x\phi_x) + \Psi_{yy} - \Psi_{xx} - T\right]^2$$

$$+ 4\left[r^2\phi_{xy} + 2(x\phi_y + y\phi_x) + \Psi_{xy}\right]^2. \qquad (9.13)$$

Results

In the manner indicated, the functions χ, $\textcircled{H}$, $4s^2$ were generated at the intersections of a square mesh of side 0.25 in the region

$$0 \le x \le 4, \qquad 0 \le y \le 2, \qquad \frac{x^2}{a^2} + \frac{y^2}{b^2} > 1.$$

Ellipses of various axial ratios were considered for each of the following problems :-

(i) uniform internal pressure P on ∂B; zero stress at infinity,

(ii) ∂B stress free; uniaxial tension T at infinity parallel to the minor axis.

Exact solutions are available for comparison from the analytic results of chapter 8.

It was found that results improved as n was increased, and good results were obtained with $n = 32$. All the results of figures 30 to 40 of pp.130 to 140 refer to this value of n. Accuracy is generally of the order of 1% except near the

boundary. It was found that results in this vicinity could be improved by using numerical differentiation of χ instead of differentiated kernels. Within this region a further slight improvement was obtained by replacing the generated values of χ by values obtained from polynomial interpolation along the mesh lines intersecting the boundary. However, for the purposes of part III, the results obtained wholly from differentiated kernels (pp.130 to 140) are acceptable.

The results are best displayed by diagrams showing contour lines on which the stress combinations are constant. These may be drawn by hand from an array of data (figure 32 is obtained from figure 30). Alternatively this process may be automated by employing a subroutine in the computer program which carries out the necessary interpolations to determine the entry and exit point of each contour as it passes through squares of the mesh. The necessary information is then stored on magnetic tape and played back to give output on a graph plotter. When this process is set up large numbers of contours may be drawn without much extra human effort. However, smoother curves may be drawn by hand unless a much finer mesh is used. An example of computer graph plotter output is included for comparison.

Analysis of Figures

The results for two different ellipses have been selected for display: 2/1 and $2/\frac{2}{5}$.

Figures 30 to 35 refer to problem (i) and the numbers refer to units of the dimensionless quantities Θ/P, $4s^2/P^2$.

Figure 30 gives a comparison between computed values of $4s^2$ and analytic values obtained from a convenient formula in Cartesian coordinates (Bhargava, 1959),

$$\frac{4s^2}{P^2} = \frac{4\,(b^4x^2 + a^4y^2)}{\left[(x^2+y^2-c^2)^2 + 4c^2y^2\right]^{3/2}} \qquad (9.14)$$

The symbol + is used when numerical results are not sufficiently accurate to be worth recording.

Figure 31 gives corresponding abbreviated results for Θ . The analytic values are derived from the formula

$$\frac{\Theta}{-P} = \nabla^2\chi = \frac{e^{-2\xi} - \cos 2\eta}{\sinh^2\xi + \sin^2\eta} \qquad (9.15)$$

which arises from (8.6) and (A5.13).

Figures 32 to 39 are placed in order so that results for the axial ratio 2 : 1 may be compared with those for $2 : \frac{2}{5}$.

Figures 32 and 34 show contours corresponding to the numerical values of figures 30 and 31.

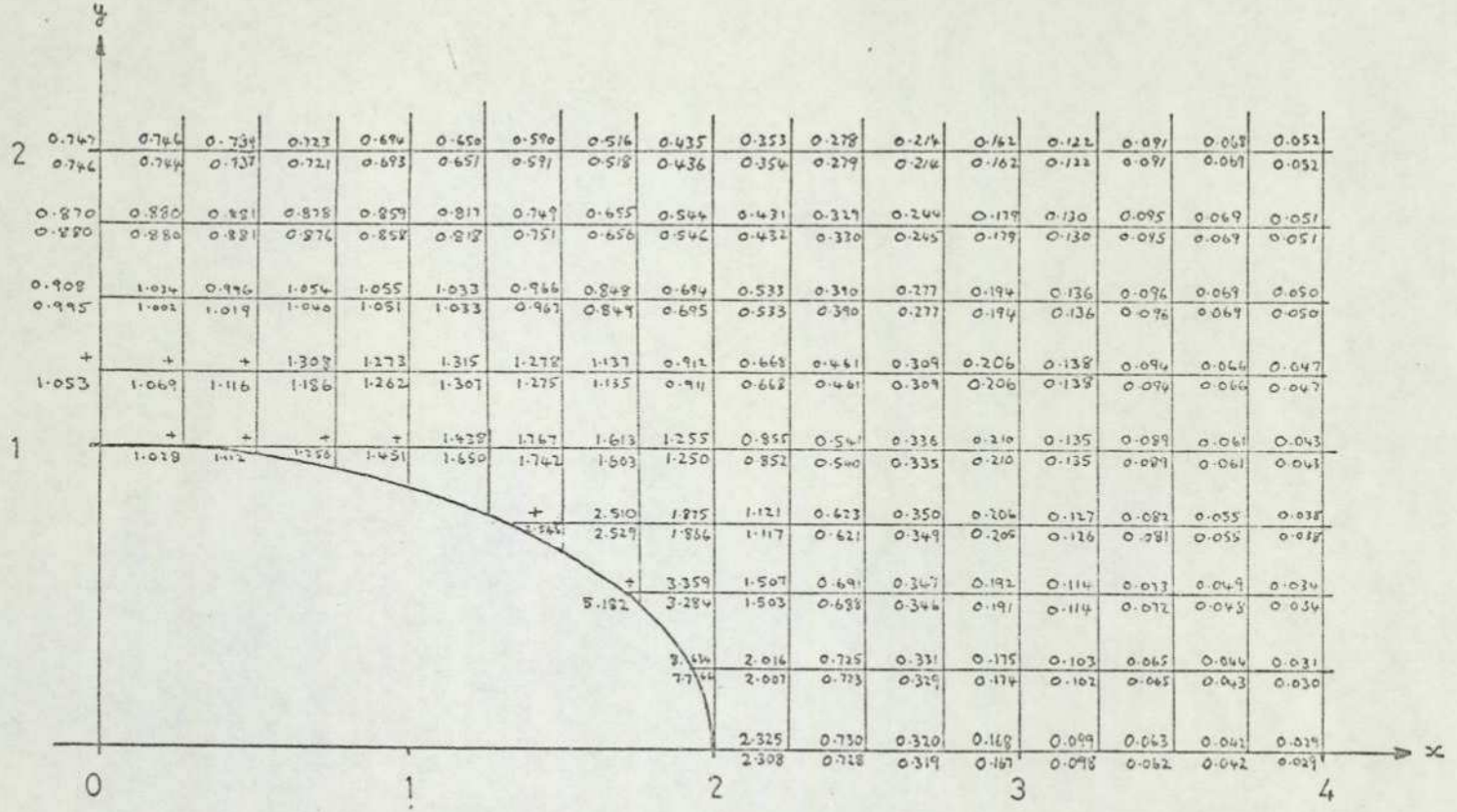
Figures 33 and 35 show the corresponding results for the $2 : \frac{2}{5}$ ellipse. In figure 33, broken lines indicate that the analytic solution has been used to complete the contours in the region where the computed solution is unacceptable. It is interesting to note that $4s^2$ is strictly increasing as the field point moves from infinity along the x-axis to the vertex of the ellipse; whereas $4s^2$ rises and then falls (unless $a = b$) as the end of the minor axis is approached along the line $x = 0$. In this case (9.14) becomes

$$4s^2 = \frac{4P^2a^4y^2}{(y^2+c^2)^3} .$$

This function of y attains a maximum value $\frac{16P^2a^4}{27c^4}$ at the points $y = \pm\sqrt{\frac{a^2-b^2}{2}}$. This, of course, does not imply that $4s^2$ attains a maximum there.

Figures 36 to 39 refer to problem (ii) and follow the same sequence as 32 to 35. Numbers refer to units of the dimensionless quantities Θ/T , $4s^2/T^2$.

Figure 40 shows graph plotter output obtained automatically from the computed results after using the contour subroutine. It should be compared with the region $2 \leq x \leq 4$, $0 \leq y \leq 2$ of figure 36.

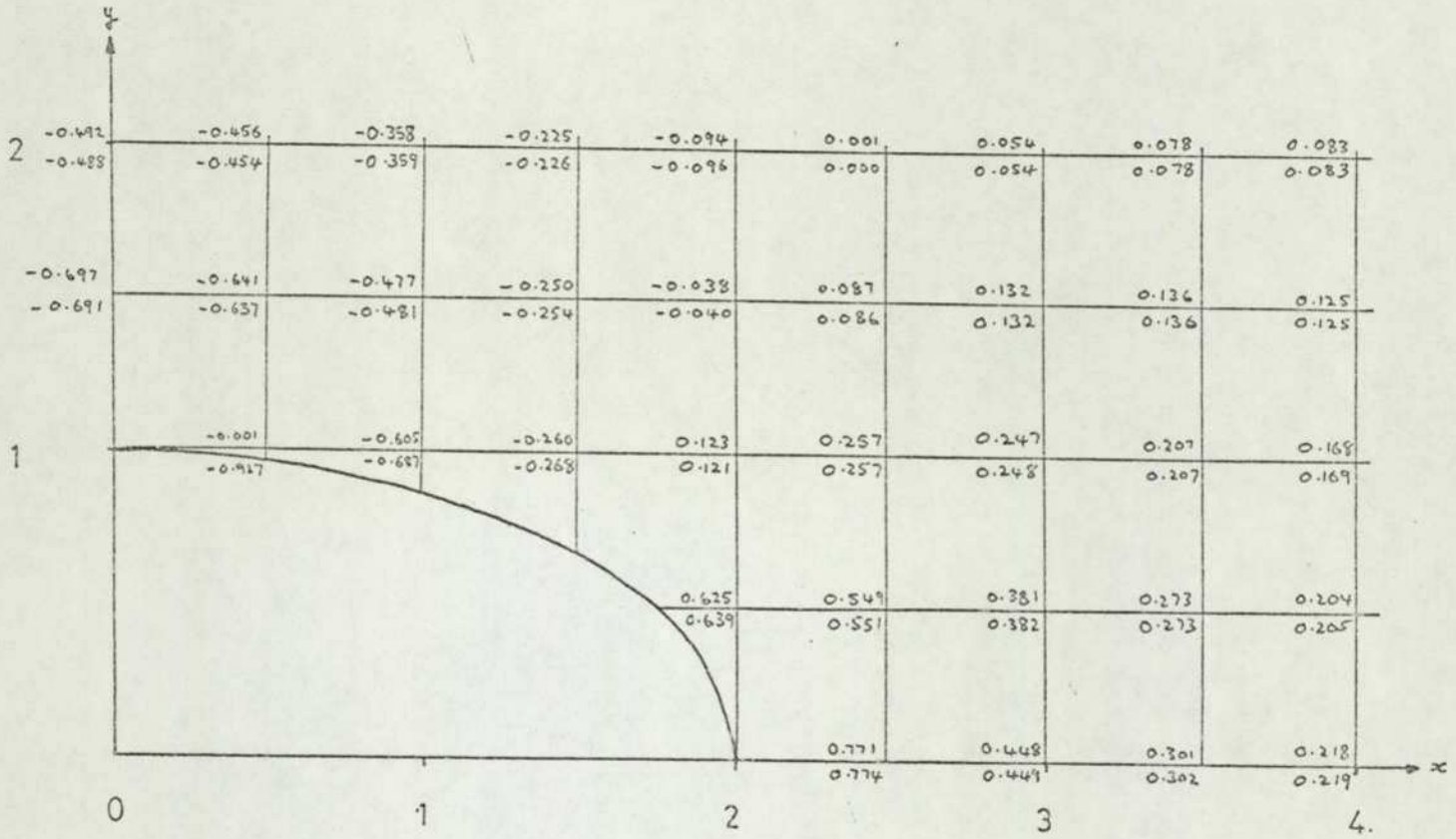


Upper figure : numerical value of $4s^2$.

Lower figure : analytical value of $4s^2$.

Uniform Pressure. 2:1 Ellipse.

Figure 30.

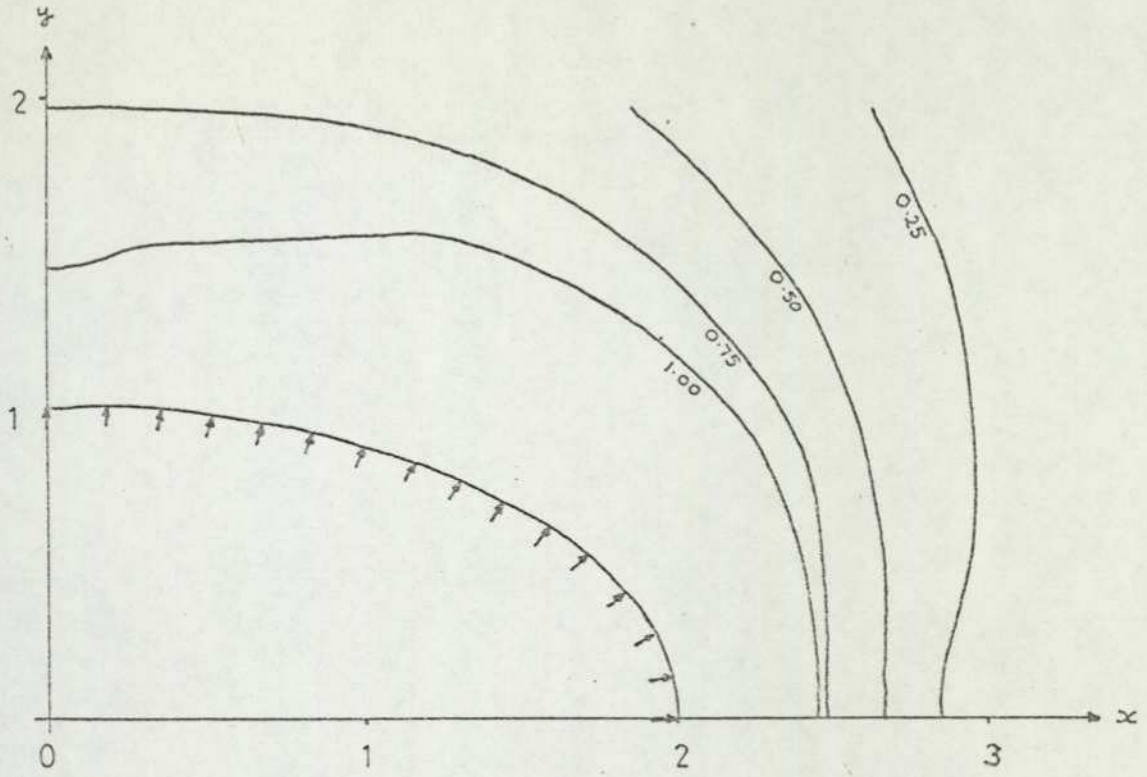


Upper figure : numerical value of Θ.

Lower figure : analytical value of Θ.

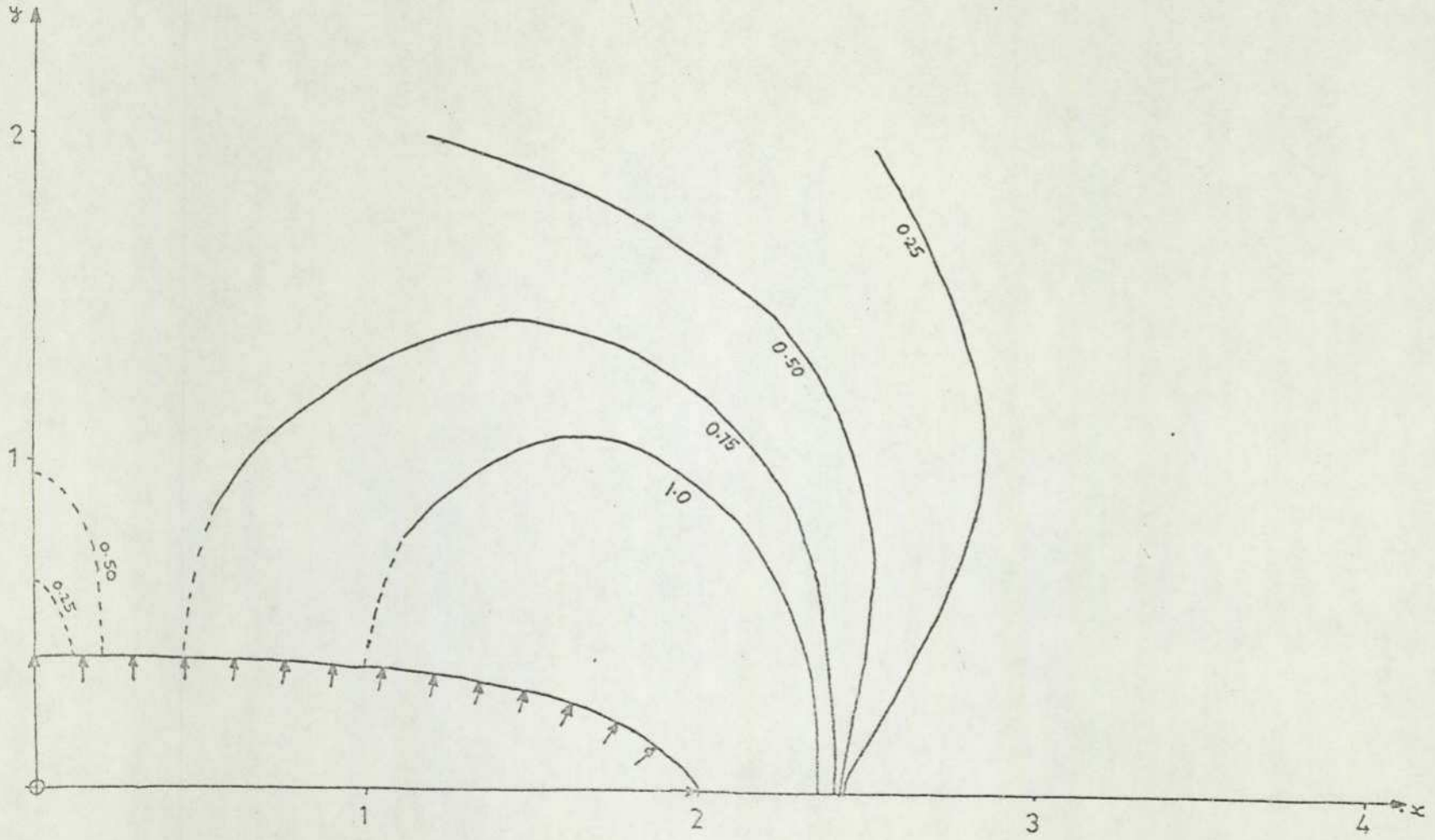
Uniform Pressure. 2:1 Ellipse.

Figure 31.



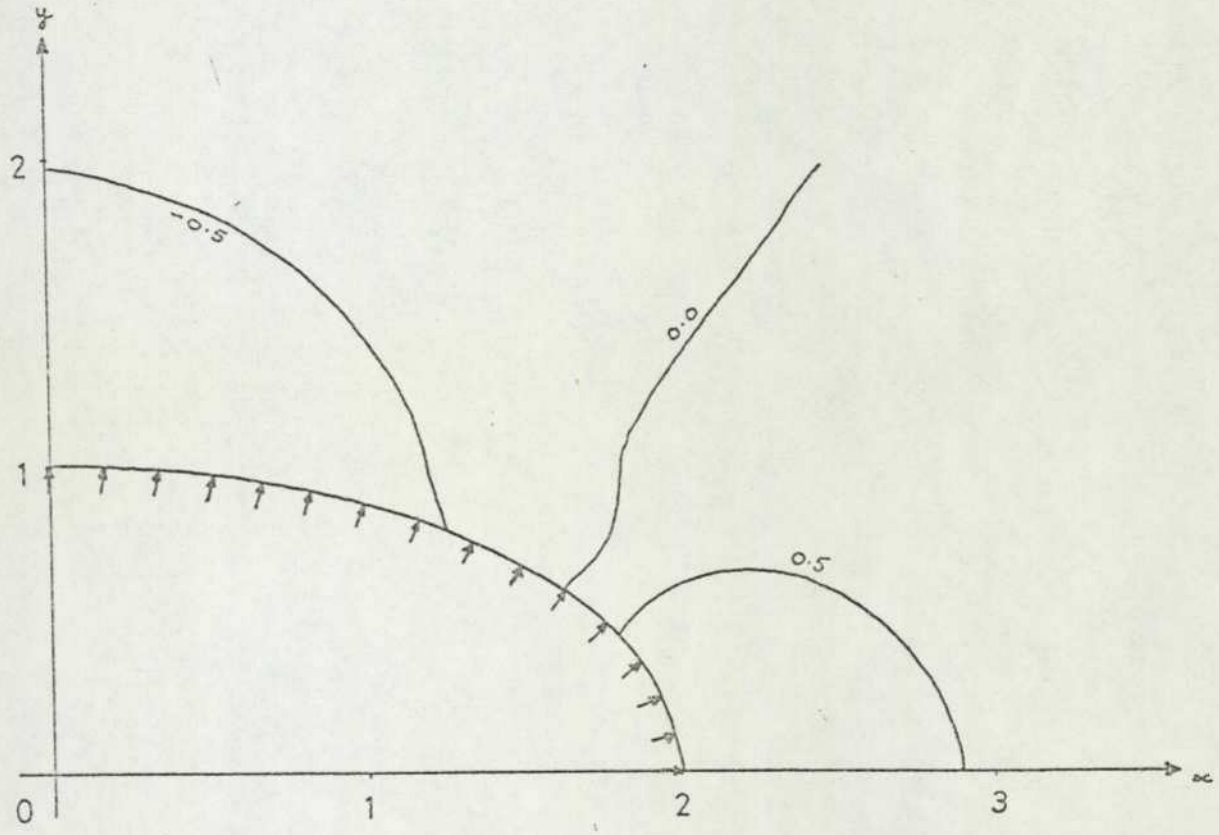
4 s². Uniform Pressure. 2:1 Ellipse.

Figure 32.



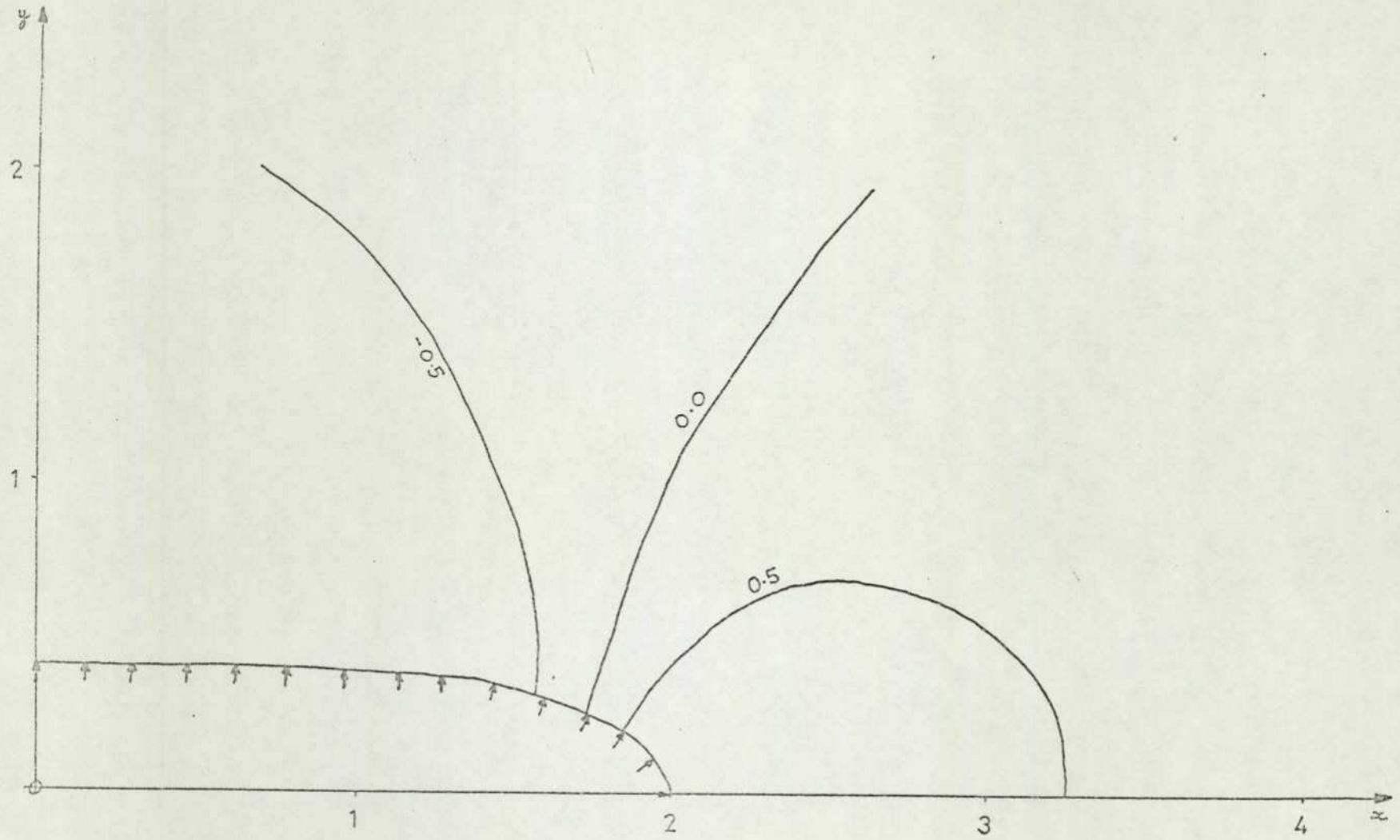
4s². Uniform Pressure. 2:⅓ Ellipse.

Figure 33.



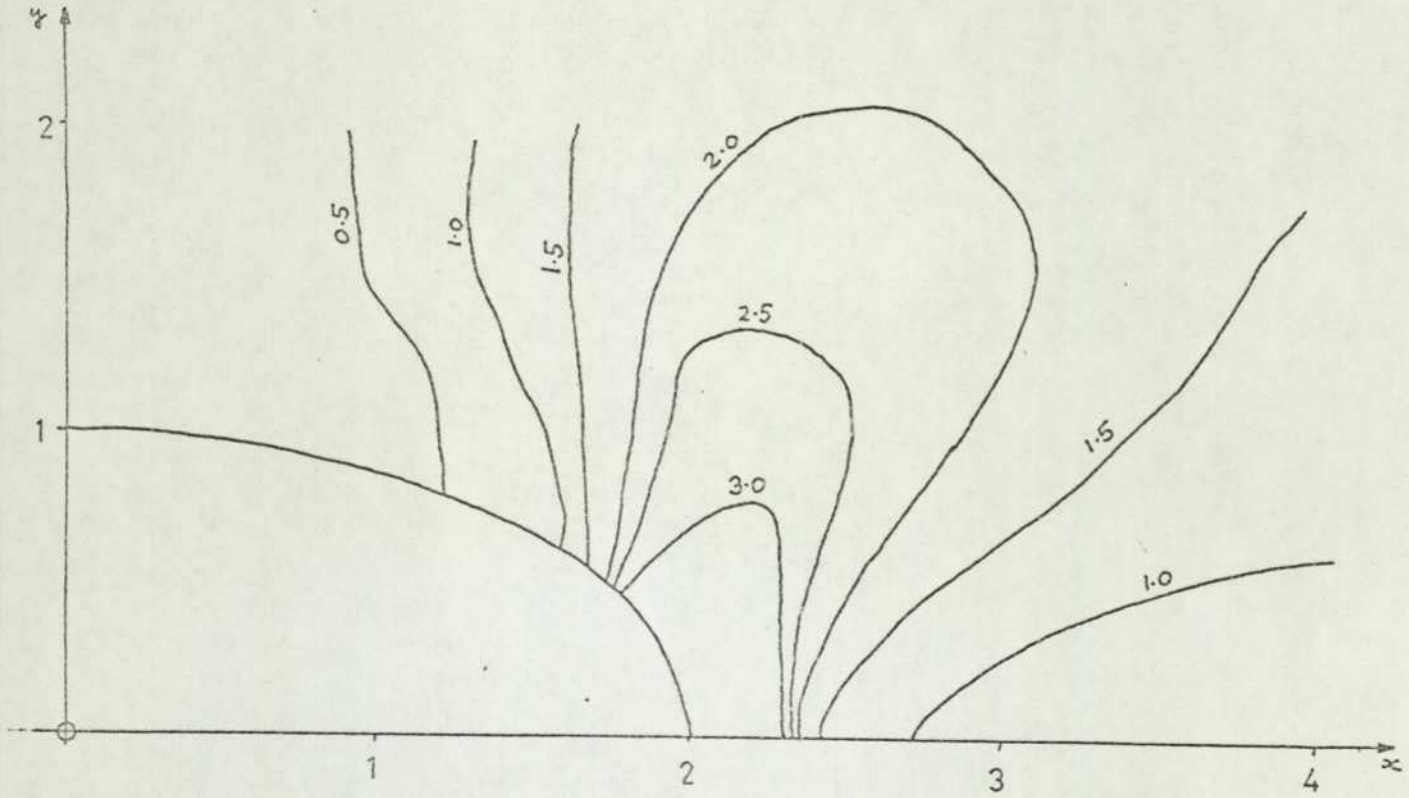
Ⓗ. Uniform Pressure. 2:1 Ellipse.

Figure 34.



(m). Uniform Pressure. 2:$\frac{1}{3}$ Ellipse.

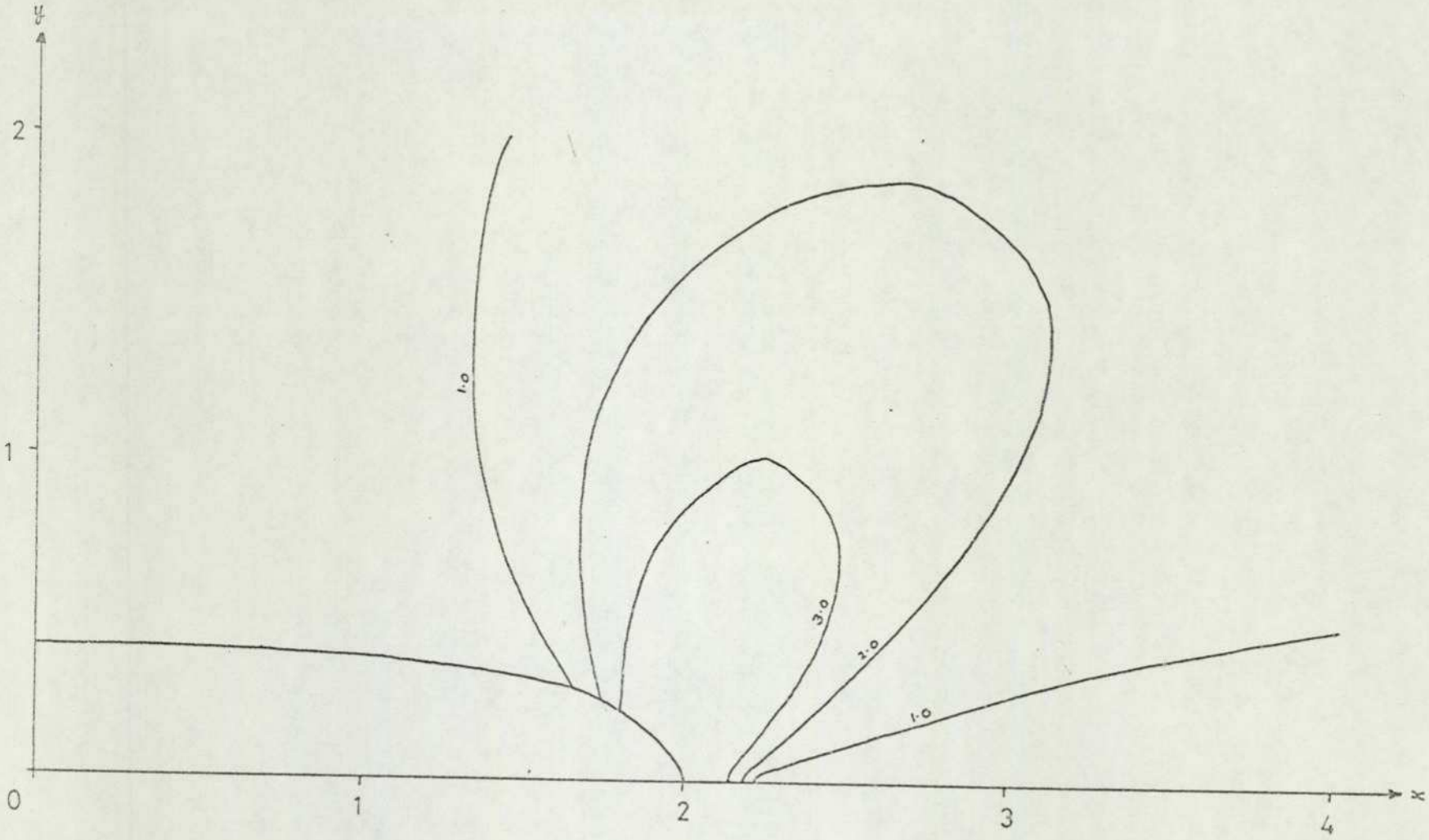
Figure 35.



4s². Simple tension at infinity parallel to the y-axis.

2:1 Ellipse.

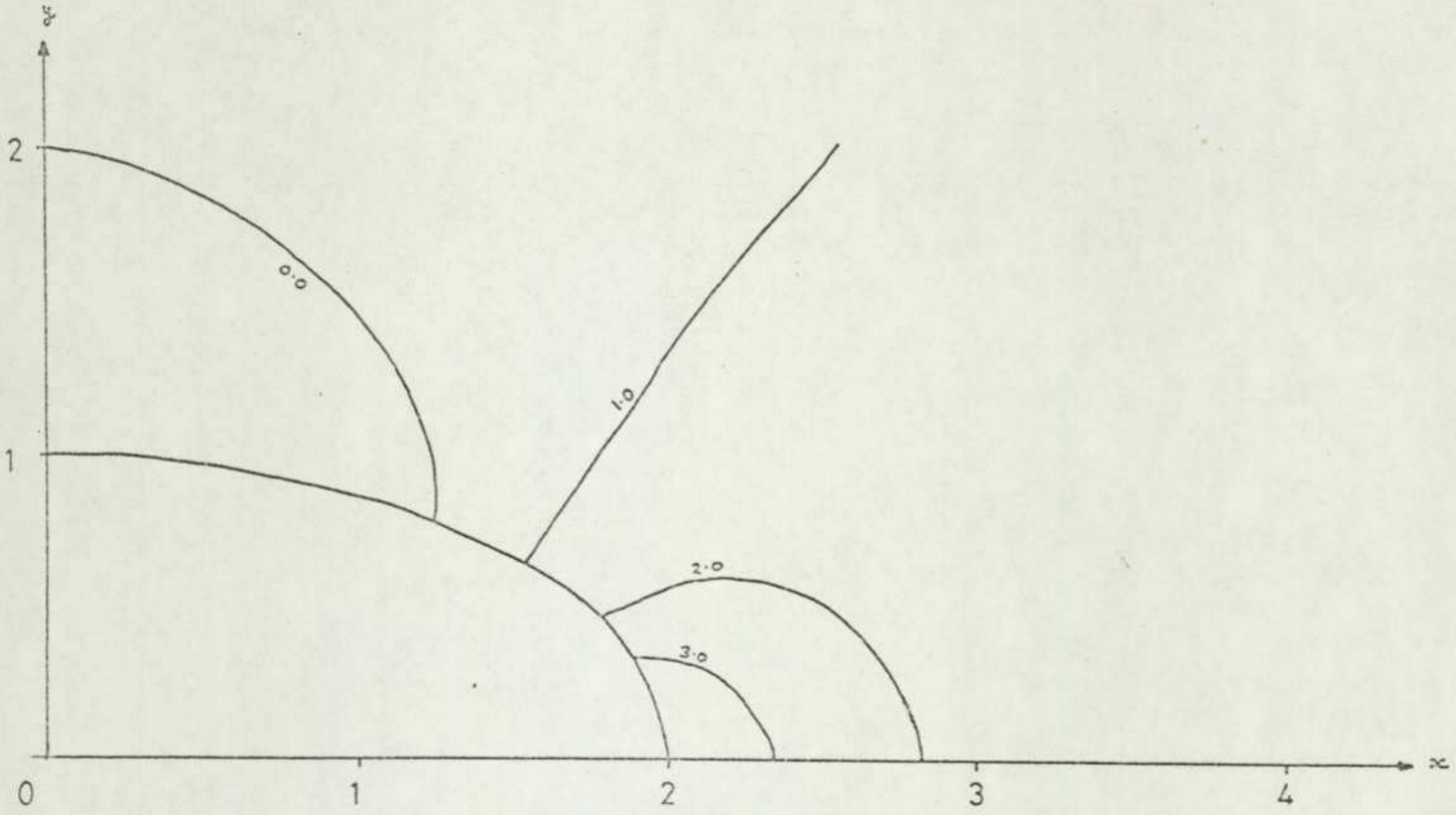
Figure 36.



4s². Simple tension at infinity parallel to the y-axis.

2:⅔ Ellipse.

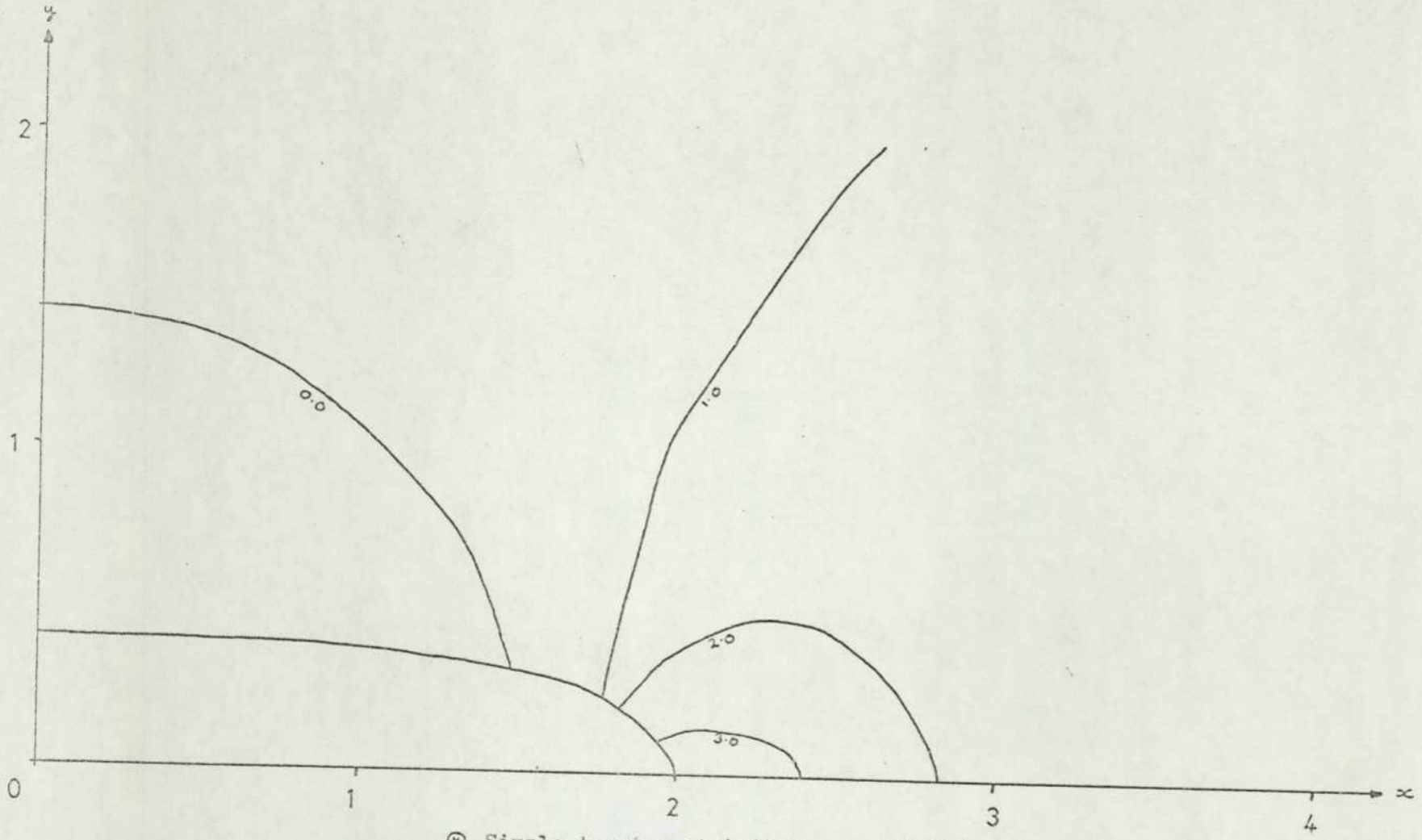
Figure 37.



Ⓗ. Simple tension at infinity parallel to the y-axis.

2:1 Ellipse.

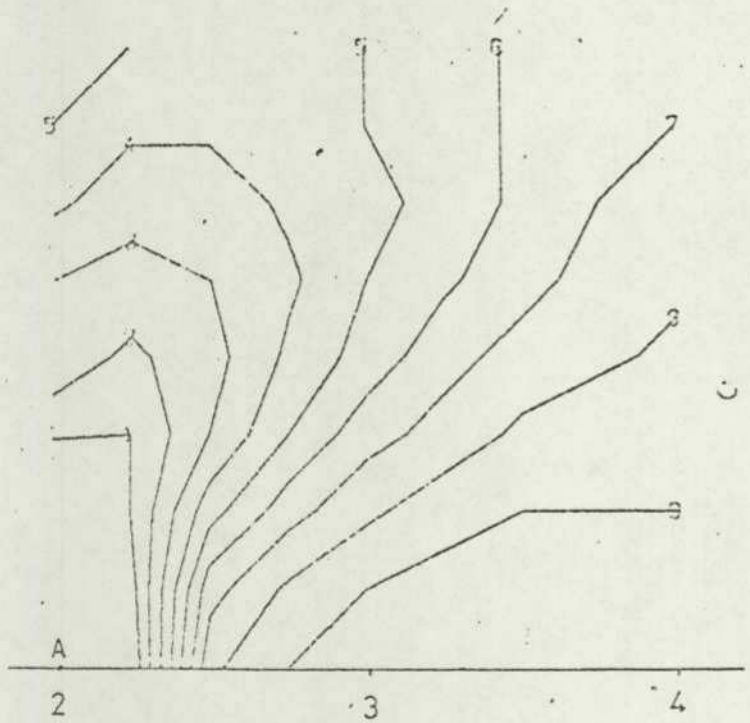
Figure 38.



(b) Simple tension at infinity parallel to the y-axis.

2: $\frac{2}{5}$ Ellipse.

Figure 39.



LEVELS PLOTTED

1	0.3000000E 01
2	0.2750000E 01
3	0.2500000E 01
4	0.2250000E 01
5	0.2000000E 01
6	0.1750000E 01
7	0.1500000E 01
8	0.1250000E 01
9	0.1000000E 01

$4s^2$. Simple tension at infinity parallel to the y-axis.

2:1 Ellipse.

Graph plotter output for the region

$2 \leq x \leq 4, 0 \leq y \leq 2$.

A denotes end of the major axis.

Figure 40.

P A R T III

ELASTO - PLASTIC STRESS ANALYSIS

CHAPTER 10

INTRODUCTION

Foundations of plasticity

In part III we are concerned with a material which behaves elastically until a limiting value of shear stress is reached, after which it suffers plastic deformation. Behaviour beyond the elastic limit depends on the properties of the material. A typical stress-strain curve for a specimen under the action of a gradually increasing uniaxial stress $\widehat{xx}$ is shown in figure 41, in which $\widehat{xx}$ is plotted against the corresponding strain ϵ_{xx} . As the load increases, it is found that the stress and strain are proportional up to a limit A where the curve begins to bend. This is the "proportional limit", but the curve may continue up to a point B, the "elastic limit", before any appreciable permanent deformation would occur if the specimen were unloaded. The portion from A to B defines a small non-linear elastic regime which we ignore. If at a point C the load is removed to a point D and then immediately reapplied, the unloading and loading curves C P D, D Q C, do not coincide. The area of the loop C P D Q C corresponds to the mechanical work dissipated during the cycle. D C is found to be parallel to O A, and beyond C the curve continues as if the cycle had not taken place. A further property of the material which is indicated in figure 41 is that, following the cycle of unloading and reapplication of the load, the stress at which plasticity occurs is higher than it was during the original load path. This is the phenomenon of "work-hardening" in which the material becomes, in a sense, stronger after the load-cycle has taken place.

The above description is of a general character since various materials react differently to this test. It is not possible to represent behaviour after the elastic limit has been reached by any one formula, far less by a linear relationship. It is necessary to idealize the behaviour in order to build up a theory. In this thesis we shall assume that no work-hardening takes place so that the line A E (figure 41) remains parallel to the strain axis.

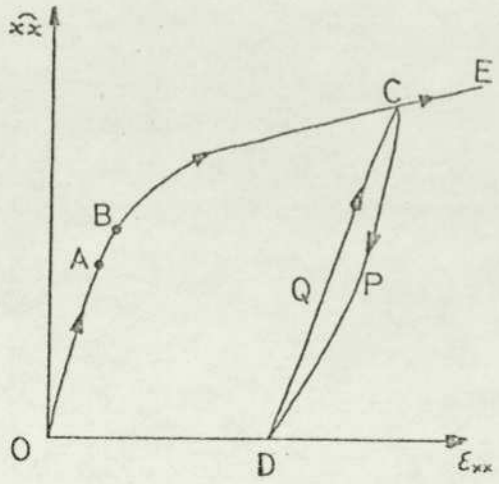


FIG. 41

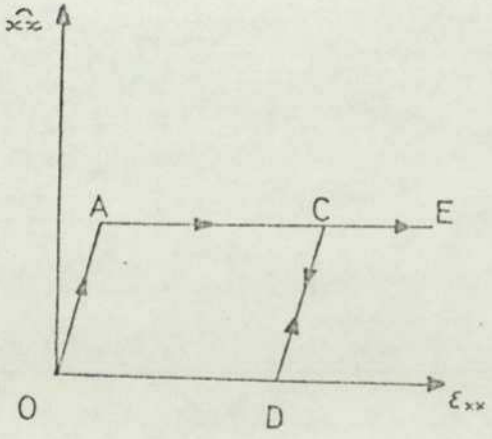


FIG. 42

Thus we consider a "perfectly plastic material", sometimes called a Saint-Venant solid, characterized by figure 42. Along A C E the stress remains constant at the yield value while the strain increases indefinitely : this is plastic flow. When the external stresses are removed there exists a new equilibrium state at D, distinguished from the equilibrium state at O by a permanent plastic strain O D. If the mechanical history of the specimen were unknown, its equilibrium state would be measured from D. Plastic deformation is therefore an irreversible process, but since D C remains parallel to O A the elastic constants of the system remain unaffected. It should be noted that for a perfectly plastic material the unloading path C D coincides with the reloading path D C.

Yield Criteria

The above discussion refers to a simple one-dimensional tension test of some hypothetical material. It is found experimentally that, when an isotropic body is loaded in a more general manner, yielding is not significantly affected by hydrostatic stress. This implies that the plasticity property of the material arises from its inability to support shear stress.

According to Tresca, yielding commences when the maximum shear stress reaches a certain critical value, i.e. when the principal stresses satisfy the condition

$$\max. \left\{ |\hat{x}\hat{x} - \hat{y}\hat{y}| , |\hat{y}\hat{y} - \hat{z}\hat{z}|, |\hat{z}\hat{z} - \hat{x}\hat{x}| \right\} = L \qquad (10.1)$$

where L is a constant characteristic of the material. According to von Mises and Hencky, yielding commences when the energy density of shear strain attains a critical value, i.e. when the principal stresses satisfy the condition

$$(\hat{x}\hat{x} - \hat{y}\hat{y})^2 + (\hat{y}\hat{y} - \hat{z}\hat{z})^2 + (\hat{z}\hat{z} - \hat{x}\hat{x})^2 = 2J^2 \qquad (10.2)$$

where J is a positive constant characteristic of the material. If we identify J and L, both criteria lead to the same result when any two principal stresses are equal. The maximum possible divergence between the criteria occurs in the case of pure shear, e.g. $\hat{x}\hat{x} = -\hat{y}\hat{y}$, $\hat{z}\hat{z} = 0$; in which (10.1) leads to $|\hat{x}\hat{x}| = J/2$, whilst (10.2) leads to $|\hat{x}\hat{x}| = J/\sqrt{3}$.

These two criteria stand out amongst others, since they have a reasonably simple form and still represent well the idealised yield properties of many materials. It has not yet proved possible to make a clear decision between (10.1) and (10.2) on experimental grounds, sometimes one and sometimes the other being favoured. Accordingly we utilise whichever criterion happens to be more mathematically convenient.

Laws of Plastic Flow

Problems of plasticity fall into two main classes:-

(i) unrestricted plastic flow occurs in at least one direction;

(ii) the plastic region is enclosed by surrounding elastic or rigid material.

In either case it is convenient to analyse the stress and strain tensors into hydrostatic and deviatoric components. Thus, using a prime to denote the latter, we write

$$\left.\begin{aligned} \hat{pq}' &= \hat{pq} - \frac{\Theta}{3}\delta_{pq}, \\ \varepsilon'_{pq} &= \varepsilon_{pq} - \frac{\Delta}{3}\delta_{pq}, \end{aligned}\right\} \qquad (10.3)$$

$$p,q = x,y,z\,; \qquad \Theta = x\hat{x} + y\hat{y} + z\hat{z}\,, \quad \Delta = \varepsilon_{xx} + \varepsilon_{yy} + \varepsilon_{zz}\,,$$

it being noted that the deviatoric quantities automatically satisfy $\Theta' = 0$, $\Delta' = 0$. The equation

$$\Theta = 3K\Delta \qquad (10.4)$$

where K is the bulk modulus, relates the hydrostatic pressure to the dilatation in both the plastic and elastic regions. Expressing (10.4) in differential form we have

$$d\Delta = \frac{1}{3K}\,d\Theta\,. \qquad (10.5)$$

The deviatoric strain components are incrementally related to the deviatoric stress components by the Prandtl-Reuss equations

$$d\varepsilon'_{pq} = \hat{pq}'\,d\lambda + \frac{d\hat{pq}'}{2\mu}\,; \qquad p,q = x,y,z\,. \qquad (10.6)$$

According to (10.6) the increment in deviatoric strain is made up of two distinct components :-

(i) a purely elastic contribution directly proportional to the deviatoric stress increment $d\hat{pq}'$. This is reversible.

(ii) a purely plastic contribution proportional to the current deviatoric stress component $\hat{p}_{ij}'$, the factor of proportionality being $d\lambda$. This is irreversible.

Unrestricted plastic flow problems may be solved using (10.6) together with any supplementary information about the individual stress and strain components.

In a zone of restricted or "contained" plastic flow, the stress components satisfy the usual Cauchy equilibrium equations provided kinematic effects may be neglected, as will be assumed in this thesis. These equations, together with the yield criterion, sometimes enable certain of the stress components to be determined directly. To evaluate the remaining stress components, and also the strain components, the Prandtl-Reuss equations must be introduced. However, even admitting various plausible approximations, such a solution presents, in general, formidable difficulties. A further serious complication concerns the location of the elasto-plastic interface, which is unknown in advance. However, some progress can be made under conditions of plane strain. This forms the main theme of subsequent chapters.

Plane Strain in Plasticity

Problems of plane strain are greatly simplified if, following Hill (1960), we assume that the maximum shear stress always lies in the plane of cross-section. This is certainly the case for an incompressible material, i.e. where $\nu = \frac{1}{2}$, and forms an extremely plausible assumption for a compressible material. Accordingly, Tresca's yield condition becomes

$$(\hat{x}_x - \hat{y}_y)^2 + 4\hat{x}_y^2 = L^2 \qquad (10.7)$$

which is satisfied by the effective stress components $\hat{x}_x$, $\hat{y}_y$, $\hat{x}_y$ in the plastic zone. When $\nu = \frac{1}{2}$, relation (10.7) also follows from the criterion of Hencky and von Mises. The equilibrium equations

$$\frac{\partial \hat{x}_x}{\partial x} + \frac{\partial \hat{x}_y}{\partial y} = 0 \quad , \qquad \frac{\partial \hat{x}_y}{\partial x} + \frac{\partial \hat{y}_y}{\partial y} = 0, \qquad (10.8)$$

together with (10.7) enable the stresses to be calculated in a plastic region with a specified boundary.

It is possible to define a stress function in the plastic region analogous to the biharmonic function of

elasticity theory. Thus we express the stresses in the form

$$\hat{xx} = \frac{\partial^2 \chi}{\partial y^2} \quad , \quad \hat{yy} = \frac{\partial^2 \chi}{\partial x^2} \quad , \quad \hat{xy} = \frac{-\partial^2 \chi}{\partial x \partial y} \quad , \qquad (10.9)$$

whereupon substitution into (10.7) yields a second-order, non-linear hyperbolic partial differential equation for χ. This means that the nature of the mathematical problem in plasticity contrasts sharply with that in elasticity where the governing equation, the biharmonic, is of elliptic type. For the latter class of problem, the tractions or displacements are prescribed on a given boundary and uniquely determine the solution within the interior. In plasticity, on the other hand, we must follow the propagation of a plastic zone from points in the material where yielding first occurs. The main difficulty here lies in determining the extent of the plastic zone as a function of the applied load. This problem will be tackled later by an elaborate numerical technique.

Conclusion

It is possible to obtain an analytical solution for a cross-section with a circular boundary (chapter 11), but for more general problems with less symmetry the stresses can only be calculated numerically. Here we exploit a method described in chapter 12, which we term "the elasto-plastic iteration procedure". This involves repeated solutions of elastic problems followed by solutions for the growing plastic zone using the slip-line technique. The latter is essentially a method of solving by characteristics the hyperbolic partial differential equation mentioned above. This procedure will be applied in chapter 13 to an elliptic cavity problem.

An analytic solution for a spherical cavity was given by Bhargava (1959) who also made an initial investigation into the iteration procedure. The originality of part III lies in our discussion of the circular cavity problem, and in the systematic application of the elasto-plastic iteration procedure. In particular we determine the zone of contained plastic flow enclosing an elliptic cavity subject to uniform internal normal pressure.

CHAPTER 11

EXACT SOLUTION FOR A CIRCULAR CAVITY

Introduction

A useful contribution to plane strain plasticity is provided by a problem which exhibits sufficient symmetry to permit an exact analytical solution. In this chapter we consider an infinite medium containing an infinite cylindrical cavity of circular cross-section, subject to a gradually increasing uniform internal pressure P. It is illuminating to analyse both the elastic and plastic contributions to the stress and strain components throughout the medium as P increases up to and beyond the critical value. Total work done on the cavity may be equated to the strain energy of the medium at any stage. Finally we discuss the residual stresses which remain in the medium if the pressure is removed.

We assume in this chapter that Poisson's ratio ν has the value $\nu = \frac{1}{2}$ in the plastic zone. Otherwise an exact solution is not possible. With the higher degree of symmetry exhibited by the analogous problem involving a spherical cavity, this assumption becomes unnecessary. The author has repeated the work of this chapter for a spherical cavity, of which details are omitted since the analysis is similar to the circular cavity problem.

Polar coordinates will be taken in the plane of cross-section with origin at the centre of the circular cavity. Axial symmetry implies that

$$\hat{r\theta} = 0 , \qquad \varepsilon_{r\theta} = 0$$

throughout, and plane strain conditions ensure that $\varepsilon_{zz} = 0$. The stress component $\hat{zz}$ has the value

$$\hat{zz} = \tfrac{1}{2}(\hat{rr} + \hat{\theta\theta}).$$

Pre-yield Solution

If the radius of the cavity is a, the purely elastic stress and strain components are

$$\hat{rr} = -\hat{\theta\theta} = \frac{-Pa^2}{r^2} ; \qquad \hat{r\theta} = 0 , \tag{11.1}$$

$$\varepsilon_{rr} = -\varepsilon_{\theta\theta} = \frac{-Pa^2}{2\mu r^2} ; \qquad \varepsilon_{r\theta} = 0 , \tag{11.2}$$

at a radial distance r from the origin. From (11.1) and (11.2) we note that

$$\Theta = 0, \qquad \Delta = 0. \tag{11.3}$$

Because of symmetry and since $\varepsilon_{rr} = \frac{du}{dr}$, the only non-vanishing displacement component is radial and given by

$$u = \frac{Pa^2}{2\mu r}. \tag{11.4}$$

The maximum shear stress is given by

$$|\hat{rr} - \hat{\theta\theta}| = \frac{2Pa^2}{r^2} \tag{11.5}$$

and yielding begins, according to Tresca's criterion, at points where (11.5) first assumes a critical value L. Thus, yielding commences at the boundary of the cavity at a critical pressure defined by

$$P_0 = \frac{L}{2} \tag{11.6}$$

i.e. when

$$\hat{\theta\theta} - \hat{rr} = L \qquad \text{on } r = a. \tag{11.7}$$

The work done per unit length of cavity in reaching the critical pressure is

$$2\pi a \int_{P=0}^{P=P_0} P \frac{du}{dP} dP = \frac{\pi a^2 P_0^2}{2\mu}. \tag{11.8}$$

The strain-energy density is given by

$$\frac{1}{2}(\hat{rr}\,\varepsilon_{rr} + \hat{\theta\theta}\,\varepsilon_{\theta\theta}) = \frac{P_0^2 a^4}{2\mu r^4} \tag{11.9}$$

whence the strain energy in the medium, per unit length of the cavity, is given by

$$\int_{r=a}^{\infty} \frac{P_0^2 a^4}{2\mu r^4} \cdot 2\pi r\, dr = \frac{\pi a^2 P_0^2}{2\mu}. \tag{11.10}$$

This is identical to (11.8) as expected.

Plastic Stresses

As the pressure increases beyond P_0 a plastic zone propagates out from the boundary. By symmetry this zone is always circular and we denote its outer radius by c when P $(>P_0)$ is the applied pressure on $r = a$. The linear elastic stress-strain relations do not hold in the plastic zone, but the Cauchy equilibrium equation

$$\frac{\partial \hat{rr}}{\partial r} = \frac{d\hat{rr}}{dr} = \frac{\hat{\theta\theta} - \hat{rr}}{r} \tag{11.11}$$

still applies. Equation (11.11), coupled with the hypothesis

$$\hat{\theta\theta} - \hat{rr} = L \; ; \qquad a \leq r \leq c, \tag{11.12}$$

determines the stress components

$$\left.\begin{aligned} \hat{rr} &= L \ln \tfrac{r}{c} - \tfrac{L}{2} , \\ \hat{\theta\theta} &= L \ln \tfrac{r}{c} + \tfrac{L}{2} , \end{aligned}\right\} \qquad a \leq r \leq c. \tag{11.13}$$

Applying (11.13) to the boundary $r = a$ we find

$$P = L \ln \tfrac{c}{a} + \tfrac{L}{2} \tag{11.14}$$

which uniquely relates the applied pressure P to the outer radius c of the plastic zone ($P > \frac{L}{2}$).

Elastic Zone Solution

We now determine the stresses in the containing elastic zone $r \geq c$. The boundary $r = c$ is just about to yield, so, by hypothesis,

$$\hat{rr} = \frac{-L}{2} \qquad \text{on} \qquad r = c. \tag{11.15}$$

Applying (11.1) with c replacing a and $\frac{L}{2}$ replacing P we find

$$\hat{rr} = \frac{-Lc^2}{2r^2} = -\hat{\theta\theta} , \qquad (r \geq c) \tag{11.16}$$

$$\varepsilon_{rr} = \frac{-Lc^2}{4\mu r^2} = -\varepsilon_{\theta\theta} , \qquad (r \geq c) \tag{11.17}$$

$$\Theta = 0, \quad \Delta = 0, \qquad (r \geq c) \tag{11.18}$$

$$u = \frac{Lc^2}{4\mu r} . \qquad (r \geq c) \tag{11.19}$$

Comparison of Elastic and Plastic Zones

In the plastic zone, by virtue of (11.13), we find

$$\hat{zz} = \tfrac{1}{2}(\hat{rr} + \hat{\theta\theta}) = L \ln \tfrac{r}{c} \quad (r \leq c) . \tag{11.20}$$

Therefore

$$\Theta = \hat{rr} + \hat{\theta\theta} + \hat{zz} = 3L \ln \tfrac{r}{c} \quad (r \leq c) , \tag{11.21}$$

which shows that a hydrostatic pressure builds up in the plastic zone whereas by (11.18) it is zero in the elastic zone.

From (11.13) and (11.16) it can be seen that the stresses $\hat{rr}$, $\hat{\theta\theta}$ are continuous across the elasto-plastic boundary $r = c$. The radial derivative of $\hat{rr}$ is also continuous but the radial derivative of hoop stress $\hat{\theta\theta}$ drops from L/c to $-L/c$ as r crosses the elasto-plastic boundary. A graph exhibits the properties of the radial and hoop stresses in figure 43.

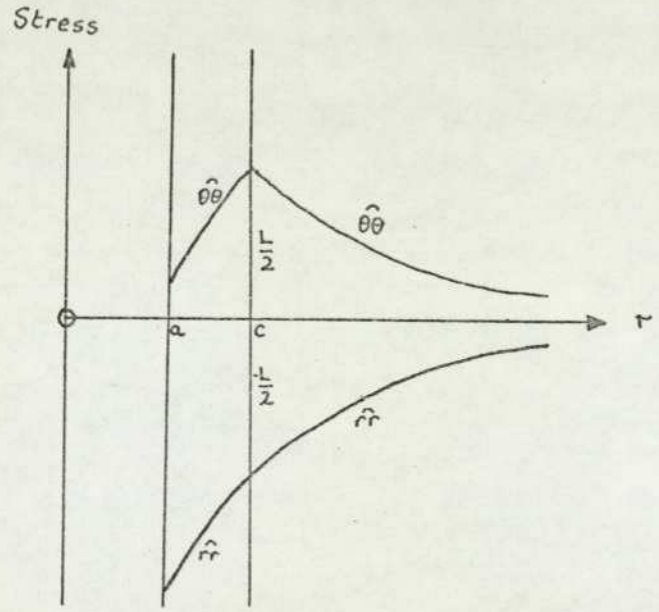


Figure 43

Total Displacements and Strains in the Plastic Zone

The divergence of the displacement vector is

$$\Delta = \frac{\Theta}{3K} = \frac{L}{K} \ln \frac{r}{c} \qquad (r < c) \qquad (11.22)$$

by (11.21), where K is the bulk modulus. Since $\varepsilon_{rr} = \frac{du}{dr}$, $\varepsilon_{\theta\theta} = \frac{u}{r}$ in the plastic zone it follows that

$$\frac{du}{dr} + \frac{u}{r} = \frac{L}{K} \ln \frac{r}{c}, \qquad (11.23)$$

whereupon integration yields

$$u = \frac{L}{K}\left[\frac{r}{2} \ln \frac{r}{2} - \frac{r}{4}\right] + \frac{B}{r} \qquad (11.24)$$

where B is a constant of integration. This may be found from the boundary condition

$$u = \frac{Lc}{4\mu} \qquad \text{on} \qquad r = c \tag{11.25}$$

arising from (11.19), whence

$$B = \frac{Lc^2}{4}\left(\frac{1}{\mu} + \frac{1}{K}\right).$$

This reduces to

$$B = \frac{3Lc^2}{4E} \qquad \text{when } \upsilon = \tfrac{1}{2}. \tag{11.26}$$

The plastic strains are therefore

$$\varepsilon_{rr} = \frac{du}{dr} = \frac{L}{4K}\left[2\ln\frac{r}{c} + 1\right] - \frac{B}{r^2}, \tag{11.27}$$

$$\varepsilon_{\theta\theta} = \frac{u}{r} = \frac{L}{4K}\left[2\ln\frac{r}{c} - 1\right] + \frac{B}{r^2}, \tag{11.28}$$

which reduce to

$$\varepsilon_{rr} = -\varepsilon_{\theta\theta} = -\frac{B}{r^2} \quad \text{if} \quad \upsilon = \tfrac{1}{2}.$$

The expressions (11.27), (11.28) are the total strain components in the plastic zone.

Analysis of Strains

In a plastic medium it is clear that strains will be made up of both elastic and plastic components. We use the superscripts $^{(e)}$, $^{(p)}$ to denote elastic and plastic components respectively. The subscripts $_{(e)}$, $_{(p)}$ denote components in the elastic and plastic zones respectively. Thus $\varepsilon^{(e)}_{(p)}$, $\varepsilon^{(p)}_{(p)}$ denote the elastic and plastic strains respectively in the plastic zone, and the total strain in the plastic zone is

$$\varepsilon_{(p)} = \varepsilon^{(e)}_{(p)} + \varepsilon^{(p)}_{(p)}.$$

The elastic strain components in the plastic zone are related to the stresses (11.13) by the usual stress-strain relations

$$E\,\varepsilon_{pq}{}^{(e)}_{(p)} = (1+\upsilon)\,\hat{p}\hat{q} - \upsilon\,\Theta\,\delta_{pq}\,; \qquad p,q = r,\theta. \tag{11.29}$$

Hence we obtain

$$\left.\begin{aligned} E\,\varepsilon_{rr}{}^{(e)}_{(p)} &= \hat{r}\hat{r}\left(1-\frac{\upsilon}{2}\right) - \frac{3\upsilon}{2}\hat{\theta}\hat{\theta}\,, \\ E\,\varepsilon_{\theta\theta}{}^{(e)}_{(p)} &= \hat{\theta}\hat{\theta}\left(1-\frac{\upsilon}{2}\right) - \frac{3\upsilon}{2}\hat{r}\hat{r}\,. \end{aligned}\right\} \tag{11.30}$$

With $\upsilon = \frac{1}{2}$, these reduce to

$$E\,\varepsilon_{rr}{}^{(e)}_{(p)} = \frac{3}{4}\left(\hat{r}\hat{r} - \hat{\theta}\hat{\theta}\right) = -E\,\varepsilon_{\theta\theta}{}^{(e)}_{(p)}\,. \tag{11.31}$$

The plastic strain components in the plastic zone are given by the equations

$$\varepsilon_{pq}{}^{(p)}_{(p)} = \varepsilon_{pq}{}_{(p)} - \varepsilon_{pq}{}^{(e)}_{(p)}\,, \qquad p,q = r,\theta. \tag{11.32}$$

Thus

$$\varepsilon_{rr}{}^{(p)}_{(p)} = \frac{L}{4K}\left[2\ln\frac{r}{c} + 1\right] - \frac{B}{r^2} + \frac{3L}{4E}\,, \tag{11.33}$$

$$\varepsilon_{\theta\theta}{}^{(p)}_{(p)} = \frac{L}{4K}\left[2\ln\frac{r}{c} - 1\right] + \frac{B}{r^2} - \frac{3L}{4E} \tag{11.34}$$

by virtue of (11.31), (11.27), (11.28) and (11.12). The importance of the assumption $\upsilon = \frac{1}{2}$ is seen when the corresponding substitution $\frac{1}{K} = 0$ is made in (11.33) and (11.34). With (11.26) there results

$$\varepsilon_{rr}{}^{(p)}_{(p)} = \varepsilon_{rr}{}'^{(p)}_{(p)} = \frac{3L}{4E}\left(1-\frac{c^2}{r^2}\right), \tag{11.35}$$

$$\varepsilon_{\theta\theta}{}^{(p)}_{(p)} = \varepsilon_{\theta\theta}{}'^{(p)}_{(p)} = \frac{-3L}{4E}\left(1-\frac{c^2}{r^2}\right). \tag{11.36}$$

We note that $\varepsilon_{rr}{}^{(p)}_{(p)} \neq \varepsilon_{rr}{}'^{(p)}_{(p)}$ unless $\upsilon = \frac{1}{2}$.

It may be observed that the strain components in the plastic zone are incrementally related to the stress components by the Prandtl-Reuss equations (10.6). If a prime denotes the deviatoric components defined by (10.3), these equations give

$$d\varepsilon'^{(p)}_{pq\,(p)} = \hat{pq}'\, d\lambda, \tag{11.37}$$

$$d\varepsilon'^{(e)}_{pq\,(p)} = \frac{d\hat{pq}'}{2\mu} \tag{11.38}$$

where $p, q = r, \theta$. Now since

$$\ominus = 3L \ln \frac{r}{c},$$

equation (11.13) provides the values of the deviatoric stress components

$$\left.\begin{aligned} \hat{rr}' &= -\frac{L}{2}, \\ \hat{\theta\theta}' &= \frac{L}{2}, \end{aligned}\right\} \quad a \leq r \leq c. \tag{11.39}$$

Since the plastic strain components are known already ((11.35) and (11.36)), the Prandtl-Reuss equations define $d\lambda$ in terms of the strain history of the material. More precisely, replacing c by s in equations (11.35) and (11.36), where s is a variable running from $s = r$ to $s = c$, we find

$$d\varepsilon^{(p)}_{rr\,(p)} = \frac{3L}{4E}\left(\frac{-2s\,ds}{r^2}\right) = -\,d\varepsilon^{(p)}_{\theta\theta\,(p)}, \tag{11.40}$$

whence either of the equations (11.39) yields from (11.37)

$$d\lambda = \frac{s\,ds}{\mu r^2}. \tag{11.41}$$

Energy Considerations

The strain energy density in the elastic zone ($r > c$) is

$$W_{(e)} = \tfrac{1}{2}\left(\hat{rr}\,\varepsilon_{rr} + \hat{\theta\theta}\,\varepsilon_{\theta\theta}\right) = \frac{L^2 c^4}{8\mu r^4} \tag{11.42}$$

by (11.16) and (11.17); whence the strain energy per unit length of cavity in the elastic zone is

$$V_{(e)} = \int_{r=c}^{\infty} \frac{L^2 c^4}{8\mu r^4} \cdot 2\pi r\, dr = \frac{L^2 c^2 \pi}{8\mu} . \qquad (11.43)$$

These could have been obtained from (11.9) and (11.10) with c replacing a and $L/2$ replacing P_o .

The strain energy density of elastic energy in the plastic zone is

$$W^{(e)}_{(p)} = \frac{1}{2}\left(\hat{r}\hat{r}\, \varepsilon^{(e)}_{rr\,(p)} + \hat{\theta}\hat{\theta}\, \varepsilon^{(e)}_{\theta\theta\,(p)} \right) . \qquad (11.44)$$

Substituting for the elastic strain components in the plastic zone (11.31) we have

$$W^{(e)}_{(p)} = \frac{3}{8E}\left(\hat{r}\hat{r} - \hat{\theta}\hat{\theta} \right)^2 = \frac{3L^2}{8E} .$$

Therefore

$$V^{(e)}_{(p)} = \int_a^c W^{(e)}_{(p)}\, 2\pi r\, dr = \frac{3L^2\pi(c^2-a^2)}{8E} \qquad (11.45)$$

represents the elastic strain energy per unit length of cavity in the plastic zone.

It is not in general valid to use a formula for plastic strain energy density analogous to the simple formulae (11.42), (11.44). We must take into account the entire strain history of the material. Thus we revert to the more basic incremental formula

$$W^{(p)}_{(p)} = \int_{s=r}^{s=c} dW = \int_{s=r}^{s=c} \left(\hat{r}\hat{r}\, d\varepsilon^{(p)}_{rr\,(p)} + \hat{\theta}\hat{\theta}\, d\varepsilon^{(p)}_{\theta\theta\,(p)} \right) \qquad (11.46)$$

which gives the plastic strain energy density at the fixed point r . Here, the variable of integration s defines the current outer radius of the plastic zone as it propagates from $s = r$ to $s = c$.
Since hydrostatic pressure does not contribute to plastic strain we replace (11.46) by

$$W^{(p)}_{(p)} = \int_{s=r}^{s=c} \left(\hat{r}\hat{r}'\, d\varepsilon'^{(p)}_{rr\,(p)} + \hat{\theta}\hat{\theta}'\, d\varepsilon'^{(p)}_{\theta\theta\,(p)} \right) .$$

Equation (11.37) yields

$$W^{(p)}_{(p)} = \int_{s=r}^{s=c} \left(\left[\hat{r}\hat{r}'\right]^2 + \left[\hat{\theta}\hat{\theta}'\right]^2 \right) d\lambda , \qquad (11.47)$$

whence, substituting for the deviatoric stress components (11.39), we obtain

$$W^{(P)}_{(P)} = \int_{s=r}^{s=c} \frac{L^2}{2}\, d\lambda . \qquad (11.48)$$

The d in equation (11.48) denotes an increment along the "strain path". Accordingly we write

$$d = \frac{d}{ds}\, ds$$

and utilise equation (11.41). Thus the plastic strain energy density is given by

$$W^{(P)}_{(P)} = \int_{s=r}^{s=c} \frac{L^2}{2\mu r^2}\, s\, ds$$

$$= \frac{-3L^2}{4E}\left(1 - \frac{c^2}{r^2}\right) . \qquad (11.49)$$

Hence the plastic energy in the plastic zone per unit length of cavity is

$$V^{(P)}_{(P)} = \int_{r=a}^{r=c} \left(\frac{-3L^2}{4E}\right)\left(1 - \frac{c^2}{r^2}\right) 2\pi r\, dr$$

$$= \frac{-3\pi L^2}{2E}\left[\frac{c^2 - a^2}{2} - c^2 \ln \frac{c}{a}\right] . \qquad (11.50)$$

Therefore the total energy in the material per unit length of cavity is

$$V_{(e)} + V^{(e)}_{(P)} + V^{(P)}_{(P)} = \frac{\pi L^2}{2\mu}\left[\frac{a^2}{4} + c^2 \ln \frac{c}{a}\right] . \qquad (11.51)$$

Work Done on the Inner Boundary

The result (11.51) may be identified with the work done on the inner boundary per unit length. Before yielding begins there is a contribution

$$V_1 = \frac{\pi L^2 a^2}{8\mu} \qquad (11.52)$$

by virtue of (11.6) and (11.10).

After the yield pressure is reached, the work done per unit length of cavity is

$$V_2 = 2\pi a \int P\, du \qquad (11.53)$$

where $P = (-\hat{rr})_{r=a}$. The pressure P and displacement u

are related since each is a function of s, the outer radius of the plastic zone. We have

$$P(s) = L\left(\ln\frac{s}{a} + \frac{1}{2}\right) \qquad \text{on } r = a, \qquad (11.54)$$

$$u(s) = \frac{Ls^2}{4a\mu} \qquad \text{on } r = a \qquad (11.55)$$

using (11.14) and (11.19). Hence

$$V_2 = 2\pi a \int_{s=a}^{s=c} P\frac{du}{ds}\,ds = \frac{\pi L^2}{\mu}\int_{s=a}^{s=c}\left(s\ln\frac{s}{a} + \frac{s}{2}\right)ds$$

$$= \frac{\pi L^2 c^2}{2\mu}\ln\frac{c}{a}.$$

The total work done on the inner boundary per unit length is

$$V_1 + V_2 = \frac{\pi L^2}{2\mu}\left[\frac{a^2}{4} + c^2\ln\frac{c}{a}\right] \qquad (11.56)$$

which is in agreement with (11.51).

Residual Stresses

We now discuss the stresses that remain in the medium if the boundary is unloaded. These "residual stresses" may be found by superimposing a pressure $-P$ on $r = a$. The resulting stresses may then be superimposed upon those obtained above. Thus for the region that has remained elastic, we have

$$\left.\begin{aligned}\hat{rr} &= \frac{-Lc^2}{2r^2} + \frac{Pa^2}{r^2},\\ \hat{\theta\theta} &= \frac{Lc^2}{2r^2} - \frac{Pa^2}{r^2},\end{aligned}\right\} \quad r \geq c, \qquad (11.57)$$

while for the region that was plastic we have

$$\left.\begin{aligned}\hat{rr} &= L\ln\frac{r}{c} - \frac{L}{2} + \frac{Pa^2}{r^2},\\ \hat{\theta\theta} &= L\ln\frac{r}{c} + \frac{L}{2} - \frac{Pa^2}{r^2},\end{aligned}\right\} \quad a \leq r \leq c. \qquad (11.58)$$

By (11.14) these become

$$\hat{rr} = \frac{L}{r^2}\left[\frac{a^2 - c^2}{2} - a^2\ln\frac{a}{c}\right], \qquad r \geq c, \qquad (11.59)$$

$$\hat{rr} = L\ln\frac{r}{c} - \frac{L}{2} + \frac{La^2}{r^2}\left[\frac{1}{2} - \ln\frac{a}{c}\right], \qquad a \leq r \leq c, \qquad (11.60)$$

$$\hat{\theta\theta} = \frac{L}{r^2}\left[\frac{c^2-a^2}{2} + a^2 \ln\frac{a}{c}\right], \qquad r \geq c, \quad (11.61)$$

$$\hat{\theta\theta} = L \ln\frac{r}{c} + \frac{L}{2} + \frac{La^2}{r^2}\left[\ln\frac{a}{c} - \frac{1}{2}\right], \qquad a \leq r \leq c. \quad (11.62)$$

Continuity of Residual Stresses and their Derivatives

It is to be noted that on $r = c$ (11.59) and (11.60) both yield

$$\hat{rr} = -\frac{L}{2} + \frac{La^2}{c^2}\left[\frac{1}{2} - \ln\frac{a}{c}\right] \quad (11.63)$$

while (11.61) and (11.62) both yield

$$\hat{\theta\theta} = \frac{L}{2} + \frac{La^2}{c^2}\left[\ln\frac{a}{c} - \frac{1}{2}\right]. \quad (11.64)$$

Thus the radial stress and hoop stress are continuous across the boundary that defined the elastic-plastic interface before the load was removed.

From (11.59) to (11.62) we find that the radial derivative of radial stress is continuous across $r = c$ while the radial derivative of hoop stress drops from

$$\frac{L}{c} + \frac{La^2}{c^3}\left[2\ln\frac{c}{a} + 1\right]$$

to

$$-\frac{L}{c} + \frac{La^2}{c^3}\left[2\ln\frac{c}{a} + 1\right]$$

at $r = c$; i.e. $\frac{\partial\hat{\theta\theta}}{\partial r}$ is discontinuous by an amount $\frac{2L}{c}$ at $r = c$.

By differentiating (11.59) to (11.62) we find that $\hat{rr}$ has a minimum at $r = a(1 + 2\ln\frac{c}{a})^{1/2}$. It is interesting to note that $\hat{rr} = \hat{\theta\theta}$ at this point. The hoop stress is strictly increasing for $r < c$ and strictly decreasing for $r > c$. A graph exhibiting the variation of $\hat{rr}$ and $\hat{\theta\theta}$ with r is provided in figure 44.

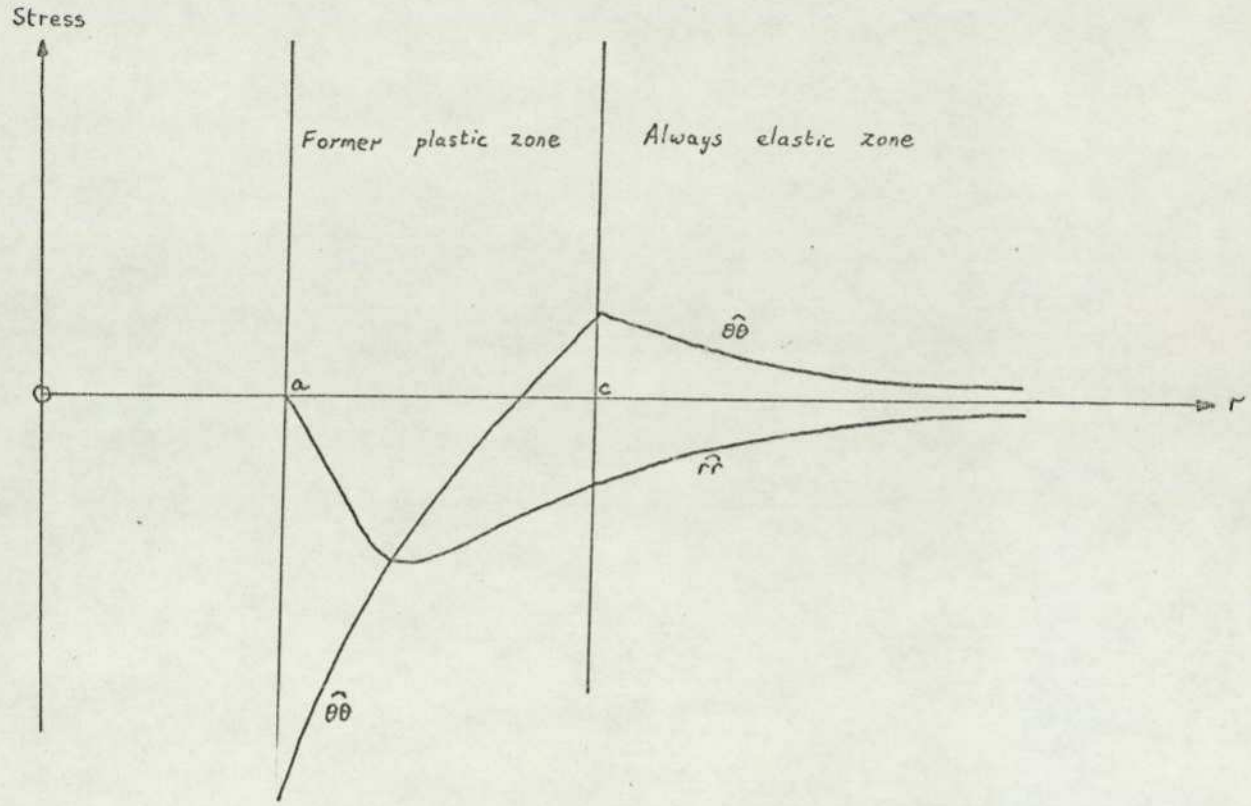

Stress
Former plastic zone
Always elastic zone
a
c
r
$\hat{\theta\theta}$
$\hat{rr}$
$\hat{\theta\theta}$

Figure 44.

CHAPTER 12

ELASTO - PLASTIC ITERATION PROCEDURE

Description of Method

Little progress has been made towards exact solutions for the location of the equilibrium elasto-plastic interface in problems of restricted plastic flow. The symmetrical conditions discussed in the last chapter constitute a very special case. However, application to a wide class of problems is possible by utilising the techniques described in this chapter. The elasto-plastic iteration procedure is a systematic method of approximating towards the true equilibrium elasto-plastic interface, C. The steps are as follows :-

(1) Solve the purely elastic problem for a given external load, and construct a curve C_1 enclosing the domain where the maximum shear stresses exceed or equal the critical value (10.7).

(2) Note that the curve C_1 is wholly enclosed by C, the true elasto-plastic interface.

(3) Now suppose that within the domain enclosed by C_1 the stresses relax slowly to values which satisfy the yield criterion (10.7). This relaxation leads to new tractions acting on the boundary of the elastic domain exterior to C_1.

(4) Subject to these boundary conditions on C_1, find the elastic stresses in the domain exterior to C_1. Enclose by a contour C_2 those domains where the maximum shear stress exceeds or equals the critical value. Evidently C_2 encloses C_1, and it forms a better approximation to C than C_1 .

(5) Continue this process and arrive at a sequence of contours C_1 , C_2 , C_3 .... which approximates more and more closely to C.

Test Example Using Analytic Solutions

For an infinite medium containing an infinite cylindrical cavity of circular cross-section under uniform internal pressure we have obtained an analytical solution for the outer boundary of the plastic region. We may use

this result to investigate the convergence of the iteration procedure. We follow the steps described above.

(1) In the same notation as (11.1) the purely elastic stresses are given by

$$\hat{rr} = -\hat{\theta\theta} = \frac{-Pa^2}{r^2} \quad ; \qquad r > a. \tag{12.1}$$

By (10.1), yielding occurs when

$$\left.\begin{aligned} |\hat{\theta\theta} - \hat{rr}| &= L, \\ \text{i.e.} \qquad \frac{2Pa^2}{r^2} &= L, \end{aligned}\right\} \tag{12.2}$$

whence C_1 is given by $r = c_1$, where

$$\left(\frac{c_1}{a}\right)^2 = \frac{2P}{L}. \tag{12.3}$$

(2) The analytical solution for C, the true elasto-plastic interface is the circle $r = c$ where c is given by (11.14), i.e.

$$\begin{aligned} \tfrac{1}{2} - \frac{P}{L} &= \ln \frac{a}{c}, \\ \frac{c}{a} &= e^{\left(\frac{P}{L} - \frac{1}{2}\right)} \end{aligned} \tag{12.4}$$

From (12.3) and (12.4) we compare $\frac{c_1}{a}$ with $\frac{c}{a}$ and observe that

$$\frac{2P}{L} < e^{\frac{2P}{L} - 1} \tag{12.5}$$

since $P > \frac{L}{2}$ by hypothesis. Hence

$$c_1 < c, \tag{12.6}$$

so c_1 is a lower bound for the radius of the elasto-plastic boundary.

(3) We now assume that the yield criterion (12.2) is satisfied in the region $a \leq r \leq c_1$ and seek to find the stresses on C_1. The general procedure is to use the slip-line technique described later in this chapter. In this particular problem we may use the analytical solution (11.13) which yields

$$\hat{rr} = L \ln \frac{c_1}{c} - \frac{L}{2}, \quad \hat{r\theta} = 0 \text{ on } r = c_1. \tag{12.7}$$

(4) Using (12.7) as boundary conditions for another elastic problem we obtain

$$\hat{rr} = \frac{Lc_1^2}{r^2}\left[\ln \frac{c_1}{c} - \frac{1}{2}\right] = -\hat{\theta\theta} \quad ; \quad r > c_1. \tag{12.8}$$

The condition $|\hat{\theta\theta} - \hat{rr}| = L$ on $r = c_2$ gives

$$\left(\frac{c_2}{c_1}\right)^2 = 1 + 2\ln \frac{c}{c_1}. \tag{12.9}$$

(5) We continue this process and obtain

$$\left(\frac{c_3}{c_2}\right)^2 = 1 + 2\ln\frac{c}{c_2} \quad , \tag{12.10}$$

$$\left(\frac{c_4}{c_3}\right)^2 = 1 + 2\ln\frac{c}{c_3} \quad , \tag{12.11}$$

etc., and observe that

$$c_1 < c_2 < c_3 < c_4 < \ldots < c \quad . \tag{12.12}$$

A simple computer program may be written to find the quantities $\frac{c_1}{a}$, $\frac{c_2}{a}$, ... from (12.3) and (12.9) to (12.11) and $\frac{c}{a}$ from (12.4) for various values of $\frac{P}{L}$ $\left(\geq \frac{1}{2}\right)$. The convergence process is illustrated in table 61, p.168. Only three or four iterations are needed to obtain an approximation for C accurate to within 1% for values of P up to four times the yield pressure.

The elasto-plastic iteration procedure was similarly tested for the analogous problem involving a spherical cavity of radius a. Equations (12.3) and (12.9) to (12.12) are replaced by

$$\left(\frac{c_1}{a}\right)^3 = \frac{3P}{2L} \quad , \tag{12.13}$$

$$\left.\begin{aligned} \left(\frac{c_{n+1}}{c_n}\right)^3 &= 1 + 3\ln\frac{c}{c_n} \\ c_n < c_{n+1} &< c \end{aligned}\right\} n = 1,2,3,\ldots \quad . \tag{12.14}$$

Results for various values of P (greater than the yield value $\frac{2L}{3}$) are given in table 62, p.169 and good convergence may be observed again. It must be admitted, however, that good results are obtained for the two problems considered here since analytic solutions are available for the stresses in the plastic zone. More generally these stresses may be found by a numerical method which we now describe.

Slip-Line Technique

This widely used numerical technique was originally devised by Hencky (1923) for integrating the system of equations

$$\frac{\partial \hat{xx}}{\partial x} + \frac{\partial \hat{xy}}{\partial y} = 0 \quad , \quad \frac{\partial \hat{xy}}{\partial x} + \frac{\partial \hat{yy}}{\partial y} = 0 \quad , \tag{12.15}$$

$$(\hat{xx} - \hat{yy})^2 + 4\hat{xy}^2 = L^2 \quad . \tag{12.16}$$

The Cartesian plastic stresses $\hat{xx}$, $\hat{xy}$, $\hat{yy}$ are not independent and we may define two independent dimensionless

variables

$$\omega = \frac{\hat{xx} + \hat{yy}}{2L} \quad , \qquad \theta = \tfrac{1}{2}\tan^{-1}\left(\frac{2\hat{xy}}{\hat{xx} - \hat{yy}}\right) + \frac{\pi}{4} \tag{12.17}$$

which enable the plastic stresses to be written in the form

$$\hat{xx} = L\omega + \frac{L}{2}\sin 2\theta, \tag{12.18}$$

$$\hat{yy} = L\omega - \frac{L}{2}\sin 2\theta, \tag{12.19}$$

$$\hat{xy} = -\frac{L}{2}\cos 2\theta. \tag{12.20}$$

With the notation of figure 28, p.108, the stresses $\hat{nn}$, $\hat{ns}$ on an element for which the normal makes an angle α with the x-axis, are given by

$$\hat{nn} = L\omega + \frac{L}{2}\sin 2(\theta - \alpha), \tag{12.21}$$

$$\hat{ns} = \frac{L}{2}\cos 2(\theta - \alpha). \tag{12.22}$$

Rearranging (12.21), (12.22) we have

$$\theta = \alpha \pm \tfrac{1}{2}\cos^{-1}\left(\frac{2\hat{ns}}{L}\right), \tag{12.23}$$

$$\omega = \frac{\hat{nn}}{L} - \tfrac{1}{2}\sin 2(\theta - \alpha). \tag{12.24}$$

Putting $\alpha = 0$ in (12.23) and (12.24) we obtain

$$\theta = \pm \tfrac{1}{2}\cos^{-1}\left(\frac{-2\hat{xy}}{L}\right),$$

$$\omega = \frac{\hat{xx}}{L} \mp \frac{\sqrt{L^2 - 4\hat{xy}^2}}{2L}.$$

From these we may recover (12.17) upon using (12.16). The ambiguity of sign may be removed by physical arguments or from boundary conditions involving the hoop stress

$$\hat{ss} = L\omega - \frac{L}{2}\sin 2(\theta - \alpha). \tag{12.25}$$

The system of equations (12.15), (12.16) are hyperbolic and accordingly possess two families of characteristics, sometimes termed first and second shear lines or slip-lines along which

$$\omega - \theta = \text{constant}, \qquad \omega + \theta = \text{constant},$$

respectively. Starting from the boundary ∂B where $\hat{nn}$ and $\hat{ns}$ are known, we determine ω and θ from (12.23) and (12.24) and then continue the characteristics into the domain B using a step-by-step procedure described in the text books (e.g. Prager and Hodge, 1968). In this way we

cover the whole plastic region with an array of nodal points at which ω and θ and hence the stress components are known.

Test Example using Slip-Line Technique

To illustrate the slip-line technique as part of the elasto-plastic iteration procedure we consider again the circular cavity subject to uniform internal pressure P. We know from (12.1) and (12.2) that yielding begins at the boundary $r = a$ when

$$\hat{\theta\theta} - \hat{rr} = L, \qquad \hat{rr} = -\frac{L}{2} . \tag{12.26}$$

Since $\hat{rr} = -P$, the initial yield pressure is given by

$$P_0 = \frac{L}{2} . \tag{12.27}$$

We will consider the case

$$P = \frac{3L}{2} . \tag{12.28}$$

The analytical value of c, the radius of the elasto-plastic boundary, is given by equation (11.14):

$$\frac{3L}{2} = L \ln \frac{c}{a} + \frac{L}{2} . \tag{12.29}$$

If $a = 2$, (12.29) yields

$$c = 2e = 5.43656 . \tag{12.30}$$

We now seek an approximation for c using the elasto-plastic iteration procedure. The first step is to utilise the numerical methods of Part II of this thesis to solve the elastic problem with boundary conditions:

$$P = \frac{3L}{2} \quad \text{on} \quad r = a = 2. \tag{12.31}$$

We take

$$P = 1, \qquad L = 2/3 \tag{12.32}$$

so that the yield criterion $s = L/2$ becomes

$$4s^2 = \frac{4}{9} = 0.4444 . \tag{12.33}$$

The computer program which produced the results of chapter 9 may be utilised to generate $4s^2$ throughout the domain $r \geq a$. In particular we find

$4s^2 = 0.573$ when $r = 3.25$,

$4s^2 = 0.426$ when $r = 3.50$.

Interpolation gives

$$4s^2 = 0.444 \quad \text{when} \quad r = r_1 \doteq 3.47 . \tag{12.34}$$

In fact the analytical solution (12.1) gives $r = 3.464$. Equation (12.34) defines the contour C_1 .

There is no need for greater accuracy in (12.34) although such could easily be obtained if required. We have simply found a lower bound for the elasto-plastic boundary $r = c$. In practice we shall use a lower bound than r_1 , at which the plastic solution can conveniently be found by the slip-line technique.

To effect a numerical plastic solution for the region between ∂B and C_1 we first select 32 equally spaced nodal points on ∂B. Because of symmetry we work only with those in the first quadrant. From (12.23) and (12.24), the θ , ω coordinates of the nodal points are

$$\theta = \alpha - \frac{\pi}{4} \quad , \quad \omega = -1 \qquad \text{on } \partial B. \tag{12.35}$$

In the notation of figure 45, if the values of θ and ω are known at the points A, B, they may be found at C using the formulae

$$\left.\begin{aligned} \omega_c &= \tfrac{1}{2}\left[(\omega_A + \omega_B) + (\theta_A - \theta_B)\right], \\ \theta_c &= \tfrac{1}{2}\left[(\omega_A - \omega_B) + (\theta_A + \theta_B)\right]. \end{aligned}\right\} \tag{12.36}$$

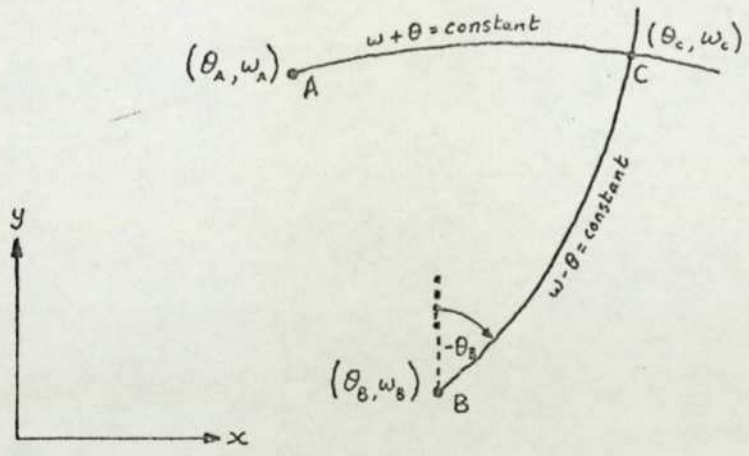


FIG. 45

It is important to distinguish between the two families of shear lines. We note that θ is the angle through which the y - axis turns in an anticlockwise sense in order to point in the "first shear direction", i.e. that of the curve

$$\omega - \theta = \text{constant}.$$

Figure 46 shows the (θ , ω) coordinates obtained from (12.36) for all points in a mesh.

We now approach the more formidable problem of finding accurately the position coordinates of all mesh points. A basic rough approximation to the position of C when A and B are known (figure 45) is the intersection of the following straight lines :

(i) through B making an angle $-\theta_B$ with the y-axis (measuring clockwise).

(ii) through A making an angle $\frac{\pi}{2}-\theta_A$ with the y-axis (measuring clockwise).

These lines meet approximately at right angles at C if the mesh size is small, the orthogonality providing a useful check.

A better approximation, however, is obtained by replacing θ_B in (i) by $\frac{1}{2}(\theta_B + \theta_C)$ and replacing θ_A in (ii) by $\frac{1}{2}(\theta_A + \theta_C)$. Using this improved approximation we computed the polar coordinates (r, ϕ) for the intersections (numbered P_1 , P_2 , P_3 ,.... in figure 46) of the first shear line originating from the boundary point (2 , 0). We observe that the first and second shear lines through the point $\phi = \alpha$ on $r = a$ are

$$r = a e^{\pm(\phi-\alpha)}, \qquad (12.37)$$

i.e. equiangular spirals. Because of symmetry we need only consider the first shear line $r = a e^{\phi}$ and this expression provides a check on the accuracy of the computed polar coordinates (r_i , ϕ_i) of P_i $(i = 1,2,3,.....)$. Results are shown in table 63, p.169.

We now use our slip-line solution to find the plastic stresses at a radius r_j where

$$r_j = \max r_i \quad \text{such that} \quad r_i < c_1 , \quad (i = 1,2,3,.....).$$

From table 63, p.169, we obtain $r_j = r_5$. Knowing that the plastic zone extends at least as far as $r = 3.47$ we are at liberty to retreat to $r = 3.27$ and find the plastic stresses there. We have

$$\omega_5 = -1 + \frac{5\pi}{32}, \qquad \theta_5 = \frac{-3\pi}{32}, \qquad \alpha_5 = \frac{5\pi}{32}$$

upon employing the subscript notation described above. Hence (12.21) and (12.22) yield

$$\hat{n}n = -1 + \frac{10\pi}{96}, \qquad \hat{n}s = 0 \qquad \text{on } r = r_5. \qquad (12.38)$$

Solving another elastic problem, this time using (12.38) as boundary conditions, we examine the computer output to determine again the region where $4s^2 \geq \frac{4}{9}$. We find C_2 to be approximately r = 4.64. (The analytic elastic solution

gives the result r = 4.6454). It is now convenient to retreat to $r = r_8 = 4.392$ (see table 63) where plastic stresses can conveniently be found by the slip-line technique. We find

$$\omega_8 = -1 + \frac{\pi}{4}, \qquad \theta_8 = 0, \qquad \alpha_8 = \frac{\pi}{4};$$

$$\hat{nn} = \frac{\pi}{6} - 1, \qquad \hat{ns} = 0. \tag{12.39}$$

It is encouraging to note that the value of $\hat{nn}$ in (12.39) agrees to three decimal places with the analytical plastic solution (11.13) at $r = r_8$.

We now utilise (12.39) as boundary conditions on r = 4.392, and solve the elastic problem again. We find C_3 is r = 5.25 and retreat to $r_9 = 4.8459$. Hence another iteration yields C_4 to be given by r = 5.381.

Conclusion

We have, therefore, the following successive approximations to r = c :

C_1	r = 3.46
C_2	r = 4.64
C_3	r = 5.25
C_4	r = 5.38

The analytical result is r = 5.44.

Another assessment of the accuracy of each approximation may be derived by observing that the hoop stress $\hat{ss}$ and the invariant $\Theta = \hat{nn} + \hat{ss}$ must be continuous across the equilibrium elasto-plastic interface. In this problem we know that $\Theta = 0$ for $r \geq c$ (11.18). For $r \leq c$ we have from (12.18) and (12.19) or (12.21) and (12.25)

$$\Theta = \hat{xx} + \hat{yy} = \hat{nn} + \hat{ss} = 2L\omega. \tag{12.40}$$

Computing (12.40) from the slip-line solution after each iteration we find that values approach zero as expected. Results are shown below :-

	ω	Θ
C_1	- 0.45	- 0.60
C_2	- 0.16	- 0.21
C_3	- 0.03	- 0.04
C_4	- 0.01	- 0.01
C	0.00	0.00

To sum up, the elasto-plastic iteration procedure has been tested both as a process, and as a numerical method involving computed plastic solutions. Although convergence has only been examined for circular and spherical boundaries, results give ground for supposing that the same convergence behaviour will be obtained for a large class of reasonably shaped boundaries.

Results

TABLE 61

P/L	0.5000	0.7500	1.0000	1.2500
c_1/a	1.0000	1.2247	1.4142	1.5811
c_2/a	1.0000	1.2813	1.6167	1.9898
c_3/a	1.0000	1.2840	1.6481	2.1095
c_4/a	1.0000	1.2840	1.6487	2.1170
c/a	1.0000	1.2840	1.6487	2.1170

P/L	1.5000	1.7500	2.0000
c_1/a	1.7321	1.8708	2.0000
c_2/a	2.3883	2.8045	3.2334
c_3/a	2.6796	3.3625	4.1571
c_4/a	2.7177	3.4857	4.4587
c/a	2.7182	3.4903	4.4817

Circular Cavity

TABLE 62

P/L	2/3	1	4/3	5/3
c_1/a	1.0000	1.1447	1.2599	1.3572
c_2/a	1.0000	1.1797	1.3775	1.5820
c_3/a	1.0000	1.1814	1.3953	1.6448
c_4/a	1.0000	1.1814	1.3956	1.6487
c/a	1.0000	1.1814	1.3956	1.6487

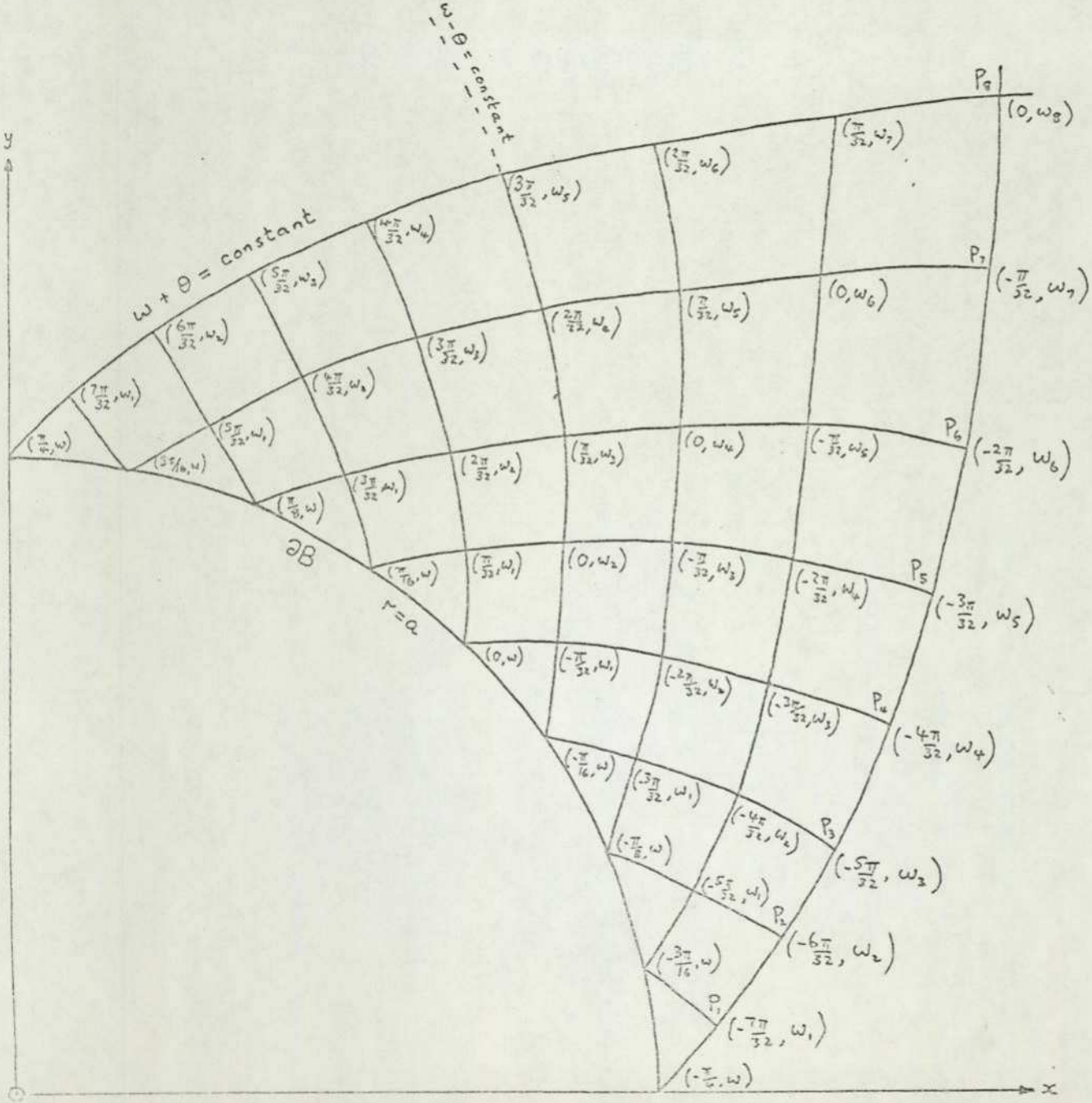
P/L	2	7/3	8/3
c_1/a	1.4422	1.5183	1.5874
c_2/a	1.7868	1.9887	2.1866
c_3/a	1.9292	2.2445	2.5854
c_4/a	1.9475	2.2989	2.7090
c/a	1.9477	2.3010	2.7183

Spherical Cavity.

TABLE 63

i	COMPUTED r_i	ANALYTIC r_i	ϕ_i
1	2.207	2.206	$\pi/32$
2	2.435	2.434	$\pi/16$
3	2.686	2.685	$3\pi/32$
4	2.964	2.962	$\pi/8$
5	3.270	3.267	$5\pi/32$
6	3.608	3.605	$3\pi/16$
7	3.981	3.976	$7\pi/32$
8	4.392	4.389	$\pi/4$
9	4.846	4.839	$9\pi/32$
10	5.347	5.338	$5\pi/16$

Polar coordinates of P_i



$\omega_8 = -1 + \frac{8\pi}{32}$

$\omega_7 = -1 + \frac{7\pi}{32}$

$\omega_6 = -1 + \frac{6\pi}{32}$

$\omega_5 = -1 + \frac{5\pi}{32}$

$\omega_4 = -1 + \frac{4\pi}{32}$

$\omega_3 = -1 + \frac{3\pi}{32}$

$\omega_2 = -1 + \frac{2\pi}{32}$

$\omega_1 = -1 + \frac{\pi}{32}$

$\omega = -1$

Net of shear lines showing (θ, ω) coordinates. Uniform internal pressure on the circle $r=a$.

Figure 46

CHAPTER 13

ELLIPTIC CAVITY SUBJECT TO UNIFORM INTERNAL PRESSURE

Introduction

In this chapter we extend the previous analysis to an infinite cavity of elliptic cross-section. The boundary ∂B, given by

$$\frac{x^2}{a^2} + \frac{y^2}{b^2} = 1 \qquad (13.1)$$

is subject to uniform internal normal pressure P. We consider the case $a = 2$, $b = 1$: and P is three times the initial yield pressure. We use our elasto-plastic iteration procedure in which the first step is to solve the elastic problem with the appropriate boundary conditions.

First Iteration

An analytical elastic solution is available (chapter 9) and the solution for the maximum shear stress s, defined in (9.14), which, expressed in confocal elliptic coordinates (Bhargava, 1959), takes the form

$$s = \frac{P\left[\left(\frac{a^2+b^2}{c^2}\right)^2 - 1\right]^{1/2}}{\left[\frac{a^2+b^2}{c^2} - \cos 2\eta\right]} \qquad \text{on } \partial B. \qquad (13.2)$$

The boundary quantity (13.2) attains a maximum value Pa/b at the extremities of the major axis. The Tresca yield criterion states that yielding begins when

$$s = \frac{L}{2}. \qquad (13.3)$$

The initial yield pressure P_o is therefore given by

$$\frac{L}{2} = \frac{P_o a}{b},$$

i.e.

$$P_o = \frac{Lb}{2a}. \qquad (13.4)$$

We considered the case

$$P = 3P_o = \frac{3L}{4}, \qquad (13.5)$$

so that by (13.3) the yield condition is expressed in the form

$$s = \frac{2P}{3}, \qquad 4s^2 = \frac{16P^2}{9}. \qquad (13.6)$$

To complete the first stage of the first iteration we draw a contour C_1 which encloses the region in which the purely elastic stresses satisfy the inequality

$$\frac{4s^2}{P^2} \geqslant \frac{16}{9} = 1.777. \qquad (13.7)$$

For this we can utilise either the analytical solution (9.14) or the numerical solution obtained by the integral equation methods of Part II. The values of $4s^2/P^2$, as obtained by each method, have already been tabulated (figure 30, p.130) for a mesh of field points. The result of applying (13.7) to construct C_1 is shown in figure 49 (p177).

It is now assumed that the stresses within C_1 are relaxed to satisfy the yield criterion and these plastic stresses are found using the slip-line technique described in chapter 12. The characteristic coordinates are known on the boundary to be

$$\theta = \alpha - \tfrac{\pi}{4}, \quad \omega = -\tfrac{1}{4} \qquad (13.8)$$

by virtue of (12.23), (12.24) and (13.5). Equal eccentric angles were used to define 32 nodal points on ∂B as before. The symmetry of the problem implies that we need only consider the first quadrant; results in the other three quadrants being obtained by reflection in the coordinate axes. We find that five nodal points in the first quadrant are enclosed by C_1 (figure 49, p.177). The characteristic coordinates (13.8) are evaluated both at these five points and, using (12.36), at all intersections within C_1 of shear lines originating from these five points. The aim is to find plastic stresses on C_1. From the point of view of accuracy it is advantageous to shrink the curve C_1 slightly so that it passes through the intersections of shear lines. The modified curve C_1 will be termed $\bar{C}_1$. We are free to retreat in this manner since we are only asserting that C_1 lies wholly within the plastic zone, i.e. C_1 is a "lower bound" for the true elasto-plastic interface. A curve $\bar{C}_1$ strictly within C_1 will clearly have the same property. Alternatively we could interpolate along shear lines to obtain stresses on the contour C_1 already defined. However, although slightly inferior as a first approximation, the curve $\bar{C}_1$ provides a superior basis for the second iteration.

For the latter, it will again be convenient to represent the boundary in terms of 8 nodal points in the first quadrant. These points are numbered 1 to 8 and their location is determined using the construction of figure 45, p165. Results are shown in figure 49, p.177, whence there is an obvious choice of 4 new nodal points on $\bar{C}_1$. Four points on ∂B will be utilised again in the second iteration. It is important for continuity that we take a nodal point (number 5) at the intersection of ∂B and $\bar{C}_1$.

By repeated use of equations (12.36) we find the characteristic coordinates of the new nodal points as follows:-

Nodal point	θ	ω
1	- 0.615	+ 0.115
2	- 0.285	+ 0.065
3	- 0.005	- 0.005
4	+ 0.205	- 0.075

We then obtain $\frac{dx}{dn}$, $\frac{dy}{dn}$ from the slope of the normal to $\bar{C}_1$, and equations (12.18) to (12.20) then provide the plastic stress components $\hat{xx}$, $\hat{xy}$, $\hat{yy}$. Thence from the formulae (7.11):

$$\left.\begin{aligned} F_x &= -\hat{xx}\,\frac{dx}{dn} - \hat{xy}\,\frac{dy}{dn}, \\ F_y &= -\hat{xy}\,\frac{dx}{dn} - \hat{yy}\,\frac{dy}{dn}, \end{aligned}\right\} \qquad (13.9)$$

we obtain the traction components per unit length of boundary F_x, F_y. The results are

Nodal point	F_x	F_y
1	0.50	0.09
2	0.47	0.34
3	0.52	0.41
4	0.41	0.56

By numerical integration we then find the partial derivatives of the Airy stress function using (7.13). Hence the normal derivative χ' may be computed from (7.15). After another numerical integration, equation (7.14) yields the function χ. To ensure continuity with the values of χ, χ' at nodal points on ∂B, the nodal point (number 5) which lies on $\bar{C}_1$ and ∂B is chosen as the point s_0 (of equations (7.13) and (7.14)).

Second Iteration

We define a contour $\overline{\partial B}$ as that enclosing the ellipse ∂B and the region enclosed by $\overline{C}_1$. A rough sketch is shown in figure 47.

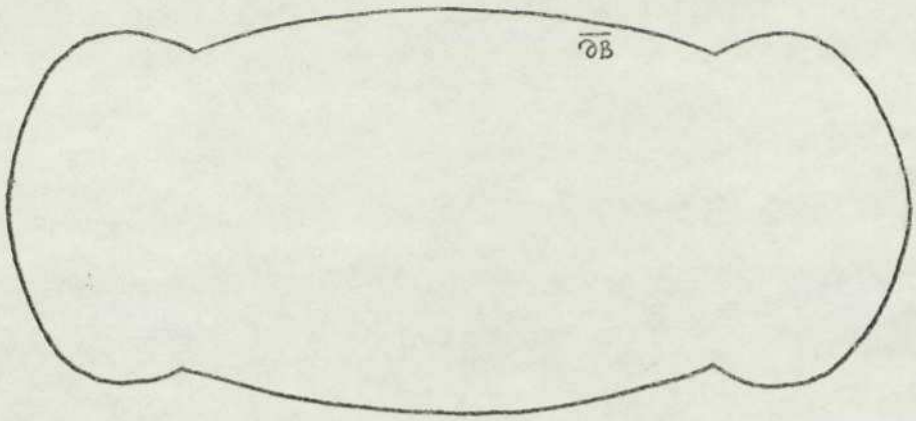


Figure 47

Values of χ and χ', which are known everywhere on $\overline{\partial B}$, are used as boundary data in the elastic cavity problem. This is solved as before by the numerical methods of Part II, and a contour C_2 is constructed (figure 50, p.178) to enclose the domain satisfying (13.7).

The characteristic coordinates θ, ω are found throughout the enclosed net of shear lines. As before we shrink C_2 and replace it by a contour $\overline{C}_2$ which passes through mesh points of the characteristic net (figure 50). We chose suitable nodal points to define $\overline{C}_2$ and found their Cartesian coordinates as follows :-

Nodal point	x	y
1	2.42	0.37
2	2.61	0.64
3	2.28	0.98
4	1.96	1.38
5	1.62	1.26
6	1.08	1.27
7	0.80	1.10
8	0.42	1.18

A computer program was written to determine $\hat{xx}$, $\hat{xy}$, $\hat{yy}$ and then F_x, F_y from the above data as in (13.9). The program also computed the quantities χ and χ' on $\overline{C}_2$ as in the first iteration. This time there was no problem concerning two parts of the boundary since the plastic zone has completely surrounded the cavity.

Third Iteration

The values of χ, χ' obtained on $\bar{C}_2$ are now used as input data for yet another numerical elastic problem. A contour C_3 is obtained by enclosing the region in which (13.7) is satisfied.

The form of the contour C_3 so obtained (figure 51) suggests that improvements could be made by choosing a smoother contour than $\bar{C}_2$. Accordingly we select the contour $\bar{\bar{C}}_2$ shown in figure 52, p.180. By the argument employed previously we are free to retreat in this way from $\bar{C}_2$ to $\bar{\bar{C}}_2$ which is wholly enclosed by $\bar{C}_2$. After modifying the input data for $\theta, \omega, x, y, x', y'$ at certain nodal points, the program for the elastic problem was run again. The contour C_3 is accordingly replaced by a modified contour which we call C_3^*.

Conclusion

The contour C_3^* appears to be more reliable than C_3. Figure 53 compares the contours C_1, C_2, C_3^*. It may be observed that C_3^* intersects C_2. This apparent illogicality is a consequence of our "retreat" procedure; but may be interpreted as an indication that we are now very close to the true equilibrium elasto-plastic interface C. The proximity of C_2 to C_3^* is also an encouraging feature.

Finally the contours C_3 and C_3^* are compared in figure 54, and bearing in mind natural numerical oscillations, an estimate of the true contour C is made on the basis of the reasonable convergence of C_1, C_2, C_3^*. A sketch of the final estimate for the whole zone of contained plastic flow is given below (figure 48). For more accurate readings, reference should be made to figure 54 (p.182) which is on a larger scale.

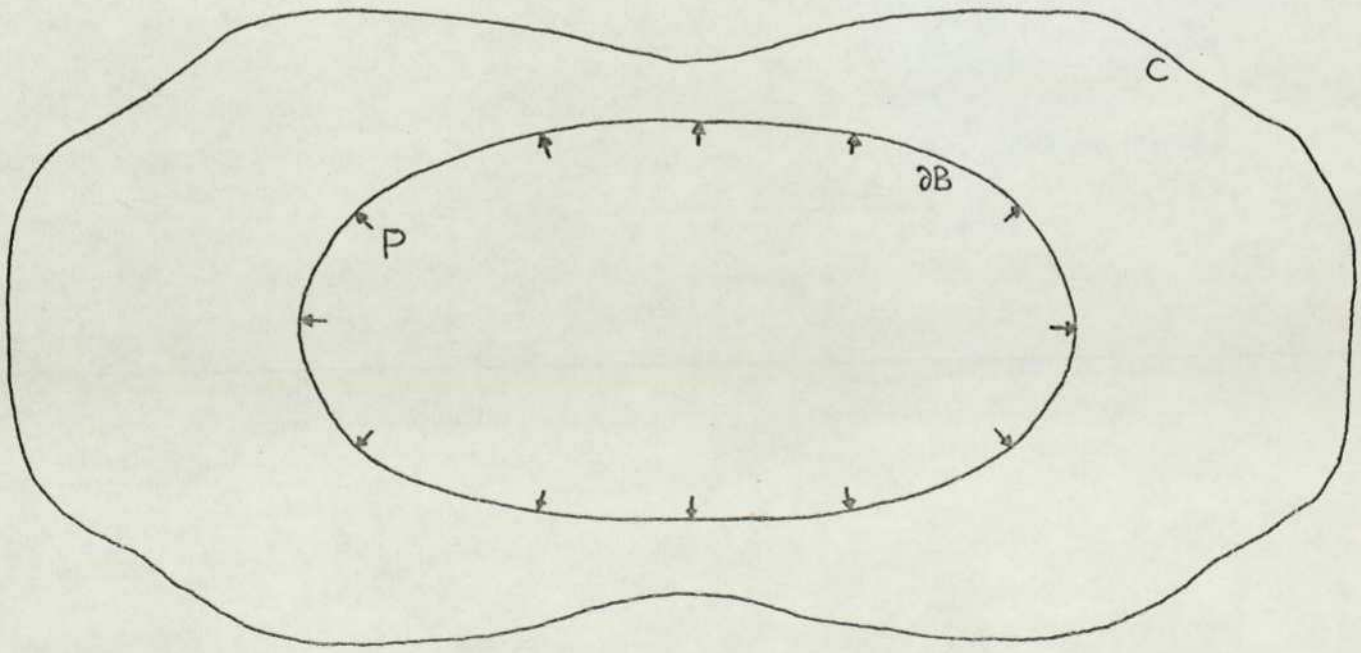


FIG. 48

We are aware of the limitations of the method; notably that of constructing shear lines accurately. It can be reasonably asserted that our final estimate of C (figure 54) is accurate to within 10%. The physical measurement of elastic constants is subject to errors of this order; it may well be that any attempt to solve this problem experimentally would be subject to greater errors, so that further approximations are irrelevant from the practical point of view.

Mathematically, the value of Part III of this thesis is that the elasto-plastic iteration procedure is exploited further than ever before, and applied in particular to the problem of the elliptic cavity subject to uniform internal pressure. The solution, obtained in this chapter, for the resulting zone of contained plastic flow, is more accurate than any previously obtained. The successive approximations are displayed in the figures on the following pages.

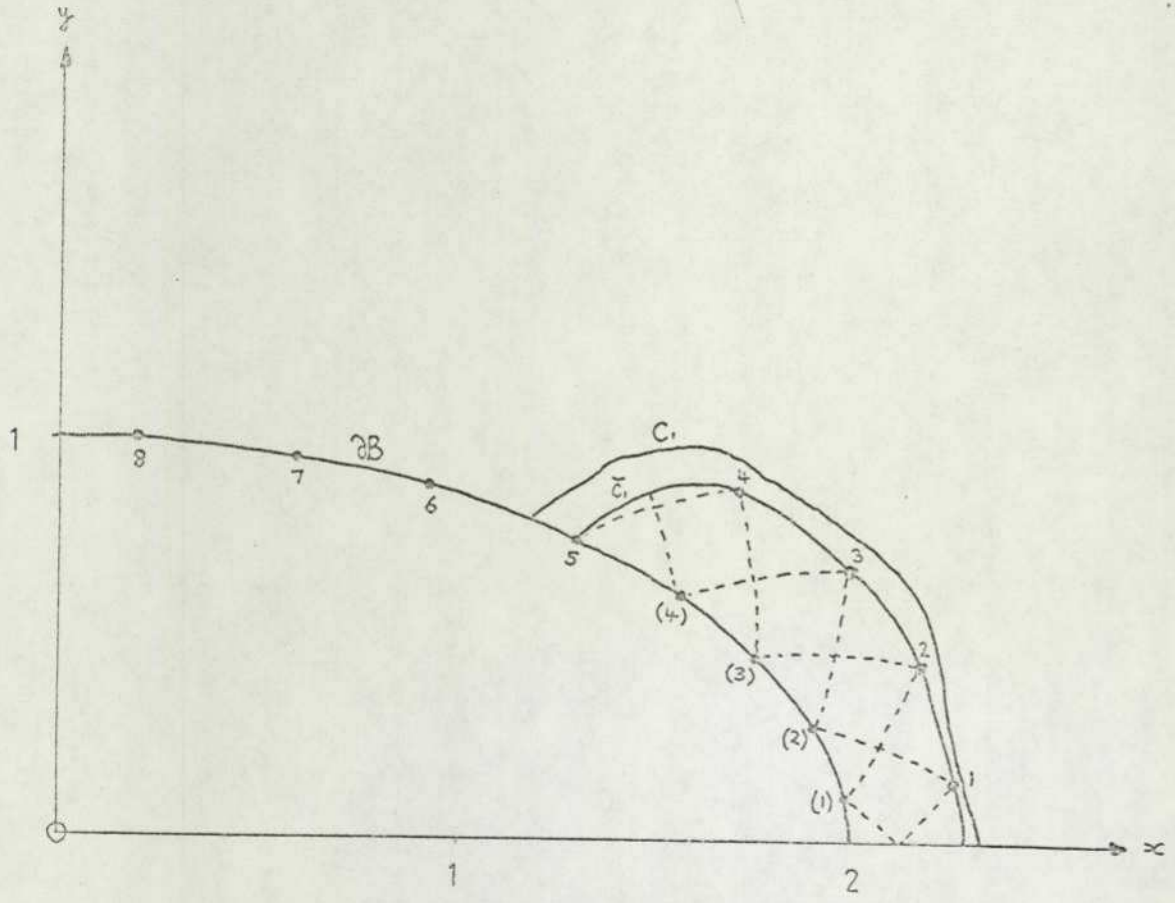


FIG. 49

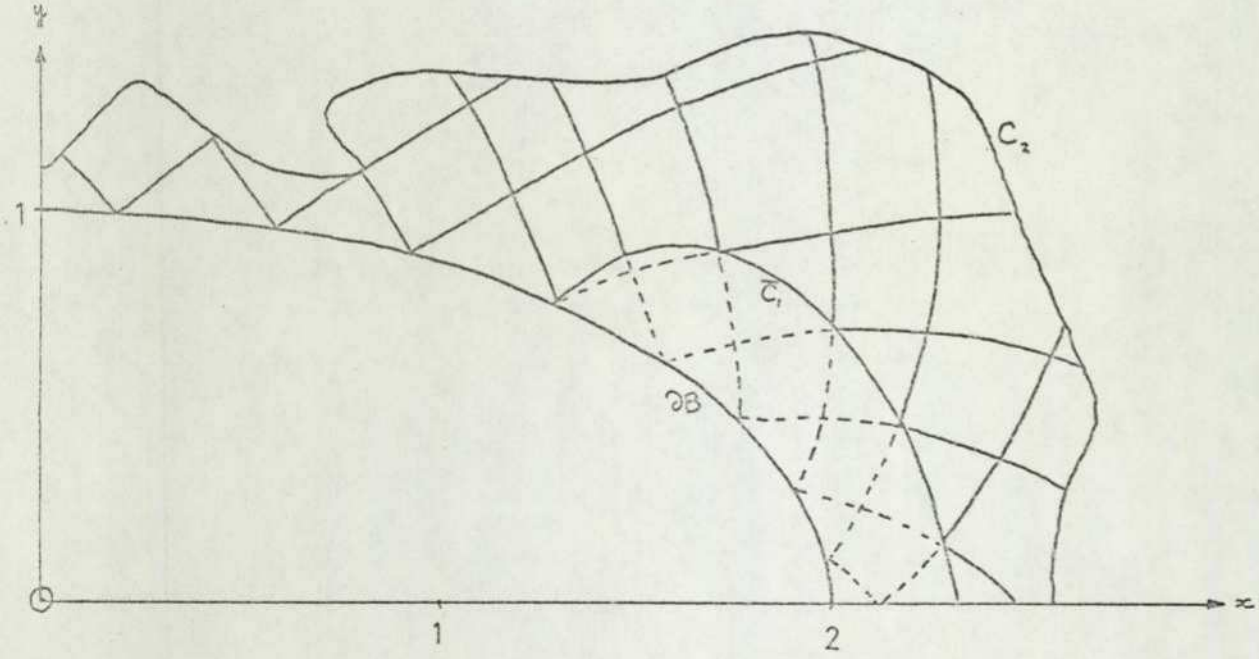


FIG. 50

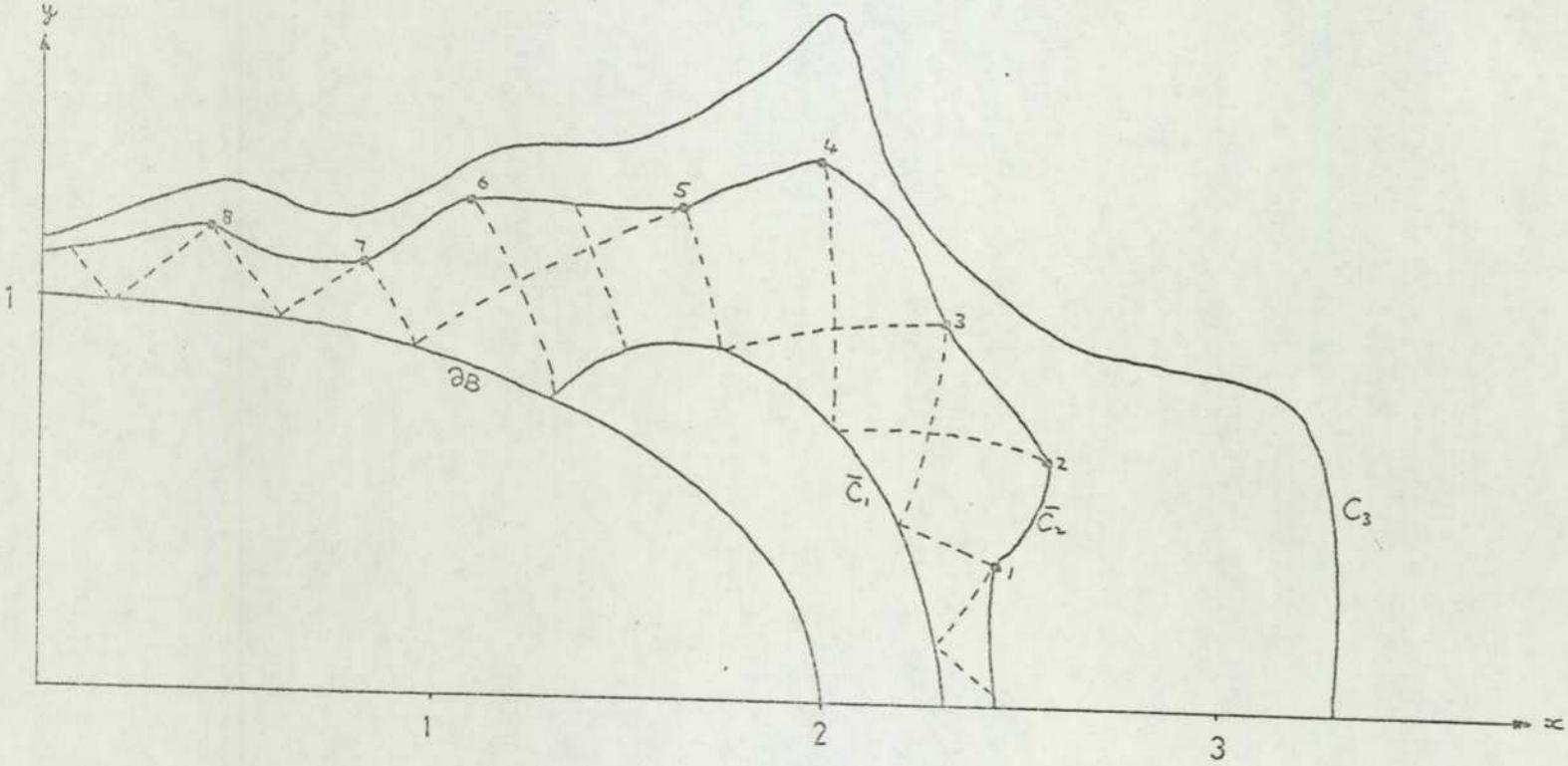


FIG. 51

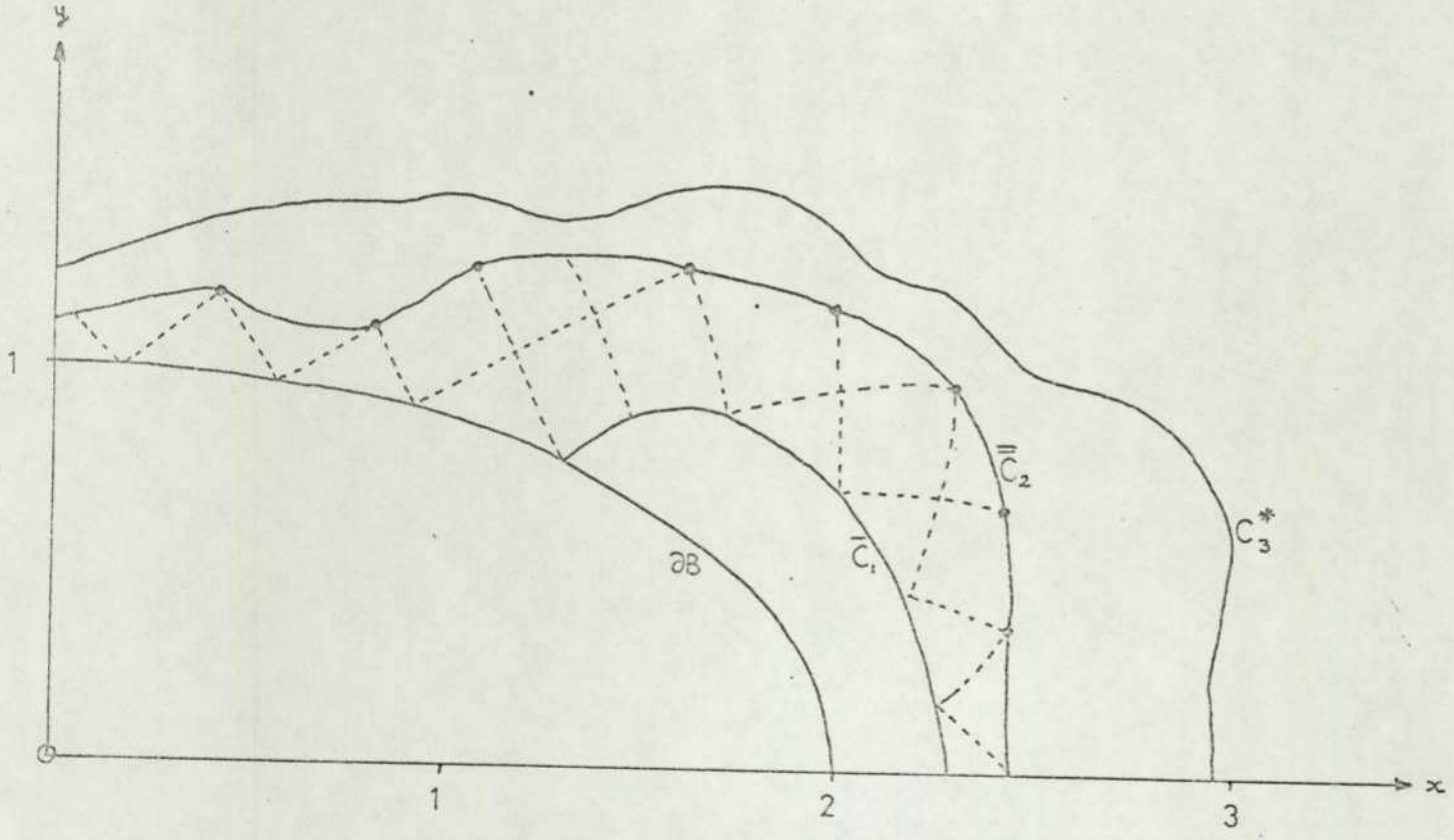


FIG. 52

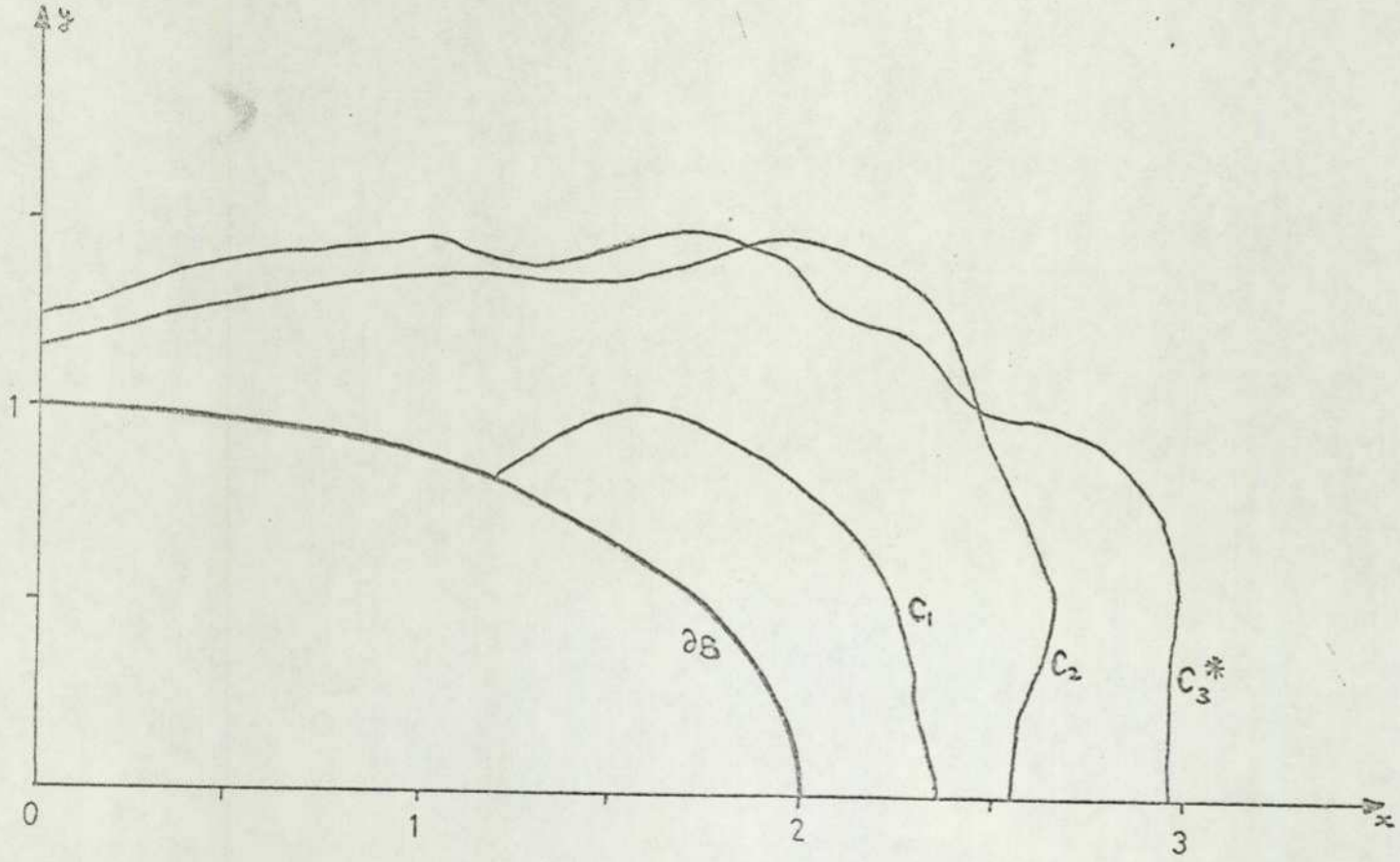


FIG. 53

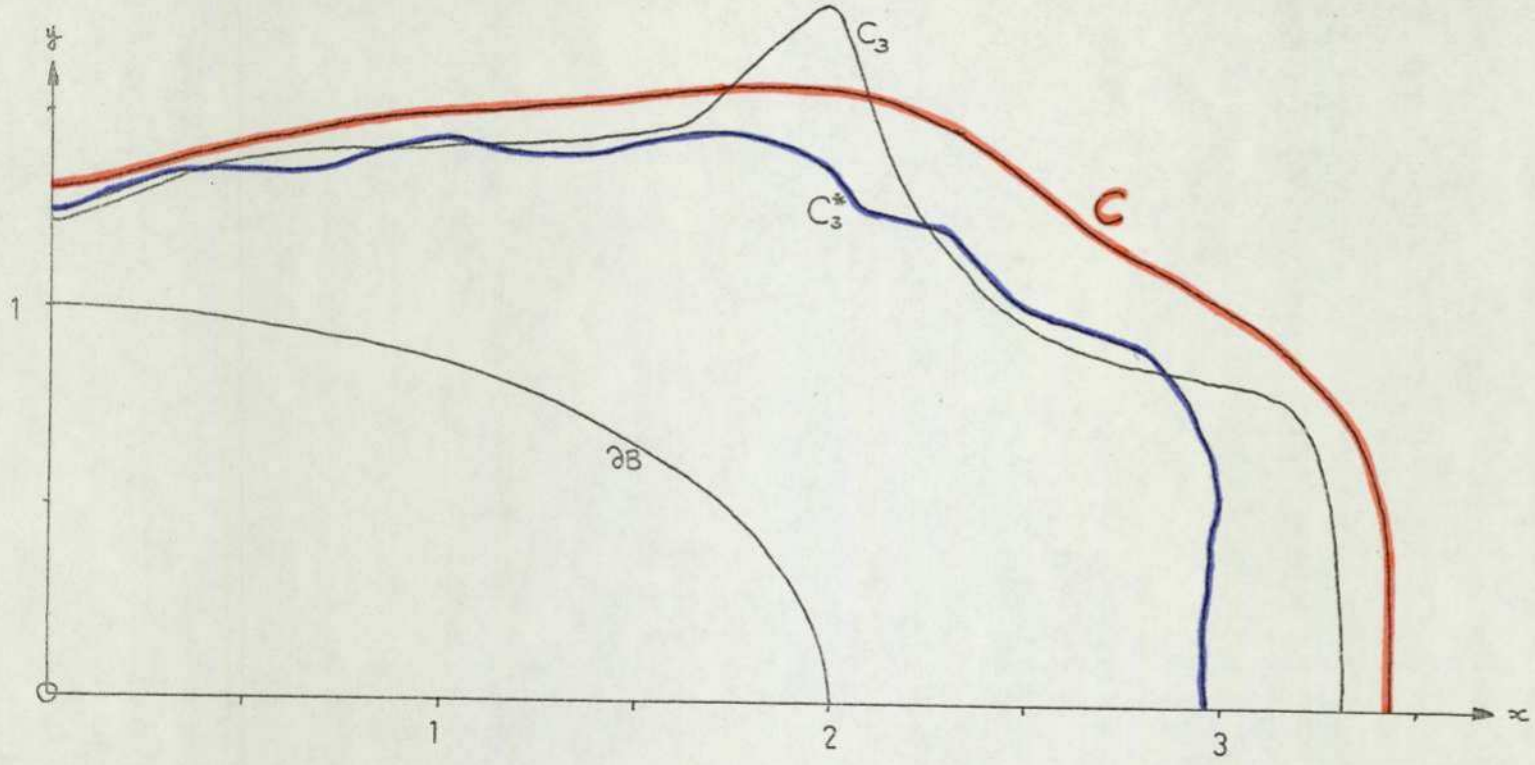


FIG. 54

APPENDICES.

APPENDIX 1

THE Γ-CONTOUR : ANALYTICAL CONSIDERATIONS

In chapter 2 we obtained the result (2.18) that

$$\int_{\partial B} \ln|\underline{p}-\underline{q}|\,\lambda(\underline{q})\,dq = \text{constant}; \qquad \underline{p}\in\partial B, \quad \text{(A1.1)}$$

possesses an effectively unique solution for any given contour ∂B. It is now necessary to decide which value the constant in (A1.1) takes for any given contour. It is to be noted that if $\lambda(\underline{q})$ satisfies (2.13) on ∂B then on a similar contour of parameter m (we replace the position vector $\underline{r}$ for ∂B by $m\underline{r}$ to obtain the geometrically similar contour ∂B_m), (2.13) is satisfied by $\Lambda(m\underline{q})$ where

$$\Lambda(m\underline{q}) = \frac{\lambda(\underline{q})}{m(1+s\ln m)},$$

$$s = \int_{\partial B} \lambda(\underline{q})\,dq,$$

since

$$\int_{\partial B_m} \ln|m\underline{p}-m\underline{q}|\,\lambda(\underline{q})\,d(m\underline{q}) = (m\ln m)\int_{\partial B_1} \lambda(\underline{q})\,dq + m\int_{\partial B_1} \ln|\underline{p}-\underline{q}|\,\lambda(\underline{q})\,dq = m(1+s\ln m).$$

Thus it is evident that it is <u>not</u> possible to define a solution for (2.13) for a contour for which $m = e^{-1/s}$ and furthermore, that there is <u>one and only one</u> such contour in any class of similar contours. This exceptional contour is called the Γ-contour. It might, of course, happen that $\partial B_1 = \Gamma$, in which case the right-hand side of the last result becomes $sm\ln m$ and since $m = 0$ is not considered anyway we have the exceptional contour characterized by $m=1$ as expected.

Thus we can state that (2.13) has a solution for all but one contour of any given class of similar regular contours. The condition for (2.14) to have a non-trivial solution is that ∂B is the Γ-contour. As a simple illustration, equation (2.13) is solved for a circle of

radius b by $\lambda(\underline{q}) = (2\pi\, b\, \ln b)^{-1}$, but has no solution when b = 1; on the other hand, equation (2.14) exhibits the non-trivial solution $\lambda(\underline{q})$ = constant when b = 1, but has no solution apart from $\lambda(\underline{q}) = 0$ when $b \neq 1$. It is not difficult to show that in three-dimensions there are no exceptional surfaces analogous with the two-dimensional Γ-contour.

The Γ-contour has no physical significance. In a numerical approach, proximity to Γ will be indicated by ill-conditioning in the relevant system of linear equations. As noted in chapter 2 we may avoid the Γ- contour simply by changing the scale.

Assuming this done, we return to equation (2.1). We multiply both sides of (2.1) by $\lambda(\underline{p})\,d_P$ and integrate around ∂B ($\neq \Gamma$). Inversion of the order of integration is justified since all functions may be assumed of class L_2 so that the Lebesgue-Fubini theorem applies. Thus we have

$$\int_{\partial B} \lambda(\underline{p}) \left[\int_{\partial B} \ln|\underline{p}-\underline{q}|\, \sigma(\underline{q})\, d_q \right] d_P = \int_{\partial B} \phi(\underline{p})\, \lambda(\underline{p})\, d_P \qquad \text{(A1.2)}$$

and hence

$$\int_{\partial B} \sigma(\underline{q}) \left[\int_{\partial B} \ln|\underline{p}-\underline{q}|\, \lambda(\underline{p})\, d_P \right] d_q = \int_{\partial B} \phi(\underline{p})\, \lambda(\underline{p})\, d_P\,, \qquad \text{(A1.3)}$$

but since λ has been chosen for a non Γ-contour this reduces to

$$\int_{\partial B} \sigma(\underline{q})\, d_q = \int_{\partial B} \phi(\underline{p})\, \lambda(\underline{p})\, d_P\,. \qquad \text{(A1.4)}$$

This result is used in chapter 2 (equations (2.26) and (2.34)) in arriving at the result that there exists a unique interior harmonic function characterized by $\phi(\underline{p})$ on ∂B ($\neq \Gamma$); and similarly there exists a unique exterior function bounded at infinity. A similar treatment can be given for the Γ-contour showing that with the partition (2.29) and the condition (2.34), equation (2.33) always exhibits a unique solution.

APPENDIX 2

THE Γ-CONTOUR : NUMERICAL CONSIDERATIONS

In appendix 1 a method was given for finding the Γ - contour analytically. It seems profitable to conduct a numerical investigation to confirm that ill-conditioning is confined to the neighbourhood of this exceptional contour as predicted. Briefly, if the "electrostatic" problem solved on $f(x, y) = 0$ yields a capacity s, the Γ-contour is given by

$$f\left(\frac{x}{m}, \frac{y}{m}\right) = 0$$

where

$$m = e^{-1/s}. \qquad (A2.1)$$

Accordingly for the particular case of the ellipse with $a = 2$, $b = 1$,

$$f(x,y) = \frac{x^2}{4} + \frac{y^2}{1} - 1 = 0.$$

The analytical value of the capacity for this ellipse is given by (3.21) as

$$s = 2.4663$$

so that (A2.1) yields $m \doteq 0.6667$. Since

$$f\left(\frac{x}{m}, \frac{y}{m}\right) = \frac{x^2}{4m^2} + \frac{y^2}{m^2} - 1 = 0,$$

the Γ-contour for the 2:1 ellipse is given by

$$b = m \doteq 0.6667.$$

A series of programs was run which solved the Dirichlet problem for the 2:1 ellipse (again with $\phi(\underline{P}) = 1$ on ∂B) taking a range of values of b from 0.5 to 2.0 giving special attention to values of b near m. As expected, ill-conditioning occurs as b approaches m from above or below. The generated value of $\phi(\underline{P})$ at the origin has the following properties

$$\phi_o \to -\infty \text{ as } b \to m^{(-)},$$

$$\phi_o \to +\infty \text{ as } b \to m^{(+)},$$

$$|\phi_o - 1| < 0.01 \quad \text{if} \quad |b - m| > 0.02.$$

Full results are given in table 64. The values of $\phi(\underline{P})$ at 8 points on the major axis were generated and each produced similar behaviour to ϕ_o. In particular for the point $\underline{P}$

defined by $x = (1.95)^{\frac{a}{2}}$, $\phi(\underline{P}) \equiv \phi_p$ is characterized by

$$\phi_p \to -\infty \text{ as } \quad b \to m^{(-)}$$

$$\phi_p \to +\infty \text{ as } \quad b \to m^{(+)}$$

$$|\phi_p - 1| < 0.01 \text{ if } \quad |b - m| \quad > \quad 0.1.$$

It was also noted that everywhere on ∂B

$$\sigma < 0, \; s < 0 \text{ if } \quad b < m \quad ,$$

$$\sigma > 0, \; s > 0 \text{ if } \quad b > m \quad .$$

We note from the analytical results (3.21) and (3.26) that s and σ become infinite when $a + b = 2$. This provides a more direct route to the Γ-contour than (A2.1) but applies only to ellipses. Clearly for the 2:1 ellipse, $b = \frac{2}{3}$ gives the Γ-contour whilst for the n:1 ellipse $b = 2/(n+1)$ defines the scale to be avoided. Theoretically

$$\sigma \to \infty, \; s \to \infty \text{ as } \quad b \to m^{(+)},$$

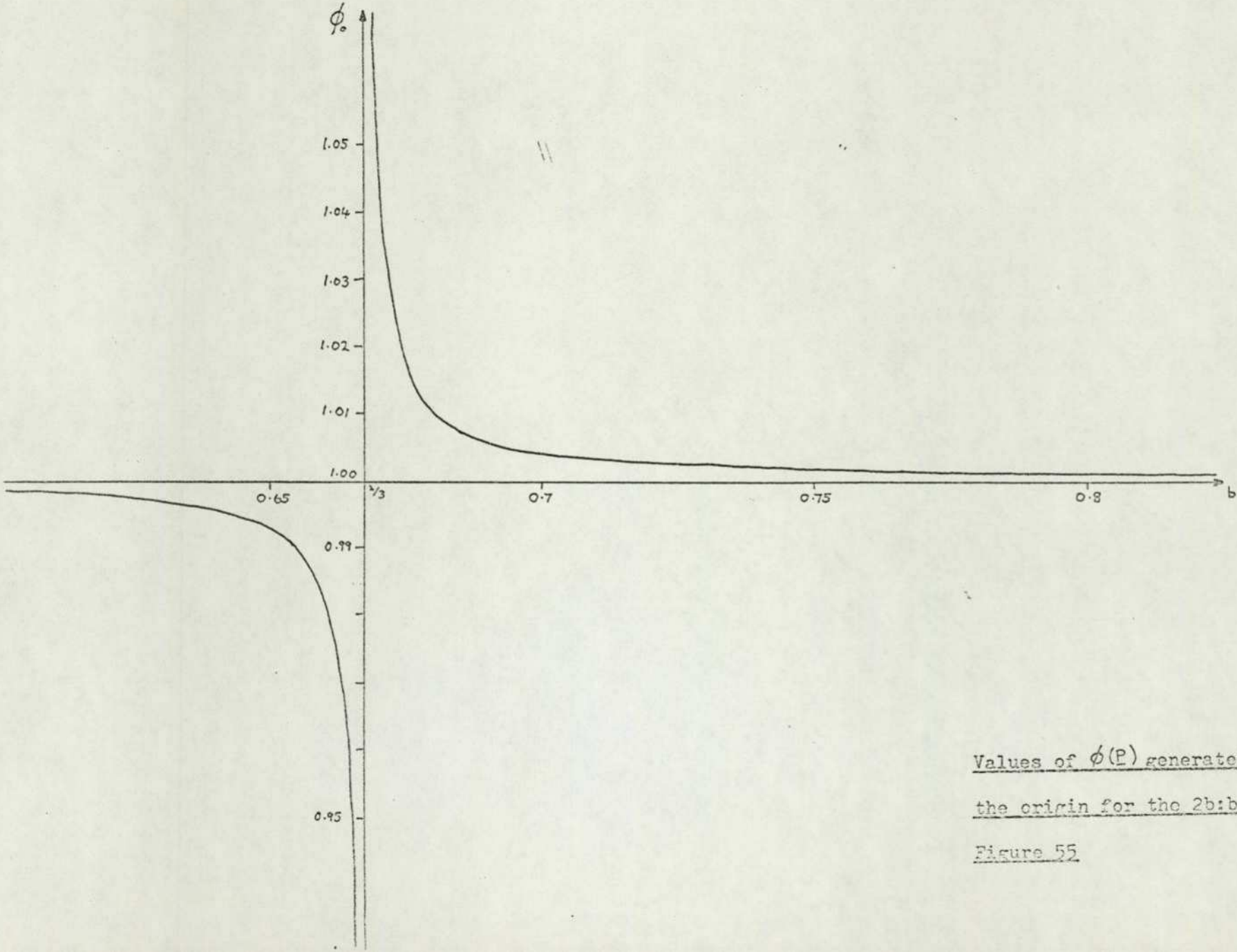
$$\sigma \to -\infty, \; s \to -\infty \text{ as } \quad b \to m^{(-)}.$$

This feature is confirmed well in the numerical results of table 64 and figure 55. The accuracy of the computed σ, s, ϕ increases steadily as the scale increases beyond the Γ-contour (as was found by a further program in which b was increased from 1 to 100). The following is a sample of the results obtained :-

TABLE 64

b	ϕ_o	ϕ_p
0.500	0.9993	0.9947
0.600	0.9981	0.9855
0.660	0.9808	0.8508
0.662	0.9727	0.7880
0.664	0.9530	0.6350
0.666	0.8324	- 0.3020
0.667	1.5965	5.6345
0.668	1.1074	1.8347
0.670	1.0407	1.3166
0.700	1.0040	1.0314
0.800	1.0011	1.0084
0.900	1.0007	1.0051
1.000	1.0005	1.0038
2.000	1.0002	1.0014

Values of $\phi(\underline{P})$ generated at the centre and near the boundary of a 2:1 ellipse of various scales.



Values of $\phi(P)$ generated at the origin for the 2b:b ellipse.

Figure 55

APPENDIX 3

A TRIAL HARMONIC PROBLEM

As a further test example, the Dirichlet problem of chapter 3 was considered, with the ellipse replaced by the square $|x| \leq 1$, $|y| \leq 1$. For this new domain equations (3.1), (3.2) and (3.5) were used again, and equal intervals were defined along each side of the square with interval points in each corner. The number of nodal points, n , was systematically increased and ϕ generated in the interior for each n. Error analysis was again carried out on the boundary and results for $\phi(\underline{P})$ generated over a square mesh of interior points were encouraging. Values of $\phi(\underline{P})$ for $n = 80$ are shown in figure 56.

A similar Dirichlet problem with different boundary conditions arises when determining the stress function χ for the torsion of a beam with uniform square cross-section. With B again defined by $|x| \leq 1$, $|y| \leq 1$, we accordingly seek a solution for χ satisfying

$$\nabla^2 \chi = -2 \quad \text{in} \quad B + \partial B$$

and

$$\chi = 0 \quad \text{on} \quad \partial B$$

using

$$\phi = \chi + \tfrac{1}{2} r^2 \quad \text{in} \quad B + \partial B,$$

$$\nabla^2 \phi = 0 \quad \text{in} \quad B + \partial B,$$

and

$$\phi = \tfrac{1}{2} r^2 \quad \text{on} \quad \partial B$$

where $r^2 = x^2 + y^2$ and ∇^2 is the two-dimensional Laplacian operator. Here the formulation is as before except that (3.1) is replaced by

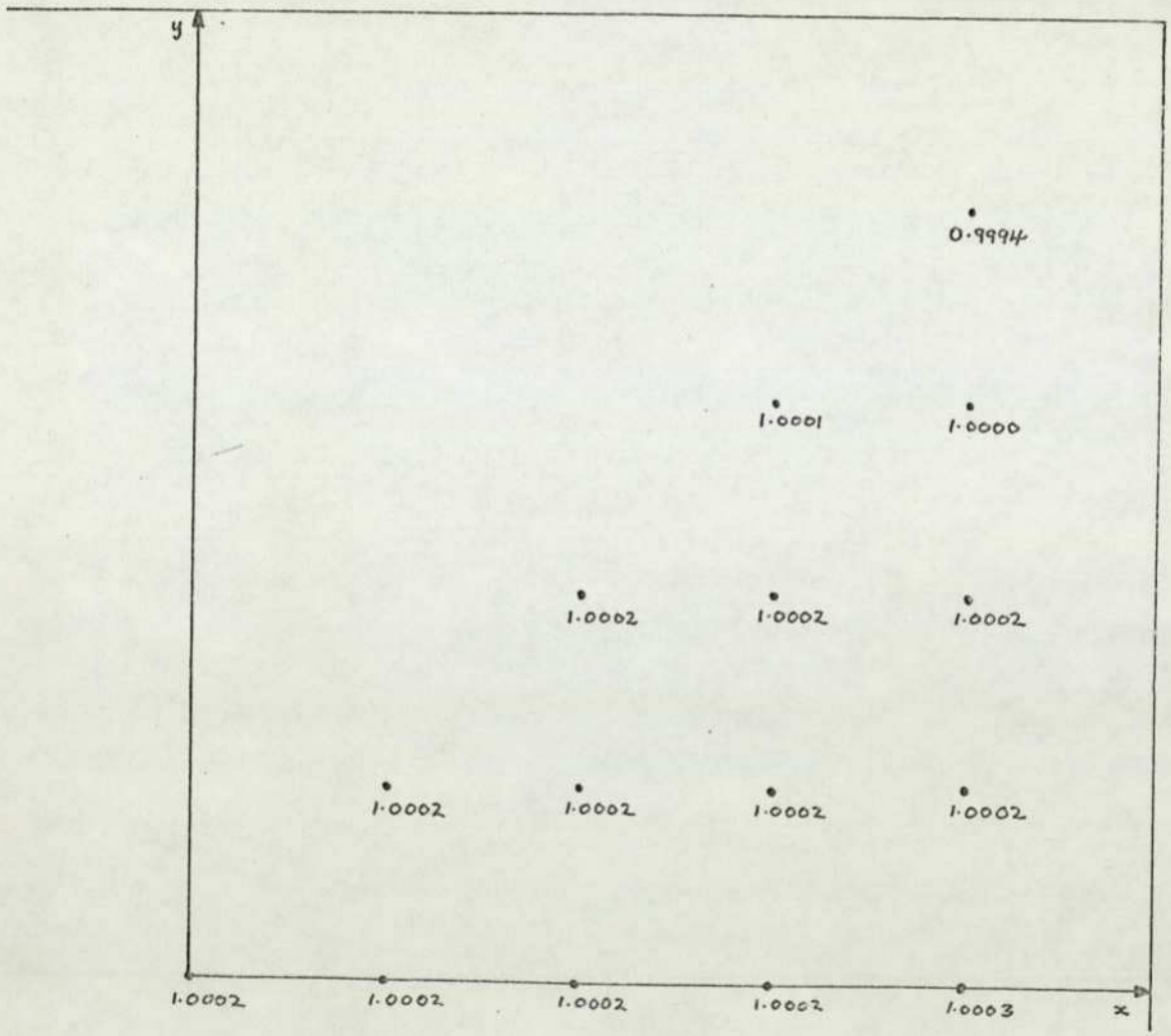
$$\int_{\partial B} \ln|\underline{P} - \underline{q}| \sigma(\underline{q}) dq = \tfrac{1}{2} \left[r(\underline{P})\right]^2, \qquad \underline{q} \in \partial B.$$

From $\phi(\underline{P})$ generated by (3.7) the solution for χ follows from

$$\chi(\underline{P}) = \phi(\underline{P}) - \tfrac{1}{2}\left[r(\underline{P})\right]^2, \quad \underline{P} \in B + \partial B.$$

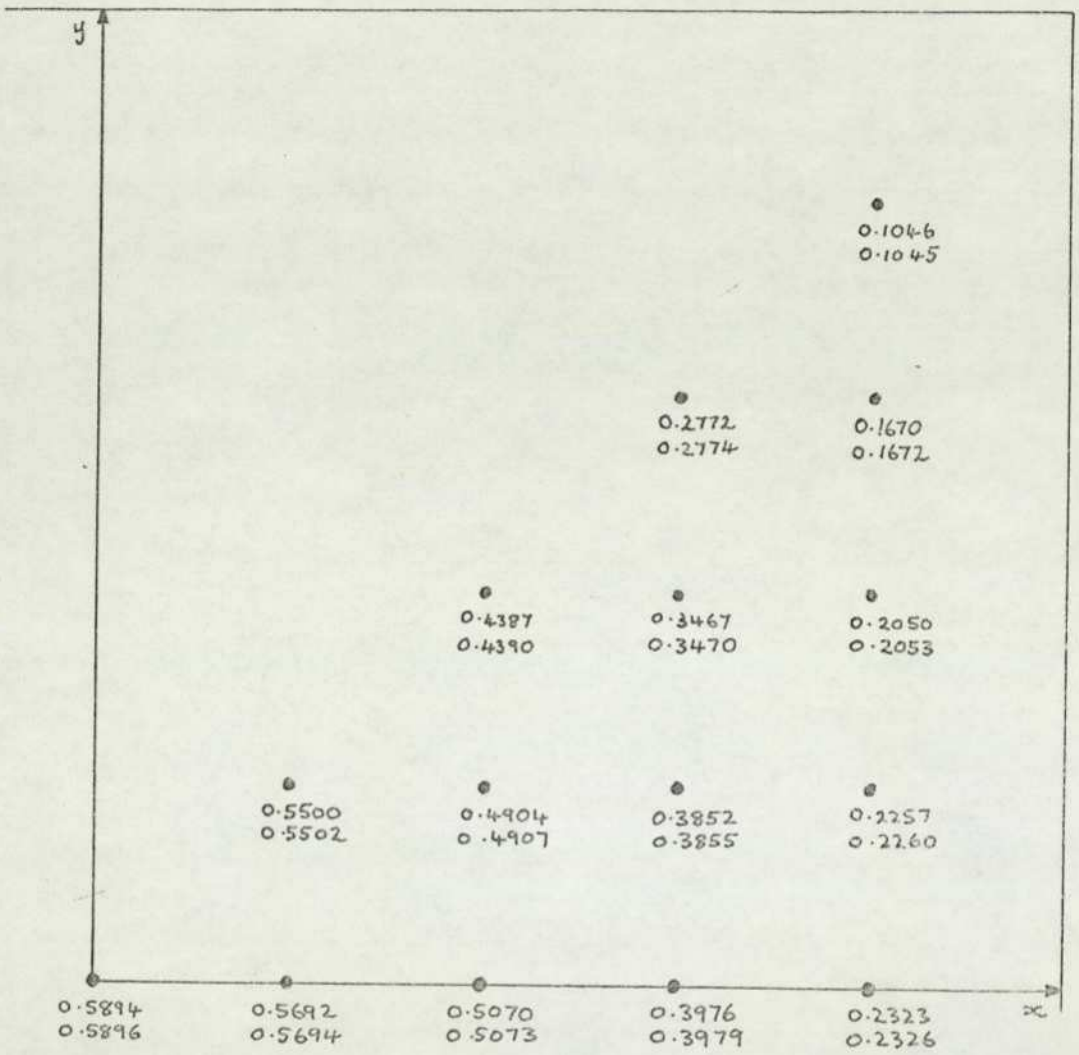
After subjecting the numerical analysis to the usual scrutiny and improvement procedures, we obtained the results shown in figure 57 using n = 80. Five times this number of lattice points does not produce a more accurate solution by relaxation methods (except very near the boundary). Our results for interior mesh points deviate from the analytic

solution by less than 0.15%. Figures 56 and 57 only show values of $\underline{P}$ corresponding to $x \geq y \geq 0$, since, by the symmetry of the last two problems about the x and y-axes and the lines $y = \pm x$, it is only necessary to consider field points within one eighth of the square. For figure 56 the analytical solution for comparison is $\phi(\underline{P}) = 1$ everywhere, whilst in figure 57 the upper figures are the analytical values and the lower figures their numerical counterparts.



Solutions of $\nabla^2\phi = 0$ inside the square $|x| \leq 1, |y| \leq 1$ with $\phi = 1$ on the boundary.

Figure 56



Solutions of $\nabla^2 \chi = -2$ inside the square $|x| \leq 1, |y| \leq 1$ with $\chi = 0$ on the boundary.

Figure 57

APPENDIX 4

REPRESENTATION OF AN ARBITRARY BIHARMONIC FUNCTION

In this appendix we prove that an arbitrary biharmonic function χ admits a representation in the form

$$\chi = x\phi + \psi \quad ; \quad \nabla^2\phi = \nabla^2\psi = 0. \qquad (A4.1)$$

This is the converse of the result proved in chapter 5 (p.57) that if χ is represented in the form (A4.1) then χ is biharmonic.

We first note that if χ is an arbitrary biharmonic function, then $\nabla^2\chi$ is a harmonic function since it satisfies

$$\nabla^2(\nabla^2\chi) = 0. \qquad (A4.2)$$

An arbitrary harmonic function may always be expressed as the derivative of another harmonic function, hence we may write

$$\nabla^2\chi = 2\frac{\partial\phi}{\partial x} \qquad (A4.3)$$

where

$$\nabla^2\phi = 0. \qquad (A4.4)$$

Since

$$\nabla^2(x\phi) = (\nabla^2\chi)\phi + x\nabla^2\phi + 2\ \text{grad}\ x\ .\ \text{grad}\ \phi$$

a particular solution of (A4.3) is $\chi = x\phi$, whence the general solution is

$$\chi = x\phi + \psi \qquad (A4.5)$$

where

$$\nabla^2\psi = 0. \qquad (A4.6)$$

Thus we may say that (A4.1) is a necessary and sufficient condition for a function χ to be biharmonic. The same result holds for the representations $\chi = y\phi + \psi$, $\chi = r^2\phi + \psi$ where $\nabla^2\phi . \nabla^2\psi = 0$.

APPENDIX 5

CONFOCAL ELLIPTIC COORDINATES

Confocal elliptic coordinates (ξ, η) may be defined in relation to Cartesian coordinates (x, y) by the equations

$$\left.\begin{aligned} x &= c \cosh\xi \cos\eta, \\ y &= c \sinh\xi \sin\eta . \end{aligned}\right\} \quad (A5.1)$$

The condition

$$\xi = \xi_0 = \text{constant} \quad (A5.2)$$

defines the ellipse

$$\frac{x^2}{a^2} + \frac{y^2}{b^2} = 1 \quad (A5.3)$$

if

$$\left.\begin{aligned} a &= c \cosh\xi_0 , \\ b &= c \sinh\xi_0 . \end{aligned}\right\} \quad (A5.4)$$

Similarly $\eta = \eta_0 = \text{constant}$ is the locus of a hyperbola. Equations (A5.4) imply

$$a^2 - b^2 = c^2 , \quad (A5.5)$$

$$\left.\begin{aligned} &\xi_0 = \cosh^{-1}\frac{a}{c} = \sinh^{-1}\frac{b}{c} = \ln\left(\frac{a+b}{c}\right), \\ &\cosh\xi_0 = \frac{a}{c}, \quad \sinh\xi_0 = \frac{b}{c}, \quad e^{\xi_0} = \left(\frac{a+b}{c}\right), \quad \cosh 2\xi_0 = \frac{a^2+b^2}{c^2} . \end{aligned}\right\} \quad (A5.6)$$

A typical point in the $x - y$ plane may be specified by

$$\underline{r} = c\cosh\xi\cos\eta\,\hat{\underline{i}} + c\sinh\xi\sin\eta\,\hat{\underline{j}} \quad (A5.7)$$

where $\hat{\underline{i}}$, $\hat{\underline{j}}$ are unit vectors along the x , y axes respectively. The scale factors $\left|\frac{\partial c}{\partial \xi}\right|$ and $\left|\frac{\partial c}{\partial \eta}\right|$ each take the value

$$c\sqrt{\sinh^2\xi + \sin^2\eta} = \frac{c}{\sqrt{2}}\sqrt{\cosh 2\xi - \cos 2\eta} . \quad (A5.8)$$

Equation (A5.7) also yields

$$r^2 = \frac{c^2}{2}(\cosh 2\xi + \cos 2\eta). \quad (A5.9)$$

Hence

$$r \to \frac{ce^{\xi}}{2} \quad \text{as} \quad \xi \to \infty , \quad (A5.10)$$

i.e.

$$\xi = O(\ln r) \quad \text{as} \quad r \to \infty . \quad (A5.11)$$

From (A5.1)

$$\tan\theta = \frac{y}{x} = \tanh\xi \tan\eta \quad ,$$

therefore

$$\theta \to \eta \text{ as } \xi \to \infty. \tag{A5.12}$$

The scale factors (A5.8) both approach r as $\xi \to \infty$ by virtue of (A5.10). There is thus a parity between confocal elliptic coordinates ξ, η that does not exist between plane polar coordinates.

The scale factors are also utilised in constructing the two-dimensional Laplacian operator

$$\nabla^2 \equiv \frac{1}{c^2(\sinh^2\xi + \sin^2\eta)} \left[\frac{\partial^2}{\partial\xi^2} + \frac{\partial^2}{\partial\eta^2} \right] \tag{A5.13}$$

so that if ϕ is a harmonic function in x and y , ϕ is also harmonic in ξ, η .

From (A5.7) it can be seen that the scalar product

$$\frac{\partial \underline{r}}{\partial\xi} \cdot \frac{\partial \underline{r}}{\partial\eta} = 0 \tag{A5.14}$$

which proves that each ellipse of the family ξ = constant intersects orthogonally each hyperbola of the family η = constant. Thus the normal to the ellipse $\xi = \xi_0$ at the point (ξ_0, η_0) is the tangent to the hyperbola $\eta = \eta_0$. Hence, employing the scale factors (A5.8) again, we may express the normal derivative operator for the ellipse in the form

$$\frac{\partial}{\partial n} = \frac{\pm 1}{c\sqrt{\sinh^2\xi + \sin^2\eta}} \frac{\partial}{\partial\xi} = \frac{\pm\sqrt{2}}{c\sqrt{\cosh 2\xi - \cos 2\eta}} \frac{\partial}{\partial\xi} \quad . \tag{A5.15}$$

The + sign applies to an exterior domain: the - sign applies to an interior domain.

REFERENCES

BHARGAVA, R.D. 1959. Ph.D. Thesis. London University.

BHARGAVA, R.D. 1965. Proc. natn. Inst. Sci. India, 31, 6.

GARABEDIAN, P.R. 1951. Pacif. J. Math., 1, 485.

GHOSH, S. 1929. Bull. Calcutta math. Soc., 21, 191.

HAPPEL, H. 1921. Math. Z., 11, 194.

HADAMARD, J. 1908. Mém. prés. div. Sav. Acad. Sci. Inst. Fr., 2, 33.

HANCOCK, H. 1958. Elliptic Integrals. New York, Dover.

HENCKY, H. 1923. Z. angew. Math. Mech., 3, 241.

HILL, R. 1960. The Mathematical Theory of Plasticity, Oxford, University Press.

JASWON, E. 1969. M.Phil. Thesis, London University.

JASWON, M.A. 1963. Proc. R. Soc., A 275, 23.

JASWON, M.A., and MAITI, M. 1968. J. Engng. Math., 2, 83.

JASWON, M.A., MAITI, M. and SYMM, G.T. 1967. Int. J. Solids Structures, 3, 309.

JASWON, M.A., and PONTER, A.R. 1963. Proc. R. Soc., A273, 237.

KANTOROVICH, L.V. and KRYLOV, V.I. 1958. Approximate Methods of Higher Analysis, Groningen, Noordhoff.

KELLOGG, O.D. 1929. Foundations of Potential Theory, New York, Ungar.

LASKAR, S.K. 1972. Ph.D. Thesis. The City University, London.

LIGTENBERG, F.K. 1954. Proc. Soc. exp. Stress Analysis, 12, 83.

LOVE, A.E.H. 1952. A Treatise on the Mathematical Theory of Elasticity, (4th edition) Cambridge, University Press.

MIKHLIN, S.G. 1957. Integral Equations, London, Pergamon.

MUSKHELISHVILI, N.I. 1963. Some Basic Problems of the Mathematical Theory of Elasticity, (4th edition) Groningen, Noordhoff.

PRAGER, W. and HODGE, P.G., 1968. Theory of Perfectly Plastic Solids, New York, Dover.

SENGUPTA, H.M. 1948. Bull. Calcutta math. Soc., 40, 17.

SENGUPTA, H.M. 1949. Bull. Calcutta math. Soc., 41, 163.

SPAIN, B. 1940. Q. Jl. Math., 11, 271.

SYMM, G.T. 1963. Proc. R. Soc., A 275, 33.

SYMM, G.T. 1964. Ph.D. Thesis. London University.

SYNGE, J.L. 1957. The Hypercircle in Mathematical Physics, Cambridge, University Press.

SZEGÖ, G. 1939. Orthogonal Polynomials, New York, Am. math. Soc., Colloquium Publications, 23.

TIMOSHENKO, S.P., and GOODIER, J.N. 1970. Theory of Elasticity, (3rd edition) New York, McGraw-Hill.

TIMOSHENKO, S.P., and WOINOWSKY-KRIEGER, S. 1959. Theory of Plates and Shells, (2nd edition) New York, McGraw-Hill.